The role of soil moisture and weather patterns for flood occurrence and characteristics at the river basin scale

Manuela Nied

Institute of Earth- and Environmental Science

The role of soil moisture and weather patterns for flood occurrence and characteristics at the river basin scale

Cumulative Dissertation

for the degree of
Doctor of Natural Sciences (Dr. rer. nat.)
in Hydrology

submitted to the
Faculty of Science
at the University of Potsdam, Germany

by
Manuela Nied

Submitted: March 2016

Referees:
Prof. Dr. Bruno Merz, University of Potsdam
Prof. Dr. Axel Bronstert, University of Potsdam
Prof. Dr. Rolf Weingartner, University of Bern

Submitted: March 2016
Defended: July 2016
Published: August 2016

Published online at the
Institutional Repository of the University of Potsdam:
URN urn:nbn:de:kobv:517-opus4-94612
http://nbn-resolving.de/urn:nbn:de:kobv:517-opus4-94612

1 Contents

2 List of Figures

3 List of Tables

4 Abstract

Flood generation at the scale of large river basins is triggered by the interaction of the hydrological pre-conditions and the meteorological event conditions at different spatial and temporal scales. This interaction controls diverse flood generating processes and results in floods varying in magnitude and extent, duration as well as socio-economic consequences. For a process-based understanding of the underlying cause-effect relationships, systematic approaches are required. These approaches have to cover the complete causal flood chain, including the flood triggering meteorological event in combination with the hydrological (pre-)conditions in the catchment, runoff generation, flood routing, possible floodplain inundation and finally flood losses.

In this thesis, a comprehensive probabilistic process-based understanding of the causes and effects of floods is advanced. The spatial and temporal dynamics of flood events as well as the geophysical processes involved in the causal flood chain are revealed and the systematic interconnections within the flood chain are deciphered by means of the classification of their associated causes and effects. This is achieved by investigating the role of the hydrological pre-conditions and the meteorological event conditions with respect to flood occurrence, flood processes and flood characteristics as well as their interconnections at the river basin scale.

Broadening the knowledge about flood triggers, which up to now has been limited to linking large-scale meteorological conditions to flood occurrence, the influence of large-scale pre-event hydrological conditions on flood initiation is investigated. Using the Elbe River basin as an example, a classification of soil moisture, a key variable of pre-event conditions, is developed and a probabilistic link between patterns of soil moisture and flood occurrence is established. The soil moisture classification is applied to continuously simulated soil moisture data which is generated using the semi-distributed conceptual rainfall-runoff model SWIM. Applying successively a principal component analysis and a cluster analysis, days of similar soil moisture patterns are identified in the period November 1951 to October 2003.

The investigation of flood triggers is complemented by including meteorological conditions described by a common weather pattern classification that represents the main modes of atmospheric state variability. The newly developed soil moisture classification thereby provides the basis to study the combined impact of hydrological pre-conditions and large-scale meteorological event conditions on flood occurrence at the river basin scale.

A process-based understanding of flood generation and its associated probabilities is attained by classifying observed flood events into process-based flood types such as snowmelt floods or long-rain floods. Subsequently, the flood types are linked to the soil moisture and weather patterns. Further understanding of the processes is gained by modeling of the complete causal flood chain, incorporating a rainfall-runoff model, a 1D/2D hydrodynamic model and a flood loss model. A reshuffling approach based on weather patterns and the month of their occurrence is developed to generate synthetic data fields of meteorological conditions, which drive the model chain, in order to increase the flood sample size. From the large number of simulated flood events, the impact of hydro-meteorological conditions on various flood characteristics is detected through the analysis of conditional cumulative distribution functions and regression trees.

The results show the existence of catchment-scale soil moisture patterns, which comprise of large-scale seasonal wetting and drying components as well as of smaller-scale variations related to spatially heterogeneous catchment processes. Soil moisture patterns frequently occurring before the onset of floods are identified. In winter, floods are initiated by catchment-wide high soil moisture, whereas in summer the flood-initiating soil moisture patterns are diverse and the soil moisture conditions are less stable in time. The combined study of both soil moisture and weather patterns shows that the flood favoring hydro-meteorological patterns as well as their interactions vary seasonally. In the analysis period, 18 % of the weather patterns only result in a flood in the case of preceding soil saturation. The classification of 82 past events into flood types reveals seasonally varying flood processes that can be linked to hydro-meteorological patterns. For instance, the highest flood potential for long-rain floods is associated with a weather pattern that is often detected in the presence of so-called ‘Vb’ cyclones. Rain-on-snow and snowmelt floods are associated with westerly and north-westerly wind directions. The flood characteristics vary among the flood types and can be reproduced by the applied model chain. In total, 5970 events are simulated. They reproduce the observed event characteristics between September 1957 and August 2002 and provide information on flood losses. A regression tree analysis relates the flood processes of the simulated events to the hydro-meteorological (pre-)event conditions and highlights the fact that flood magnitude is primarily controlled by the meteorological event, whereas flood extent is primarily controlled by the soil moisture conditions.

Describing flood occurrence, processes and characteristics as a function of hydro-meteorological patterns, this thesis is part of a paradigm shift towards a process-based understanding of floods. The results highlight that soil moisture patterns as well as weather patterns are not only beneficial to a probabilistic conception of flood initiation but also provide information on the involved flood processes and the resulting flood characteristics.

5 Zusammenfassung

Hochwasserereignisse in großen Flusseinzugsgebieten entstehen durch das Zusammenwirken der hydrologischen Vorbedingungen und der meteorologischen Ereignisbedingungen. Das Zusammenwirken findet auf verschiedenen räumlichen und zeitlichen Skalen statt und steuert dabei unterschiedliche Prozesse der Hochwasserentstehung. Diese führen zu Hochwassern mit vielfältigen Eigenschaften, die sich unter anderem in maximalem Pegelstand, räumlicher Ausdehnung, Andauer und sozio-ökonomischen Folgen unterscheiden. Für ein prozessbasiertes Verständnis der zugrunde liegenden Zusammenhänge zwischen Ursache und Wirkung sind systematische Ansätze notwendig. Diese müssen die gesamte kausale Hochwasserprozesskette, von dem Hochwasser auslösenden meteorologischen Ereignis welches auf die hydrologischen Vorbedingungen im Einzugsgebiet trifft, über Abflussbildung, Wellenablauf und mögliche Überflutungen, bis hin zum Hochwasserschaden umfassen.

Die vorliegende Arbeit hat das Ziel, zu einem umfassenden probabilistischen, prozessbasierten Verständnis der Ursachen und Auswirkungen von Hochwassern beizutragen. Neben der räumlichen und zeitlichen Dynamik von Hochwasserereignissen werden die an der kausalen Hochwasserprozesskette beteiligten geophysikalischen Prozesse analysiert. Systematische Zusammenhänge von Ursachen und Wirkungen innerhalb der Hochwasserprozesskette werden durch die Analyse von Klassifizierungen der hydrologischen Vorbedingungen und der meteorologischen Ereignisbedingungen offengelegt. Des Weiteren wird der Einfluss der klassifizierten Bedingungen bezüglich Hochwasserentstehung, Hochwasserprozessen und Hochwassereigenschaften sowie deren Verbindungen untereinander auf Ebene des Flusseinzugsgebiets quantifiziert.

Das Wissen über hochwasserauslösende Bedingungen, welches bisher auf die Analyse von Großwetterlagen und deren Einfluss auf die Hochwasserentstehung beschränkt war, wird um den Einflussfaktor der großskaligen hydrologischen Vorbedingungen ergänzt. Am Beispiel des Einzugsgebiets der Elbe wird eine Klassifizierungsmethode für die Bodenfeuchte, einer bedeutenden hydrologischen Vorbedingung, entwickelt. Durch die Klassifizierung der Bodenfeuchte kann ein probabilistischer Zusammenhang zwischen räumlichen Bodenfeuchtemustern und dem Auftreten von Hochwasser hergestellt werden. Die Bodenfeuchteklassifizierung wird angewandt auf Bodenfeuchtedaten, die mit dem konzeptionellen Niederschlags-Abfluss-Modell SWIM durch kontinuierliche Simulation erzeugt werden. Eine Hauptkomponenten- und anschließende Clusteranalyse identifizieren dabei Tage ähnlicher räumlicher Bodenfeuchteverteilung im Zeitraum November 1951 bis Oktober 2003.

Die meteorologischen Ereignisbedingungen werden durch eine gängige Wetterlagenklassifikation beschrieben, welche die charakteristischen atmosphärischen Zustände abbildet. Gemeinsam mit der neu entwickelten Bodenfeuchteklassifizierung bildet dies die Grundlage für die Untersuchung des kombinierten Einflusses der hydrologischen Vorbedingungen und der großräumigen meteorologischen Ereignisbedingungen auf die Entstehung von Hochwasser auf Flussgebietsskala.

Das prozessorientierte Verständnis der Hochwasserentstehung und die damit einhergehenden Wahrscheinlichkeiten werden durch die Klassifizierung von vergangenen Hochwasserereignissen in prozessbasierte Hochwassertypen wie Schneeschmelzhochwasser oder Hochwasser auf Grund von langanhaltendendem Regen erzielt. Anschließend werden den Hochwassertypen die jeweils vorliegenden Bodenfeuchtemuster und Wetterlagen zugeordnet. Die Hochwasserprozesse werden zudem durch Simulation der gesamten kausalen Hochwasserprozesskette unter Einbeziehung eines Niederschlags-Abfluss-Modells, eines 1D/2D hydrodynamischen Modells sowie eines Hochwasserschadensmodells modelliert. Ein neu entwickelter Permutationsansatz basierend auf der Wetterlage und dem Monat ihres Auftretens generiert synthetische meteorologische Datensätze, welche der Modellkette als Eingangsdaten dienen, um eine repräsentative Anzahl von Hochwasserereignissen zu erzeugen. Durch die Vielzahl an simulierten Hochwasserereignissen kann der systematische Einfluss der hydrometeorologischen Bedingungen auf verschiedene Hochwassermerkmale mit Hilfe von bedingten Verteilungsfunktionen und Regressionsbäumen gezeigt werden.

Die Ergebnisse belegen die Existenz von Mustern der Bodenfeuchte auf Ebene von Flusseinzugsgebieten. Die Muster bilden sowohl großräumige jahreszeitliche Schwankungen der Bodenfeuchte als auch kleinskalige heterogene Prozesse im Einzugsgebiet ab. Häufig vor Hochwassern auftretende Bodenfeuchtemuster werden identifiziert. Im Winter wird Hochwasser vornehmlich durch eine flächendeckend hohe Bodenfeuchte eingeleitet. Im Sommer sind die Bodenfeuchtemuster zeitlich variabler und die mit Hochwasser in Verbindung stehenden Muster zahlreicher. Die Ergänzung der Bodenfeuchtemuster um die Wetterlagenklassifikation zeigt für die Hochwasserentstehung, dass die Beiträge der einzelnen hydrometeorologischen Muster sowie deren Zusammenwirken jahreszeitlich variieren. Im Untersuchungszeit-

raum resultieren 18 % der Wetterlagen nur bei vorangehender Bodensättigung in einem Hochwasser. Die Zuordnung von 82 Hochwasserereignissen zu prozessbasierten Hochwassertypen zeigt ebenfalls saisonal unterschiedliche Prozesse auf, welche mit den hydro-meteorologischen Mustern in Verbindung gebracht werden können. Beispielsweise ist das größte Hochwasserpotenzial auf Grund von langanhaltendem Regen auf eine Wetterlage zurückzuführen, die häufig in Gegenwart von sogenannten "Vb" Zyklonen beobachtet wird. Regen-auf-Schnee und Schneeschmelz-Ereignisse werden im Zusammenhang mit westlichen und nordwestlichen Windrichtungen beobachtet. Die prozessbasierten Hochwassertypen und die resultierenden Hochwassereigenschaften können durch die angewandte Modellkette wiedergegeben werden. Insgesamt werden 5970 Ereignisse simuliert, welche die beobachteten Hochwassereigenschaften zwischen September 1957 und August 2002 reproduzieren. Zusätzlich können durch die Modellkette auch Aussagen über auftretende Hochwasserschäden gemacht werden. Eine Regressionsbaum-Analyse setzt die Hochwasserprozesse der simulierten Ereignisse in Beziehung zu den hydro-meteorologischen Bedingungen. Dabei wird deutlich, dass der Pegelstand primär durch die meteorologischen Ereignisbedingungen bestimmt wird, wohingegen die räumliche Ausdehnung des Hochwassers primär durch die Bodenfeuchtebedingungen beeinflusst wird.

Die vorliegende Arbeit ist Teil eines Paradigmenwechsels hin zu einem prozessbasierten Hochwasserverständnis. Die Beschreibung von Hochwasserentstehung, Hochwasserprozessen und Hochwassereigenschaften in Abhängigkeit von hydro-meteorologischen Mustern zeigt, dass Bodenfeuchtemuster sowie Wetterlagen nicht nur zu einer probabilistischen Analyse der Hochwasserentstehung beitragen, sondern auch Aufschluss über die ablaufenden Hochwasserprozesse und die daraus resultierenden Hochwassereigenschaften geben.

Chapter 1:
Introduction

1.1 Background

Ever since, the world has experienced devastating flood events causing the displacement of people, loss of human lives as well as private, economic, and infrastructural losses. According to the World Bank (Jha et al., 2012), floods are the most frequent and devastating natural hazard worldwide. Since the 1950s, the number of reported events along with the number of affected people and losses due to flooding has increased significantly (Jha et al., 2012). Worldwide, the estimated damage reached US $ 486 billion between 1950 and 2010. Thereof US $ 216 billion arose between 2000 and 2010 alone (Guha-Sapir et al., 2015), highlighting the recent increase in flood impact worldwide.

The nature and origin of floods is manifold. Broad categories are coastal floods, fluvial floods and flash floods. Coastal floods are triggered by storms, typically during high tide, or by tsunamis caused by marine earthquakes or landslides. Fluvial floods are usually rainfall-driven, in coherence with saturated soils and occasionally snowmelt. Ice jams in the river channel can cause fluvial flooding, too. Flash floods are observed in ephemeral rivers and mountain torrents (European Union, 2007). They are either triggered by heavy rain associated with severe thunderstorms and tropical storms or by the bursts of natural and artificial dams. This work investigates fluvial floods. In the course of this work, the terms 'flood(s)', 'flooding' and 'event(s)' therefore refer to fluvial flood(s) excluding flooding due to ice jams.

Recent extreme events in Central Europe, e.g. the Rhine flood in 1995 (Chbab, 1995; Engel, 1997), the Elbe floods in 2002 and 2013 (Conradt et al., 2013; Merz et al., 2014b; Ulbrich et al., 2003a, b) and the Danube flood in 2013 (Blöschl et al., 2013) illustrated that coping with floods is not merely a question of local flood defense structures such as dikes and dams. Instead, an entire chain of processes is involved. For a comprehensive understanding of the underlying cause-effect relations, a process based understanding of floods is required to not only increase the reliability of flood estimates but also to improve the prediction of future floods under climate and land use change (Merz et al., 2014a). Likewise, a paradigm shift towards a process based understanding of floods is observed in flood frequency analysis and entitled 'flood frequency hydrology' by Merz and Blöschl (2008a, b). In this work, the implementation of 'flood frequency hydrology' is advanced by focusing on a process based understanding of floods. This is achieved by revealing (i) the spatial and temporal dynamics of flood events and (ii) the geophysical processes involved in the causal flood chain, as well as by (iii) deciphering the systematic interconnections within the flood chain by means of the classification of their causes and effects.

1.2 Spatial and temporal dynamics

The European Union (2007) defines a flood as "the temporary covering by water of land not normally covered by water" and thereby highlights that a flood is composed of a temporal as well as of a spatial component. Depending on the flood generating mechanism, the temporal component can range from minutes up to months. The spatial extension can range from few square meters up to ten thousands of square kilometers (Hirschboeck, 1988). Flood magnitude is variable within space and time. This notion of floods is in contrast to flood frequency analysis and design value estimation where a flood event is defined for one point in time at one particular location in the river network. Usually in flood frequency analysis, spatial interactions of flood events along the river network are neglected and uniform return periods in the entire catchment are assumed. However, this spatially uniform return period approach is only valid for local flood assessment and tends to overestimate flood risk on larger spatial scales (Falter et al., 2015; Ghizzoni et al., 2012; Keef et al., 2009, 2013; Thieken et al., 2014). In contrast, for the assessment of flood impact at the river basin scale as requested by the European Union (2007), a flood has to be considered as the simultaneous or time shifted occurrence of peak discharges of various magnitudes at several gauges within the entire river network (Ghizzoni et al., 2012; Merz and Blöschl, 2003; Rodda, 2005; Uhlemann et al., 2010).

Beyond this hazard oriented definition, a flood may also be defined through its impact on a vulnerable society, economy and environment. Accordingly there is a need to address floods from a risk perspective incorporating hazard, exposure and vulnerability (Merz et al., 2010a).

1.3 Geophysical processes

The causal flood chain (Fig. 1.1) outlines the geophysical processes involved, from flood triggering physical (pre-)event conditions, through runoff generation and concentration, wave propagation and superposition as well as inundation to the flood impact. The flood triggering physical (pre-)event conditions are in particular the hydrological pre-event conditions such as soil saturation and snow water equivalent and the meteoro-

logical event conditions, such as the amount and spatial distribution of precipitation or the inflow of warm air masses (Brocca et al., 2008; Froidevaux et al., 2015; Merz and Blöschl, 2008b, 2009b; Parajka et al., 2010). Together, they affect the varying runoff generation mechanisms as well as runoff concentration. This in turn can result in the accumulation of excess water in the river channel. Subsequently, the water is routed through the river network. Propagating along the river network to the catchment outlet, the flood wave is modulated and superimposes with inflowing flood discharges. In case the flood water level overtops the river banks, adjacent areas may be inundated which may cause losses and impact society. A multitude of characteristic numbers can be used to describe the flood event quantitatively. These include flood loss, flood magnitude and extent as well as event duration and are termed flood characteristics in the further course.

For a comprehensive understanding of flood cause and effect, each link of the chain demands attention. Observations of precipitation, water levels, discharge, etc. can give partial insight into the ongoing processes and their causes and effects. However, the limited sample size of flood events as well as the wide variety of possible process combinations hinder the establishment of a clear link between cause and effect. A promising complement to analyzing observational data is the modeling of flood events by continuous simulation of the entire causal flood chain (e.g. Falter et al., 2015; Haberlandt and Radtke, 2014). Since all inputs, influences and processes are integrated in the river basin, this is the consequential unit to carry out this analysis. Furthermore, the river basin is the scale of interest for national risk policy as well as disaster management and planning (European Union, 2007).

1.4 Systematic interconnections within the flood chain

The hydrological pre-event conditions, meteorological event conditions, flood generation processes as well as flood characteristics are highly variable between and within flood events. However, these factors act on characteristic spatio-temporal scales. Therefore, in order to understand the cause and effect relationships of floods in a holistic way, systematic approaches are required which unveil the causal mechanisms, systematics and dominant processes in the atmosphere, the catchment and the river system (Blöschl et al., 2007; Merz et al., 2014a). Classification is such an approach.

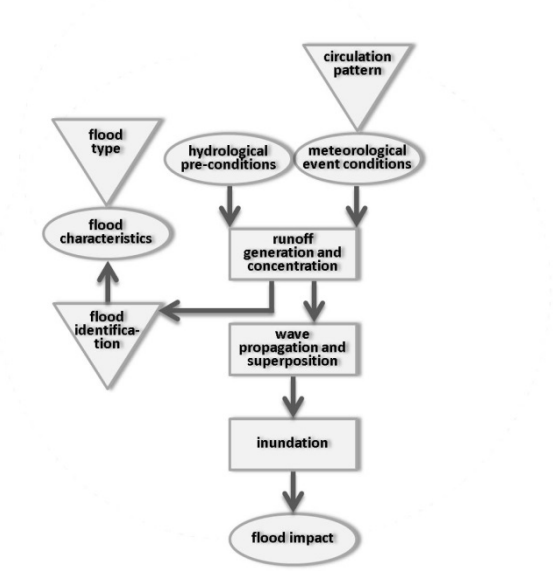

Fig. 1.1: The causal flood chain, its processes (rectangles) and states (ellipses). Triangles mark classifications of the system under study.

All individual factors under consideration are first characterized and afterwards grouped into categories according to a similarity criterion. By doing so, the classification highlights similarities among individuals in the same category as well as differences between categories. In Fig. 1.1 several classification systems of the causal flood chain are highlighted by triangles. The identification of a flood event itself is already a classification step, as it categorizes a time series into flood and no-flood periods. Various flood identification approaches are applicable, e.g. according to a discharge time series or the occurrence of flood related damage.

Classification is an established concept in meteorology where the daily synoptic situation is classified into circulation or weather patterns, which describe the main modes of variability of the atmospheric state (Philipp et al., 2010). These daily atmospheric circulation patterns are linked to flood occurrence as well as flood magnitude, and a probabilistic relation between atmospheric circulation patterns and flood occurrence/magnitude is sought (e.g. Bárdossy and Filiz, 2005; Jacobeit et al., 2006; Parajka et al., 2010; Petrow et al., 2007, 2009; Prudhomme and Genevier, 2011; Wilby and Quinn, 2013). In contrast, for other causal factors of flood generation, such as the hydrological pre-event conditions, no studies are available that attempt to classify and link them to floods. This is remarkable, since for instance the causal link of the catchment's soil moisture state and flood generation is widely acknowledged in the literature (e.g. Brocca et

al., 2008; Merz and Blöschl, 2008b, 2009b; Schröter et al., 2015). Therefore, the classification of the hydrological pre-event conditions and their linkage to flood initiation is an obvious step to investigate the presence and characteristics of underlying systematics. Moreover, the combined effects of flood triggering causes, i.e. hydrological pre-event conditions and meteorological event conditions, is not yet systemized at the regional scale ($\geqslant$10,000 km^2), where flooding can affect many sites simultaneously, whereas other sites remain unaffected (Merz and Blöschl, 2008b).

Likewise to atmospheric classification, flood events can also be classified (e.g. Alila and Mtiraoui, 2002; Hirschboeck, 1987; Merz and Blöschl, 2003). Categories that generalize the findings about flood events are termed flood types. This concept assumes that "the causal mechanisms and dominant processes in the atmosphere, catchment and river system [...] leave their fingerprints on flood characteristics" (Merz et al., 2014a). According to the causal flood chain, floods originating from the same flood generating process exhibit the same flood characteristics and can be assigned to the same flood type. For this reason, a probabilistic relation between the classified flood triggering causes and the resulting flood characteristics as well as flood types should be recognizable.

Overall, the concept of classification encompasses the entire causal flood chain: the atmosphere, flood identification, flood type classification as well as the newly developed classification of the antecedent soil moisture state (Fig. 1.1). Accordingly, the classifications of different factors are linked to each other in order to decipher cause and effect of flooding in a probabilistic framework. Flood frequency estimation and flood risk management may benefit from an understanding of how the hydro-meteorological (pre-)conditions, the resulting flood processes as well as the different flood characteristics are interconnected.

1.5 Objective and research questions

The great variability of the pre-event hydrological catchment conditions and the meteorological event conditions as well as their complex interaction results in diverse flood generating processes leading to manifold flood characteristics. Consequently, a flood is a complex spatio-temporal phenomenon that requires the application of systematic approaches to gain insight into its processes as well as to quantify the economical and societal impact of these processes. The objective of this thesis is to systematically investigate the impact of pre-event hydrological catchment conditions and meteorological event conditions on flood occurrence, flood processes and flood characteristics as well as their interconnections at the river basin scale.

The objective is addressed by the following research questions:

1. Flood generation is triggered by the interaction of pre-event hydrological catchment conditions and the meteorological event characteristics. Previous studies focused on the classification of the large-scale meteorological event conditions and their linkage to flood generation. Large-scale hydrological pre-event conditions are commonly neglected and no systematic analysis has been presented so far. With respect to soil moisture as a key variable of pre-event catchment conditions several questions arise: Do large-scale soil moisture patterns exist? What is the dominant spatio-temporal behavior of soil moisture at the river basin scale? Do flood-prone soil moisture patterns exist?
2. The linkage between the large-scale meteorological event conditions and flood occurrence is widely acknowledged in the literature. However, it is unclear if and to what extent large-scale meteorological event conditions are related to the flood generation processes that find their expression in different flood types. Furthermore, the influence of the hydrological catchment conditions on the linkage between large-scale meteorological event conditions and flood occurrence is unknown. The following research questions arise: Does a specific weather pattern/soil moisture pattern generate a specific flood type and can thus be linked to a particular flood generating process? How do large-scale soil moisture conditions modify the relation between weather patterns and flood occurrence by amplifying or hindering flood generation?
3. The hydro-meteorological conditions that drive the water input into the catchment govern the flood generation processes and result in miscellaneous flood characteristics, e.g. flood magnitude and extent, event duration and flood loss. Previous studies focused on the hydro-meteorological conditions and their influence on flood occurrence as well as flood peaks in small catchments. So far, the control of the hydrological pre-event conditions and meteorological event conditions over the variety of flood characteristics has not been investigated systematically. The following questions arise: Which flood characteristics are controlled by the hydrological pre-event conditions and which ones by the meteorological event conditions? Does the presence of a particular soil moisture pattern and/or weather pattern determine

the magnitude of the flood characteristic under consideration? Does knowledge about the flood characteristics allow conclusions on the involved flood processes?

1.6 Tasks and structure

This thesis compromises 5 chapters including this introduction. The chapters are based on articles that have been published in (chapters 2 and 3), or, are currently reviewed by international peer-reviewed scientific journals (chapter 4). The methodology developed in these articles is exemplarily applied to the Elbe/Labe Basin located in Central Europe. The catchment encompasses 148,268 km² and is situated in the transition zone between maritime and continental climate. As both summer and winter floods are observed in the Elbe basin (Beurton and Thieken, 2009), the hydro-meteorological controls can be studied based on a broad range of flood types. In the recent past, the Elbe catchment experienced severe flood events such as the disastrous summer floods of August 2002 (Ulbrich et al., 2003a, b) and June 2013 (Conradt et al., 2013; Merz et al., 2014b). These events were part of large scale transbasin floods affecting Central and Eastern Europe. In total, in 2013, losses amounted to US $ 12.6 billion whereas US $ 16.5 billion accrued for the 2002-floods (Munich RE, 2015).

Figure 1.2 highlights the tasks undertaken in this study to better understand cause and effect of flooding. The accomplished tasks are outlined in the following.

Chapter 2: Flood-initiating catchment conditions

A classification of daily soil moisture patterns at the scale of large river basins is developed. Therefore, soil moisture is simulated with a semi-distributed rainfall-runoff model. Soil moisture pattern types are identified in two steps. First, principal component analysis reduces the dimensionality of the soil moisture data and identifies the main modes of soil moisture variability. Subsequently, cluster analysis assesses the similarity in daily soil moisture distributions within the catchment and assigns each day of the investigation period to one soil moisture pattern type. The soil moisture pattern types are afterwards linked to past flood events in the Elbe River basin identified from observed discharge time series. This task as well as its placement in the causal flood chain is highlighted in Fig. 1.2 left by the blue arrows. The newly established link is marked by the blue dashed line.

Chapter 3: On the relationship between hydro-meteorological patterns and flood types

A classification of flood events at the river basin scale is introduced. According to a variety of flood type indicators, it categorizes the identified flood events into process-based flood types. In the next step, the flood types are assigned to the occurring soil moisture patterns and weather patterns. Based on an efficiency index, patterns favoring a certain flood type are identified. Besides, the efficiency index quantifies the combined impact of soil moisture patterns and weather patterns on flood occurrence. This task as well as its placement in the causal flood chain is highlighted in Fig. 1.2 middle by the brown arrows. The newly established links are marked by the brown dashed lines.

Chapter 4: Hydro-meteorological controls on flood characteristics

A large number of flood events are generated based on a reshuffling approach of the catchment's meteorology to obtain a representative sample. The permuted fields of meteorological event conditions drive a model chain that incorporates the complete causal flood chain. The simulated events should give an adequate reproduction of the observed event characteristics as well as generate flood events beyond the existing range of observed variables. The flood characteristics are analyzed by cumulative distribution functions and regression tree analysis to decipher the large-scale control of soil moisture patterns and weather patterns. This task as well as its placement in the causal flood chain is highlighted in Fig. 1.2 right by the green arrows. The newly established links are marked by the green dashed lines.

Chapter 5: Discussion, conclusions and outlook

The chapter synthesizes the achievements reached in understanding the interaction of the hydrological pre-event conditions and the meteorological event conditions with their associated flood generating processes as well as their flood characteristics. The chapter summarizes the findings of the tasks by concluding remarks and provides overall conclusions. It outlines further research needs and discusses the implications of the findings of this thesis for flood risk estimation and management.

Fig. 1.2: The causal flood chain, its processes (rectangles) and states (ellipses). Triangles mark classifications of the system under study. Additionally, the graph highlights the tasks undertaken in this study for a better understanding of cause and effect of flooding. Newly established links in this study are marked by the dashed lines. Left: The first task is highlighted in blue. A classification of the catchment's soil moisture state is developed. The derived soil moisture patterns are linked to floods identified from observed discharge time series. Middle: The second task is highlighted in brown. The observed flood events are categorized into process based flood types. Afterwards, the flood types are linked to the soil moisture conditions preceding the event and the meteorological conditions during the event. Furthermore, the interaction of the antecedent conditions and the meteorological conditions on flood generation is investigated. Right: The third task is highlighted in green. The complete causal flood chain is simulated. An adequate number of floods are synthetically generated. The control and interaction of patterns of the hydro-meteorological (pre-)conditions on a variety of flood characteristics including losses as well as on the underlying flood processes is investigated.

1.7 Author contribution

The comprehensive tasks required for the development of the methodology and its application to understand floods in the Elbe River basin, the control of hydro-meteorological patterns on flood generation (cause) and impact (effect) were realized by the author in cooperation with a team of scientists. The author's contribution is the development of the soil moisture classification, the identification and characterization of flood events, the classification of flood events into flood types, the hydrological model simulations and the linkage of the single results as well as the analysis of the final results. The weather pattern classification was accomplished by Tobias Pardowitz. Damage simulations were undertaken by Kai Schröter. Viet-Dung Nguyen performed the hydraulic modelling. As indicated in Chapter 2-4, the listed co-authors contributed to the conceptual design of the papers, discussion of results as well as final formulations of the manuscript.

Chapter 2:
Flood-initiating catchment conditions

Flood-initiating catchment conditions: a spatio-temporal analysis of large-scale soil moisture patterns in the Elbe River basin

Abstract

Floods are the result of a complex interaction between meteorological event characteristics and pre-event catchment conditions. While the large-scale meteorological conditions have been classified and successfully linked to floods, this is lacking for the large-scale pre-event catchment conditions. Therefore, we propose classifying soil moisture as a key variable of pre-event catchment conditions and investigating the link between soil moisture patterns and flood occurrence in the Elbe River basin. Soil moisture is simulated using a semi-distributed conceptual rainfall-runoff model over the period 1951-2003. Principal component analysis (PCA) and cluster analysis are applied successively to identify days of similar soil moisture patterns. The results show that PCA considerably reduced the dimensionality of the soil moisture data. The first principal component (PC) explains 75.71 % of the soil moisture variability and represents the large-scale seasonal wetting and drying. The successive PCs express spatially heterogeneous catchment processes. By clustering the leading PCs, we identify large-scale soil moisture patterns which frequently occur before the onset of floods. In winter, floods are initiated by overall high soil moisture content, whereas in summer the flood-initiating soil moisture patterns are diverse and less stable in time.

Published as:

Nied, M., Hundecha, Y., and Merz, B.: Flood-initiating catchment conditions: a spatio-temporal analysis of large-scale soil moisture patterns in the Elbe River basin, Hydrol. Earth Syst. Sci., 17, 1401-1414, 2013.

2.1 Introduction

Flood generation and magnitude are the result of a complex interaction between meteorological conditions, such as the amount and spatial distribution of precipitation or the inflow of warm air masses, and pre-event hydrological catchment conditions, such as soil saturation and snow water equivalent (Brocca et al., 2008; Marchi et al., 2010; Merz and Blöschl, 2008b; Merz and Blöschl, 2009b; Parajka et al., 2010). In order to capture the variety of large-scale flood generation mechanisms, flood events have been classified and analyzed according to their hydro-meteorological conditions along with their interactions between catchment state and meteorological conditions (e.g. Alila and Mtiraoui, 2002; Apipattanavis et al., 2010; Merz and Blöschl, 2003). These interactions vary from decade to decade (Alila and Mtiraoui, 2002), seasonally (Merz and Blöschl, 2003; Parajka et al., 2010; Sivapalan et al., 2005), and from event to event as well as from catchment to catchment (Merz and Blöschl, 2003). In addition to the occurrence and interaction of the hydro-meteorological conditions, their spatial patterns related to flooding need to be taken into account (Merz and Blöschl, 2003), which can be especially important in larger catchments (Merz and Blöschl, 2008b).

On the regional scale, the automated classification of meteorological conditions has already identified a close relationship between the occurrence and persistence of meteorological circulation pattern types and floods (e.g. Bárdossy and Filiz, 2005; Jacobeit et al., 2006; Parajka et al., 2010; Petrow et al., 2009; Prudhomme and Genevier, 2011).

As far as hydrological catchment conditions are concerned, several studies identified soil moisture pattern types on the local or regional scale applying an automated classification (Ibrahim and Huggins, 2011; Jawson and Niemann, 2007; Kim and Barros, 2002; Korres et al., 2010; Perry and Niemann, 2007; Wittrock and Ripley, 1999). However, the analyzed soil moisture data (remotely sensed or ground-based point measurements) are either limited in their spatial extent covering a small (< 1 km²) study area (e.g. Perry and Niemann, 2007) and/or in their temporal resolution (monthly/annual values or a small number of subsequent days) (e.g. Jawson and Niemann, 2007; Wittrock and Ripley, 1999). No studies are available that attempt to automatically classify the patterns of regional hydrological catchment conditions and to link them to flood initiation.

Complementary to the classification of meteorological conditions, we therefore propose the classification of the hydrological catchment conditions at the regional (Elbe) scale to get a probabilistic insight into the link between flood initiation and the hydrological catchment conditions. As soil moisture is a key variable of hydrological catchment conditions, we examine whether flood initiation in the Elbe River basin can be linked to specific soil moisture pattern types.

For the estimation of the hydrological catchment conditions concerning soil moisture, ground-based soil moisture measurements (e.g. time domain reflectometry, frequency domain reflectometry, gravimetric), remotely sensed soil moisture measurements (Brocca et al., 2009), model-based soil moisture (Merz and Blöschl, 2003; Norbiato et al., 2009) and surrogate measures such as mean annual precipitation (Merz et al., 2006; Merz and Blöschl, 2009b), antecedent precipitation index (Brocca et al., 2009; Merz et al., 2006), Gradex method (Merz and Blöschl, 2008b), and event runoff coefficient (Merz and Blöschl, 2003; Merz et al., 2006; Merz and Blöschl, 2009b; Sivapalan et al., 2005) have been applied. In the present paper, the link between the hydrological catchment conditions and flood initiation in the Elbe Basin is investigated by using daily profile soil moisture simulated by a rainfall-runoff model and validated against remotely sensed soil moisture. It is assumed that the implemented rainfall-runoff model incorporates the hydrological processes that enable the estimation of soil moisture. Afterwards, a principal component analysis (PCA) and a subsequent clustering of the leading principal components (PCs) yield different pattern types. PCA is by far the most commonly applied method among the automated techniques to classify the structure of spatially variable data, and has also been applied in soil moisture pattern studies (Ibrahim and Huggins, 2011; Jawson and Niemann, 2007; Kim and Barros, 2002; Korres et al., 2010; Perry and Niemann, 2007; Wittrock and Ripley, 1999). In parallel, regional flood events are identified and linked to the derived pattern types.

The remainder of this paper is organized as follows: first, the study area and input data are described in Sect. 2.2. The methods to identify distinct types of daily soil moisture patterns and flood events are provided in Sect. 2.3. Section 2.4 describes the retrieved soil moisture pattern types, their characteristics as well as their relation to flood initiation. These results are discussed in the subsequent section. Section 2.6 concludes our findings and suggestions for future research.

2.2 Study area and data

2.2.1 Study area

The Elbe/Labe River (Fig. 2.1) originates in the Giant Mountains 1386 m a.s.l in the Czech Republic, crosses northeastern Germany and reaches the North Sea after 1094 km. The Czech Republic and Germany are the main riparian states of the 148268 km² large drainage basin. Negligible parts belong to Austria and Poland. About 50 % of the Elbe drainage basin has an elevation below 200 m a.s.l. One-third is hilly country with an elevation between 200 and 500 m a.s.l. The low mountain range (500-750 m a.s.l.) accounts for 15 % and the mountain range for less than 2 %. Major tributaries are the Moldau/Vltava contributing an average of 154 $m^3 s^{-1}$ of river discharge (60 %) at its confluence with the Elbe River, the Eger/Ohře (38 $m^3 s^{-1}$), the Mulde (67 $m^3 s^{-1}$), the Saale (117 $m^3 s^{-1}$), the Schwarze Elster (21 $m^3 s^{-1}$) and the Havel (114 $m^3 s^{-1}$). The Elbe River basin is situated in a transition zone between temperate (lower Elbe) and continental climate (middle and upper Elbe). Especially in the upper Elbe, the climate is strongly modified by the relief (IKSE, 2005). Mean annual precipitation in the river basin is 715 mm (1961-1990). However, there is a large variation within the basin. In the mountainous areas mean annual precipitation is above 1000 mm, whereas in the middle Elbe mean annual precipitation is around 450 mm. In the wintertime, precipitation falls as snow in the mountainous areas. Depending on snow depth and elevation, snow melts predominantly in March although it can persist until May, resulting in a snowmelt-influenced discharge regime. Mean annual evapotranspiration in the Elbe River basin is 455 mm (IKSE, 2005). In the highlands, thin cambisols are the main soil type, whereas in the lowlands, sandy soils and glacial sediments dominate. In the valleys, loamy soils are found. The western Elbe is covered by loess (chernozems and luvisols) (Hattermann et al., 2005). Land use is dominated by cropland (50.8 %), forest (evergreen 21.8 %, mixed 5.3 %, deciduous 3.1 %) and grassland (10.2 %). Settlements account for 6.5 % of the total basin area (CORINE European Environment Agency, 2000). Dams have been built in the Elbe headwaters and dikes have been installed along the river for flood protection purpose. The Havel region is strongly influenced by past mining activities. Previously observed flooding was predominantly generated by snowmelt in combination with rainfall in winter and spring in the upper Elbe. In summer, large-scale flooding due to long-lasting rainfall as well as small-scale flooding due to convective events were observed (IKSE, 2005).

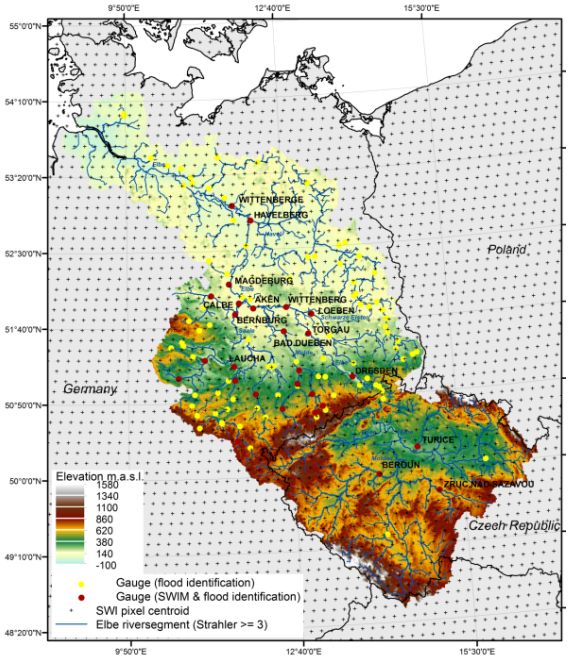

Fig. 2.1: Topographic map of the Elbe River basin. Yellow dots: Discharge gauges applied in flood identification. Red dots: Discharge gauges applied in flood identification as well as hydrologic model calibration and validation. Crosses: Location of pixel centroids of the scatterometer data.

2.2.2 Data

The data used in this study include climatic data as well as soil and land use information for driving a hydrologic model. Discharge observations are utilized for hydrologic model calibration and validation as well as flood event identification. Scatterometer soil moisture estimates are used to validate the simulated soil moisture. The analysis time period is 1 November 1951 to 31 October 2003.

2.2.2.1 Climatic and hydrologic data

Daily meteorological data (maximum, minimum and mean air temperature, precipitation amounts, relative humidity, sunshine and total cloud cover durations) were provided by the German Weather Service (DWD) and the Czech Hydrometeorological Institute (CHMI). In the Czech part of the basin, the climate station network is less dense. The station data were corrected for inconsistencies, data gaps and inhomogeneities (Österle et al., 2006, 2012).

The soil map was generated by merging the German soil map 'BUEK 1000' provided by the Federal Institute for Geosciences and Natural Resources (BGR) and the FAO-UNESCO soil map for the Czech part.

The resolution and quality of the soil maps are different, which may influence the results of the rainfall-runoff model.

The land use information is taken from the CORINE 2000 land cover data set of the European Environment Agency and is considered as static during the analysis period.

Discharge data were provided by various German water authorities and the Global Runoff Data Centre (GRDC, 2010). 114 gauging stations (Fig. 2.1, dots), including a large number of nested catchments, were used for flood identification. While the selected gauges are densely and approximately equally distributed in the German part, six gauges were available in the Czech part. Catchment size varies between 104 km² and 131950 km². Half of the gauges covered at least 94 % of the analysis time period. Hydrological years with more than 60 days of missing data were excluded from the flood identification resulting in between 57 (1951) and 114 (1981) gauges in the analysis. 27 discharge gauges (Fig. 2.1, red dots) were used for the calibration and validation of the rainfall-runoff model.

2.2.2.2 Scatterometer data

The remotely sensed soil water index (SWI) (Wagner et al., 1999) was provided by the Vienna University of Technology, Institute of Photogrammetry and Remote Sensing (http://www.ipf.tuwien.ac.at/radar/ ers-scat/home.htm). Surface soil moisture is derived from the radar backscattering coefficient of the scatterometers onboard of the satellites ERS-1 (1991-2000) and ERS-2 (1995-2011). First, the backscattering coefficients are standardized to a reference incidence angle (40°) by applying a change detection method. Afterwards, they are rescaled between their minimum and maximum value to represent the driest and wettest soil moisture conditions of the topmost soil layer. The soil moisture content in the first meter of the soil (SWI) is derived by applying an exponential two-layer water model to the surface soil moisture estimates (Wagner et al., 1999). The temporal resolution of the SWI is 10 days. As soil moisture retrieval is not possible under snow and frozen soil conditions, the SWI sample times are restricted from April/May to November. 228 sample times overlap with the hydrological simulation. The distance between the pixel centroids is approximately 12.5 km (Fig. 2.1, crosses).

2.3 Methodology

Profile (layer-depth weighted average) soil moisture content is simulated with a rainfall-runoff model. For the comparability of the profile soil moisture content of different soil types, the values are standardized by the field capacity of each soil type. In the following, the standardized profile soil moisture content is termed soil moisture index (SMI). PCA is used to map daily spatial SMI onto specific spatial patterns that express large parts of the spatial variability of the soil moisture series. Cluster analysis groups days of similar soil moisture patterns. In parallel, flood start days are derived from observed discharge time series and flood prone soil moisture patterns are identified.

2.3.1 Flood event identification

For the investigation of the link between large-scale soil moisture patterns and flood initiation, a flood definition that takes into account the simultaneous or time shifted flooding at several gauges is required. Several flood identification methods taking the spatio-temporal coherence of flooding into account have recently been proposed by e.g. Rodda (2005), Merz and Blöschl (2003), Keef et al. (2009), Uhlemann et al. (2010) and Ghizzoni et al. (2012). We identified large-scale flood events in the Elbe River basin using an approach proposed by Uhlemann et al. (2010) as the method is non-restrictive to a certain return period and takes the simultaneous or time shifted occurrence of peak discharges at many sites into account. A flood event is identified if at least one gauge within the catchment exceeds its 10-yr flood (POT). In a subsequent step, one searches for further significant peak discharges in a time frame three days in advance and ten days after the date of the POT. All peak dates around the POT are pooled into one flood event. Two flood events are independent from each other if the last occurrence of a significant peak of the previous flood and the first significant peak of the following flood event are separated by at least four days. Otherwise they are considered as one flood event. In this way, each flood event is characterized by a flood start date (first gauge showing significant peak around POT) and a flood end date (last gauge showing significant peak around POT). Furthermore, each flood is characterized by a measure of the overall event severity. The severity measure combines the overall flood extent and the flood magnitude (for details see Uhlemann et al., 2010).

To explore the link between flood initiation and the occurrence of soil moisture patterns, the soil moisture patterns at the start dates of the respective flood events are examined.

2.3.2 Hydrological modeling

2.3.2.1 Model description

The continuous daily eco-hydrological model SWIM (Krysanova et al., 1998) is a conceptual, semi-distributed model based on SWAT (Arnold et al., 1993) and MATSULA (Krysanova et al., 1989). The

model has three levels of spatial disaggregation: the basin (entire considered river basin), subbasins (subdivision of the basin) and hydrotops. Hydrotops are units of unique land use and soil type which are assumed to have a specific hydrological reaction. Climate input and the groundwater routine act on the subbasin scale. Daily values of relative humidity, global radiation, precipitation, mean, maximum and minimum air temperature are interpolated at the subbasin centroids. The snow routine and the soil water balance are calculated at the hydrotops and river routing at the basin scale. 1945 subbasins with a median catchment size of 33 km² (minimum 2 km², maximum 1034 km²) were implemented upstream of Wittenberge (Fig. 2.1).

The snow module is based on the degree-day method. Snow accumulation and melt depend on threshold air temperatures and a degree-day factor. Surface runoff is calculated with a modified version of the SCS–curve number method (Arnold et al., 1993; USDA Soil Conservation Service, 1972). In the soil routine, the soil root zone is subdivided into several soil layers in accordance with the soil profile of the specific soil type. To calculate percolation, a storage routing technique is applied on water inflow divided into slugs of 4 mm. Percolation in each layer depends on the soil water content which has to exceed field capacity and on the travel time through the layer governed by the saturated hydraulic conductivity. If the subjacent layer is saturated or if the soil temperature in a layer is below 0 °C no percolation occurs. Lateral subsurface flow is a function of the remaining drainable water volume and the return flow travel time which depends on the baseflow factor and on the saturated conductivity. If the considered soil layer is saturated, water is assumed to rise to the overlying layer.

Potential evapotranspiration is estimated with the Priestley-Taylor method (Priestley and Taylor, 1972). Based on potential evapotranspiration, plant transpiration and soil evaporation are calculated separately as a function of the leaf area index according to Ritchie (1972). The actual soil evaporation is estimated on the upper 0.3 m of the soil zone. As long as the soil evaporation accumulated since the last rainfall event is below 6 mm, actual soil evaporation equals potential soil evaporation. If the soil evaporation exceeds 6 mm, actual evaporation is assumed to decay exponentially. In the case of a snow cover, the soil evaporation is retained from the snow water content. For the estimation of the actual plant transpiration, the potential water use by plants based on the root development is calculated first. Secondly, potential water use is adapted to actual water use by the soil water content and field capacity.

The groundwater module consists of a shallow and a deep aquifer. The shallow aquifer is recharged by the percolation from the bottom soil layer with an exponential delay weighting function. The return flow is the groundwater contribution to the streamflow from the shallow aquifer. The amount of seepage from the shallow aquifer to the deep aquifer and the capillary rise from the shallow aquifer back to the soil profile are estimated as linear functions of recharge and actual evapotranspiration, respectively.

Routing is calculated with the Muskingum method (Maidment, 1993, chap. 10.2.3). Surface runoff and the sum of subsurface and groundwater are routed separately.

2.3.2.2 Model calibration and validation

The Elbe River basin is subdivided into 27 regions, assuming homogeneous parameterization within each region (Fig. 2.1, red dots). Nine sensitive parameters controlling snow accumulation and melt, potential evapotranspiration, saturated hydraulic conductivity, recharge as well as discharge routing (Table 2.1) are calibrated over the period 1981-1989 and validated over 1951-1980 as well as 1990-2003. Parameters were estimated for each region progressively from upstream to downstream by nesting the upstream regions for which parameters are already estimated in the next step. A weighted Nash-Sutcliffe efficiency coefficient (Hundecha and Bárdossy, 2004; Nash and Sutcliffe, 1970) was used as an objective function:

$$\mathrm{NS} = 1 - \frac{\sum w(t)(q_c(t)-q_o(t))^2}{\sum w(t)(q_o(t)-\bar{q}_o)^2}, \qquad (1)$$

where q_c and q_o are simulated and observed discharge, respectively. $\bar{q}_o$ is the average observed daily discharge in the calibration/validation period. $w(t)$ gives weight to certain parts of the hydrograph. To emphasize high flows $w(t)$ equals $q_o(t)$. The first 90 days of the simulation period are used as model initialization and excluded from the efficiency calculation.

As several parameter combinations can lead to the same model performance (Beven and Binley, 1992), a Monte Carlo uncertainty analysis is carried out to identify an ensemble of parameter sets that lead to behavioral model performances. A model performance is considered as behavioral, if an a-priori set threshold of goodness of fit is exceeded.

Table 2.1: Model parameters and their calibration range.

Model parameter	Description	Calibration range
tsnowfall	Snowfall temperature [°C]	-1.0 - 2.5
tmelt	Snowmelt temperature [°C]	0.0 - 3.0
snowmeltrate	Melting rate [mm d^{-1}]	1.0 - 4.0
thc	Correction factor for potential evapotranspiration on sky emissivity [-]	0.1 - 1.2
sccor	Correction factor for saturated conductivity [-]	0.1 - 20.0
abf0	α-factor for groundwater [-]	0.0 - 1.0
bff	Baseflow factor [-]	0.0 - 2.0
roc2/roc4	Routing coefficient surface/subsurface runoff [-]	0.1 - 15.0

The Monte Carlo simulation results in *i* data matrices **SMI** *(m* x *n)*, where *m* is the number of observations in time (i.e. 18993), *n* is the number of subbasins (i.e. 1945) and *i* refers to the number of behavioral parameter combinations (Monte Carlo parameter sets).

$$\mathbf{SMI}_i = \begin{matrix} \mathbf{SMI}_{1,1} & \cdots & \mathbf{SMI}_{1,n} \\ \vdots & \ddots & \vdots \\ \mathbf{SMI}_{m,1} & \cdots & \mathbf{SMI}_{m,n} \end{matrix} \quad (2)$$

In a next step, the simulated SMI is validated. The verification with soil moisture point measurements (e.g. gravimetric) is not feasible as these are highly variable over short distances, whereas satellite-based and hydrological-simulated soil moisture estimates are spatially integrated values (Parajka et al., 2006). For this reason, the temporal SMI progression is validated against the remotely sensed soil water index (SWI) by calculating the Pearson correlation coefficient between SMI and SWI. In accordance with the area share of overlaying SWI grid points, an area-weighted average SWI is assigned to each subbasin. For each subbasin between 122 and 197 SWI estimates are available for model validation.

2.3.3 Principal component analysis

The standardized soil moisture simulations of the behavioral Monte Carlo runs are arranged consecutively in time reshaping **SMI** into a matrix **SMI*** of size *((i* x *m)* x *n)*. PCA is applied to reduce the data dimensionality of **SMI***. First, the spatial linear Pearson correlation matrix **R***(n* x *n)* of **SMI*** is calculated giving equal weight to all subbasins and Monte Carlo parameter sets. As **R** is square and symmetric and therefore diagonalizable, one can identify the eigenvectors **u** (specific spatial patterns expressing large parts of the spatial SMI variability) and the eigenvalues diag(**λ**) of the matrix **R**:

$$\mathbf{R}\,\mathbf{u} = \boldsymbol{\lambda}\,\mathbf{u}, \quad (3)$$

by solving

$$(\mathbf{R} - \boldsymbol{\lambda}\mathbf{I})\mathbf{u} = 0, \quad (4)$$

where **I** is the *(n* x *n)* identity matrix. The eigenvectors **u** are sorted in decreasing order of their corresponding eigenvalues λ as the eigenvalue λ_k is a measure of the explained variance ev_k of the corresponding principal component PC_k:

$$ev_k = \frac{\lambda_k}{\sum_{k=1}^{n} \lambda_k}. \quad (5)$$

Hence, the leading first eigenvector points in the direction of the highest variance of **SMI*** and the next eigenvector explains the subsequent highest variance with the condition being orthogonal to the already identified eigenvector.

The PCs are obtained by projecting the standardized (zero mean, unit variance) data matrix of **SMI*** onto the eigenvector $\boldsymbol{u}_k$.

$$\mathbf{PC}_k = \mathbf{SMI}^*_{std}\boldsymbol{u}_k \quad (6)$$

As **SMI*** compromises all behavioral Monte Carlo runs, uncertainty bounds of each $\mathbf{PC}_k$ are obtained by decomposing $\mathbf{PC}_k$ of size *((i* x *m)* x *1)* into *i* time series of length *m*.

The PCs are tested for significance using the rule-N approach (Overland and Preisendorfer, 1982). The calculated normalized eigenvalues are compared against the normalized eigenvalues of a random Gaussian matrix. Those leading normalized eigenval-

ues that are higher than the 95th percentile of the simulated random eigenvalues (1000 Monte Carlo runs) are treated as significantly different from a random field. For further details on PCA see e.g. Hannachi et al. (2007), Joliffe (1986) or Preisendorfer (1988).

2.3.4 Cluster analysis

The hierarchical Ward cluster algorithm (Ward Jr., 1963) is implemented on the leading PCs to identify days of similar soil moisture patterns. At the beginning, every day D represents a single cluster. At each analysis step, the union of all possible cluster pairs is considered and the cluster pair t that offers the smallest increase in variance V is merged.

$$V_t = \sum_D \sum_k |PC_{tDk} - \overline{PC}_{t \cdot k}|^2, \quad (7)$$

where PC_{tDk} denotes the value of the k-th PC at day D belonging to cluster t. The algorithm merges the days consecutively until all days are united in a single cluster.

Including all behavioral Monte Carlo runs, the extent of a single PC is *((i x m) x 1)* i.e. ((38 x 18993) x 1). Due to limits in the computer capacity, it is not feasible to accomplish a cluster analysis directly on the leading PCs. Thus, we execute the cluster analysis in two steps. First, cluster analysis is carried out on the leading PCs of each behavioral Monte Carlo run separately. To merge the cluster results of the behavioral Monte Carlo runs, a second cluster analysis is applied on the cluster centroids (median of respective cluster members) of the behavioral Monte Carlo runs. It is assumed that the number of clusters in the first and second cluster step is the same.

Depending on the parameterization of a particular Monte Carlo run, a single day D may have different pattern characteristics and is thus assigned to different clusters t. Subsequently, each day D is assigned to the cluster with the highest probability of occurrence expressed as p_D:

$$p_D = max\left(\frac{|D \in t|}{i}\right). \quad (8)$$

In order to estimate the influence of model parameterization on the cluster t, the median p_D of all days belonging to a specific cluster t is calculated, which defines the probability of cluster membership p_t:

$$p_t = median(p_D \in t). \quad (9)$$

Thus, a small probability of cluster membership p_t indicates a strong influence of the model parameterization on the cluster assignment, while a large probability of cluster membership p_t indicates a weak influence.

To determine the number of leading PCs in the clustering as well as the number of clusters (Eq. 7), a sensitivity analysis is conducted varying the number of PCs and the number of clusters. Based on p_t (Eq. 9) the optimum PC-cluster combination is selected.

2.4 Results

2.4.1 Identified flood events

From the observed discharge time series, 94 flood events are identified, out of which 60 % are winter (November–April) events. Figure 2.2 displays the flood events separated by the month of the flood start date and the severity class s. In February, March, June and December more than ten flood events are initiated. September and October have by far the lowest number of flood initiation. In November, no flood events are initiated. High severities (s > 100) are found in the winter months December as well as March and in the summer months June to August. The severe events are not restricted to the months with the highest number of flood initiation. As the severity is a combined measure of flood magnitude and extent (affected river network), one has to take their respective influence into account. Winter events are characterized by a large spatial extent of minor magnitudes. In contrast, summer events are either characterized by a small spatial extent of very few extreme magnitudes or by a large spatial extent of miscellaneous magnitudes.

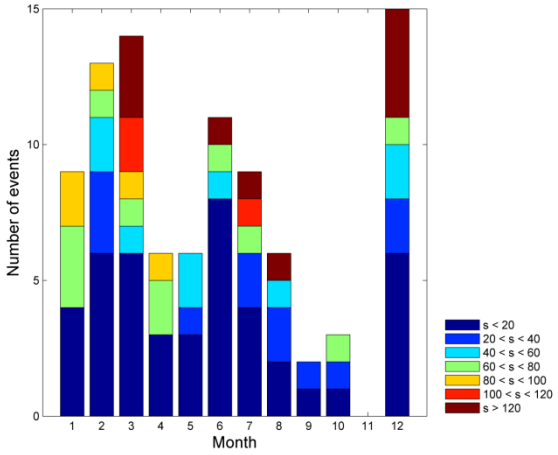

Fig. 2.2: Number of flood start dates per month and severity class s.

2.4.2 Hydrological modeling

The application of the Monte Carlo approach resulted in 38 behavioral parameter sets. In the calibration period, all gauges have a median weighted Nash-Sutcliffe efficiency between 0.55 and 0.8. The performance difference between the behavioral Monte Carlo parameter sets is negligible. Their median weighted Nash-Sutcliffe efficiency ranges between 0.71 and 0.74. In the validation period, the gauges median weighted Nash-Sutcliffe efficiency ranges between 0.53 and 0.81 (1951-1980) as well as 0.26 and 0.87 (1990-2003). Gauge Havelberg has by far the lowest efficiency which can be attributed to various lakes and strong anthropogenic modifications (mining) not represented in the model. Due to the chosen model performance measure, the calibration puts more emphasis on high flows compared to low flows. As a consequence, runoff volume is in the median overestimated by 33 % in the calibration period and by 28 % in the validation period 1951-1980 (40 % in 1990-2003).

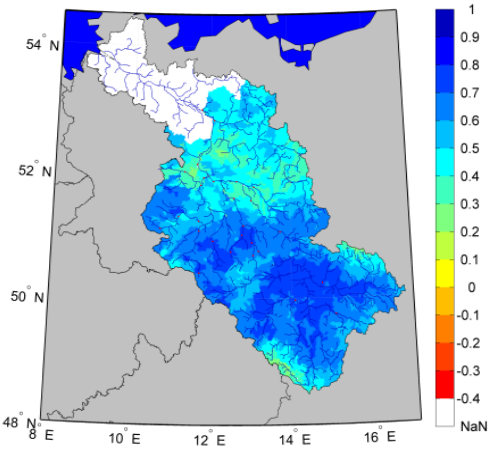

Fig. 2.3: Pearson correlation coefficient (significant level 5 %) between the median simulated SMI and the remotely sensed SWI.

For the validation of the SMI, the Pearson correlation coefficient (significant level 5 %) between the median simulated SMI and the remotely sensed SWI was calculated (Fig. 2.3). Except for a few local spots, basin-wide high correlations are observed. The median correlation is 0.57, the difference between the 25th and 75th quantile is 0.2. The individual examination of the Monte Carlo parameterizations leads to the same findings. Hence, the simulated temporal progression of the SMI is well represented in the hydrological model.

2.4.3 Soil moisture pattern classification

2.4.3.1 Principal component analysis

The leading 43 out of 1945 PCs are significantly different from a random field explaining 97.66 % of the total variance. The leading four PCs and their corresponding eigenvectors are displayed in Fig. 2.4. The eigenvectors indicate geographic regions of simultaneous anomalies in the SMI. The minimum and maximum values of the PCs correspond to the parameter uncertainty introduced by the rainfall-runoff model.

The first PC explains 75.71 % of the total variance and has a seasonal behavior. The influence of the parameter uncertainty on the PC is small. The corresponding loadings show a low spatial variability across the catchment (Fig. 2.4, top). The subsequent PCs have a damped and lagged seasonal behavior and their loadings are spatially heterogeneous. The second PC explains 8.60 % of the total variance, seasonality is still visible. Compared to the first PC, the influence of the parameter uncertainty on the PC increased, although the general behavior is the same. Its corresponding loadings show a north-south partition. The German part of the river basin has positive loadings excluding the upstream areas of the Saale and Mulde, whereas the Czech part of the river basin has negative loadings. The third PC, explaining 1.87 % of the total variability, has no apparent periodic behavior. High positive loadings are found in the Saale region and the mountainous area of the catchment. The fourth PC shows the highest influence of parameter uncertainty of the presented PCs. The explained variance is 1.49 %. The loadings are positive in large parts of Saale region, slightly positive in the central Czech part of the catchment and highly negative in the downstream Havel region.

2.4.3.2 Cluster analysis

Up to 15 of the leading PCs were chosen as variables in the cluster analysis to identify days of similar soil moisture patterns. This implies that between 75.71 % (first PC) and 94.10 % (all leading 15 PCs) of explained variance are involved in the clustering. Applying the variance criteria of Ward (Eq. 7), the weight assigned to a particular PC depends on its explained variance, as the individual PCs are not standardized, i.e. the first PC has the highest weight.

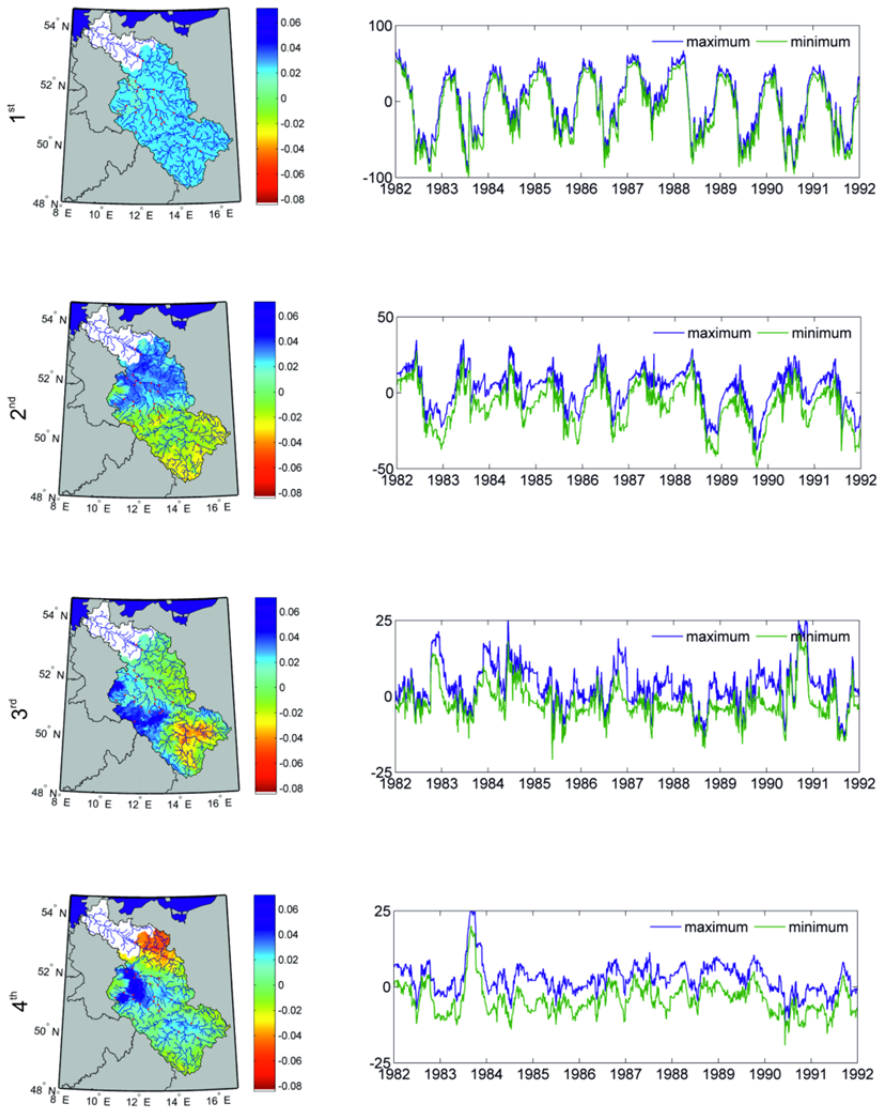

Fig. 2.4: Eigenvectors (left) and their corresponding PCs (right) of the leading four PCs. PCs are displayed for the sub-period 1982-1991. Minimum and maximum values correspond to the parameter uncertainty introduced by the rainfall-runoff model.

The probability of cluster membership p_t (Eq. 9), which evaluates the influence of model parameterization, was used to select an optimum PC-cluster combination. Figure 2.5 (left) displays the median p_t of different PC-cluster combinations. A division in two clusters leads in the median to well distinguishable clusters independent of model parameterization (median p_t ~1). The median p_t decreases up to a division in approximately 12 clusters and remains stable for a higher number of clusters. In general, the median p_t is independent of the number of PCs in the cluster analysis. An exception is the clustering of three or less PCs. In this case, the included variability is insufficient to derive a high number of distinguishable clusters as indicated by a low median p_t. In the following, the number of PCs in the cluster analysis is fixed to four since the variability (86.67 % of explained variance) is sufficient to derive a high number of distinguishable clusters.

Henceforward, clustering the leading four PCs, Fig. 2.5 (right) displays the distribution of p_t for different cluster numbers. In almost all cases, clusters with a very high p_t and thus independent of model parameterization and clusters with low p_t (< 0.5) and

thus dependent on model parameterization can be found. In a subsequent step, the analysis is restricted to ten clusters, since the median p_t peaks for ten clusters (0.74) and decays for more clusters.

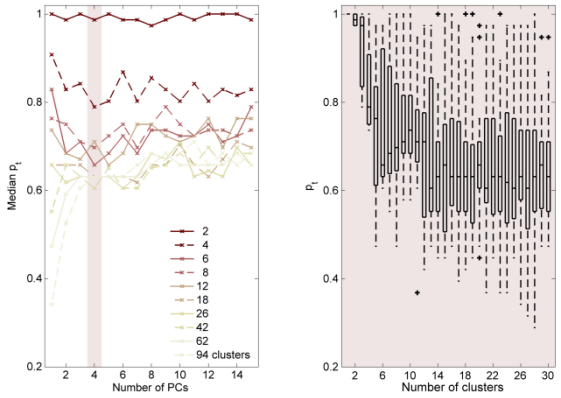

Fig. 2.5: Median probability of cluster membership p_t of different PC-cluster combinations (left). PC-cluster combinations with a small median p_t are strongly influenced by model parameterization. Distribution of p_t for different numbers of clusters when clustering the leading four PCs (right).

The SMI patterns of the cluster centroids, when separating the leading four PCs into ten clusters, are presented in Fig. 2.6. Cluster one, seven and eight show the driest soil moisture patterns. Between 87.8 % and 97.5 % of the catchment area has an SMI below 0.6. Clusters two and ten have intermediate SMI. Around 72 % of the catchment area has an SMI below 0.6. High SMI values are mainly restricted to the mountainous areas. Around 4 % of the catchment area has an SMI above 0.8. The remaining clusters change consecutively into highly saturated soil moisture patterns. Initially, a high SMI is restricted to the mountainous areas and intermediate values dominate in the mid- and lowlands (pattern six). The SMI rises in the upstream part of the basin (pattern five). The northern part of the basin gets wetter (pattern four) and the SMI in the upstream part of the basin increases additionally (pattern three). Here, 28.4 % of the catchment area has an SMI above 0.8. Finally, cluster nine shows high SMI over the entire basin. 43.8 % of the catchment area has an SMI above 0.8 and 90.1 % of the catchment area has an SMI above 0.6.

Table 2.2 displays the statistics of the ten clusters. Each day is represented 38 times, corresponding to the number of behavioral parameter sets. Cluster nine is the biggest cluster, containing 24.1 % of total days. Clusters two and seven are the smallest clusters, containing around 5 % of total days. The probability of cluster membership p_t ranges between 1.0 and 0.58.

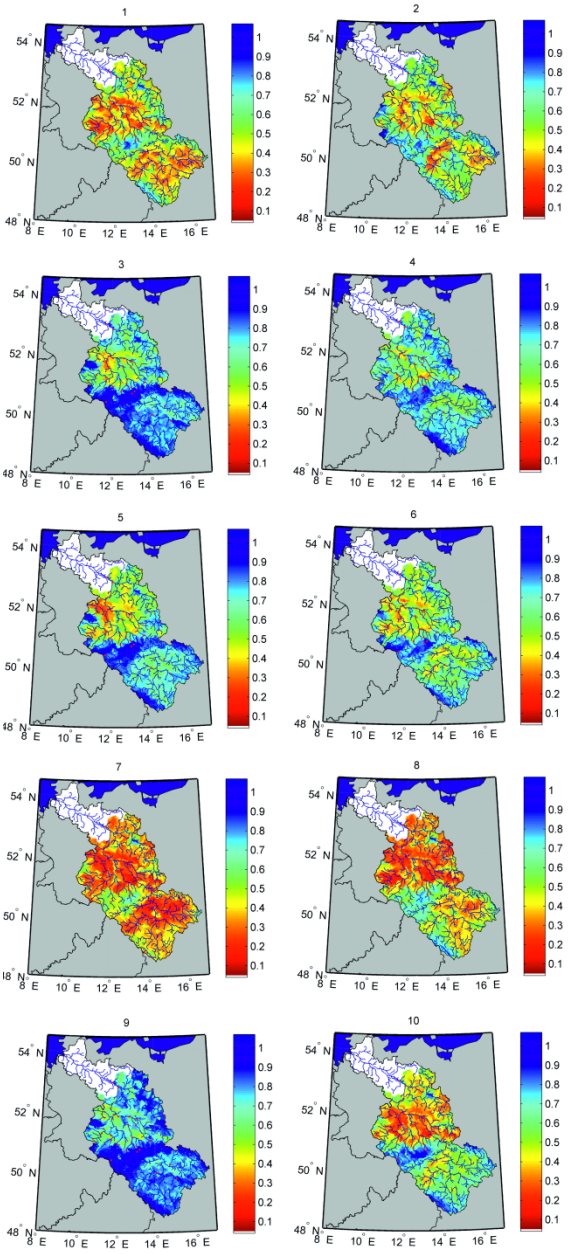

Fig. 2.6: Soil moisture index (SMI) patterns of cluster centroids.

Cluster nine has the highest p_t. Clusters two and six have the lowest p_t. Here, in the median 22 out of 38 parameter sets assign a respective day to the clusters. In order to indicate the day-to-day variability of the classification, the median persistence of each pattern type/cluster is calculated. Cluster nine has the highest persistence. In the median, the pattern persists for eleven days (average of 43 days). With a median duration of seven days, clusters three and seven have the

Table 2.2: Cluster statistics.

Cluster #	1	2	3	4	5	6	7	8	9	10	no clustering
Days [%]	7.3	5.3	13.6	9.3	7.9	10.4	5.2	8.0	24.1	8.9	100
p_t [-]	0.82	0.58	0.68	0.71	0.68	0.58	0.79	0.82	1.0	0.76	1.0
Median persistence [days]	5	4	7	5	5	4	7	5	11	5	1
Flood start days [%]	4.8 (172)	4.8 (172)	11.0 (393)	8.2 (292)	6.7 (241)	8.2 (293)	0.2 (7)	1.9 (69)	52.9 (1888)	1.3 (45)	100 (38 x 94)
Frequency of flood start days [%]	0.33	0.45	0.40	0.44	0.43	0.39	0.02	0.12	1.08	0.07	0.49
Median flood severity [-]	1.9	4.6	37.1	27.5	20.8	7.4	1.0	21.7	46.1	4.6	25.68

second highest persistence. The other pattern types have a median duration of either four or five days. The monthly frequencies of the different pattern types are presented in Fig. 2.7 (top). The frequencies express the relative occurrence of a particular pattern type in each month. Seasonal differences between the pattern types are visible. For instance, cluster three and nine are winter patterns. Cluster seven occurs in summer. Cluster four predominates in April, whereas cluster one predominates in June. In winter and in particular at the beginning of the year, clusters three and nine are the dominant patterns, whereas in summer/autumn the occurring clusters are more various.

2.4.3.3 Soil moisture patterns and their relationship to flood initiation

In the following, the soil moisture pattern types are characterized according to their relationship with flood initiation. Since the flood start days are considered for all parameter sets separately, 38 times 94 flood start days are included in the analysis. Cluster nine comprises the highest percentage (52.9 %) of flood start days (Table 2.2). Clusters eight and ten contain less than 2 % of flood start days each. Cluster seven contains nearly no flood start days. The frequency of the flood start days within each cluster expresses how often the respective pattern type can be related to flood initiation. Cluster nine has the highest frequency of flood start days. The frequency of flood initiation is 1.08 %.

The frequency of flood start days in cluster eight is one order of magnitude lower. In comparison with no clustering, flood start days are accumulated in cluster nine and the remaining clusters account for relatively few flood start days. The relative frequency of flood start days within a respective month and pattern type are presented in Fig. 2.7 (bottom). In summer, the highest relative frequencies of flood start days can be found and a multiplicity of pattern types are related to flood initiation. In winter, cluster three and in particular cluster nine, both characterized by high soil moisture across the entire basin, are related to flooding. Here, the relative frequency of flood start days is approximately constant from January until April/May. Although the two clusters have approximately the same seasonal distribution (Fig. 2.7, top), cluster nine is primarily relevant for flood initiation in winter, whereas cluster three is of primary importance in summertime flood initiation. In June, cluster three has the highest relative frequency of flood start days of all clusters. This seasonality shift between pattern frequency in general (Fig. 2.7, top) and pattern flood initiation (Fig. 2.7, bottom) also occurs in the case of clusters four and two.

Beside the pattern type frequency and relationship to flood initiation, the pattern type persistence three days in advance and after the flood start date was investigated (not shown). On the one hand, the patterns after the flood start date are more persistent than in the days ahead of the flood start date. On the other hand, there is a clear difference in the pattern persistence between summer and winter events. In wintertime, the soil moisture pattern types are persistent both in advance and after the flood start date. Occasionally, the patterns shift from cluster three into cluster nine and vice versa in the days ahead of the flood start date. In summer, either pattern type three is persistent in advance of the flood start date or a continuous wetting (transformation from pattern six, five or four) occurred. The summer patterns of low SMI are either

persistent or transform into wetter patterns after the flood start date.

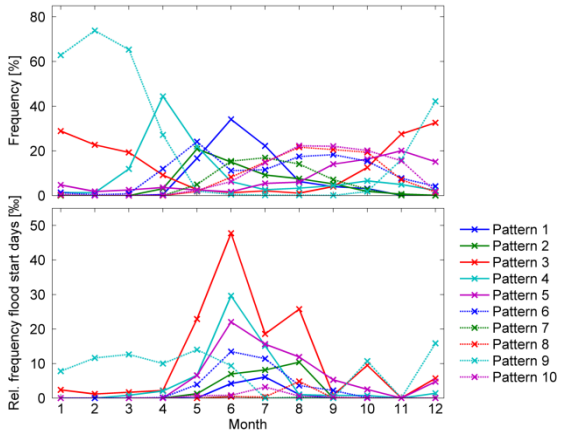

Fig. 2.7: Frequency of occurrence per month of different soil moisture pattern types [%] (top). Relative frequency of flood start days per month and respective soil moisture pattern type [‰] (bottom).

Finally, the relationship between the soil moisture patterns types and flood severity is analyzed (Table 2.2). For high SMI (patterns three, four and nine) the median flood severity increases with the degree of saturation. For dry soil moisture conditions this is not the case. Cluster eight has a median flood severity of 21.7, whereas the wetter pattern six has a median flood severity of 7.4.

2.5 Discussion

2.5.1 Soil moisture pattern classification

Large-scale soil moisture dynamics were simulated with a hydrologic model. As the model was calibrated on discharge, an integrated measure of catchment processes, the spatially distributed processes within the gauged catchment may not be well represented and small-scale patterns may be a calibration artifact. In the present study, especially the temporal SMI progression was of relevance since the PCA was based on the spatial correlation matrix (Eq. 3). The validation of the simulated SMI with the remotely sensed SWI proved the basin-wide reliability of the temporal SMI progression. As there is no obvious difference in the correlations between the Czech and the German part of the basin, an impact of the different soil maps and climate station densities on the temporal progression of simulated soil moisture can be excluded. Applying a different hydrologic model in Austria, Parajka et al. (2006) obtained considerably lower correlation coefficients of root zone soil moisture (median of 0.07 (1991-1995) and 0.12 (1996-2000)). As soil and land use properties are included in the model, there is a physical meaning behind the soil moisture patterns. For this reason, we did not interpolate the SMI on a regular grid as done by other studies (e.g. Kim and Barros, 2002; Perry and Niemann, 2007). Rather, we conducted the PCA at the subbasin scale with the drainage divides as natural boundaries.

The large amount of total variability explained by the first PC indicates that there is one dominant mode controlling the temporal soil moisture variability. This temporal mode has a seasonal behavior with maximum values in winter and spring and minimum values in summer (Fig. 2.4, top right). These seasonal soil moisture changes are mainly attributable to seasonal changes in evapotranspiration, leading to soil moisture depletion in summer and rise in winter and spring (Parajka et al., 2010). Additionally, snowmelt may have an impact. All subbasins respond in the same direction in terms of seasonality, indicating considerable similarity in the processes controlling soil moisture variability (Fig. 2.4, top left). Heterogeneous hydrological processes and catchment properties are overruled by seasonality. Perry and Niemann (2007) reported similar findings for the leading PC. Limiting the analysis to a smaller area receiving evenly distributed precipitation would possibly identify PCs attributable to single precipitation events. As the loadings are not only positive across the catchment but also approximately of the same magnitude, the first PC is a measure of the catchment average SMI. In contrast, the subsequent PCs are a measure of the disparity, describing local variations departing from the regional value. Their damped and lagged temporal progression might be attributable to the antecedent soil moisture conditions, i.e. the previous spatial distribution of precipitation.

The PCA showed that the retrieved soil moisture patterns have a stronger signal than the parameter uncertainty introduced by the rainfall-runoff model (Fig. 2.4, right). The first PC has the smallest relative difference between the members of the parameter ensemble and is least influenced by model parameterization. The relative differences between the ensemble members are higher for the subsequent PCs revealing a greater impact of model parameterization on spatially heterogeneous hydrological processes, as e.g. infiltration and soil storage, than on the seasonal progression of soil moisture.

The cluster analysis identified days of similar soil moisture patterns. Each soil moisture pattern type can be attributed to a pattern frequency, a pattern persistence and seasonal characteristics (Table 2.2, Fig. 2.7)

in the same manner as in weather type classifications (e.g. Philipp et al., 2010). The probability of cluster membership p_t yielded an objective choice of the number of PCs as well as clusters with respect to the parameter uncertainty of the rainfall-runoff model. Pattern nine characterized by high soil moisture content over the entire catchment is least dependent on model parameterization (highest p_t) and most persistent. Independent of model parameterization, any additional rainfall will be transformed into runoff without leading to alteration of the pattern type. Dry SMI patterns have a high p_t too. Likewise, the absence of rainfall doesn't lead to an alteration of the pattern type. Intermediate SMI patterns show the lowest p_t and are comparatively less persistent, as these patterns are a transitional stage to either wetter or dryer soil moisture conditions.

2.5.2 Soil moisture patterns and their relationship to flood initiation

In flood frequency analysis and design value estimation, flood events are defined for one particular gauge. An extreme value distribution is fitted to annual maxima series or a peak-over-threshold series of observed discharge. In the present study, the flood identification differed from this commonly applied approach. Instead, a flood identification method that takes into account the large-scale response has been adopted (Uhlemann et al., 2010). This is a more suitable approach in terms of the linkage between floods and large-scale soil moisture pattern types. Among the 94 detected flood events, the most severe events are well documented in terms of hydro-meteorological conditions, e.g. the flood events of August 2002 (Engel, 2004; Ulbrich et al., 2003a, b), July 1954 (Boer et al., 1959; Hauptamt für Hydrologie, 1954), or December 1974/January 1975 (Schirpke et al., 1978). Nevertheless, the flood event set may be incomplete due to ungauged small catchments receiving convective rainfall, as well as due to the requirement of an observed 10-yr flood. Furthermore, the flood event set may be biased towards flooding in the German part of the Elbe catchment, as only six gauges were available in the Czech Republic.

Previously, Uhlemann et al. (2010) highlighted the occurrence of summer flooding in the Elbe Basin. However, when analyzing trans-basin German floods, they found that the severe events were limited to the winter period. Our study, which is limited to flood identification in the Elbe, results in events of high severity ($s > 100$) both in winter and summer. Analyzing annual maximum flood series in Austria, Merz and Blöschl (2009b) didn't detect a dependence between the flood moments and seasonality. Instead, mean annual flood flows were positively correlated with average antecedent rainfall as a surrogate for the catchment soil moisture state (Merz and Blöschl, 2009b). Comparing the soil moisture pattern types and their respective median flood severity (Table 2.2), the results are heterogeneous and reflect different flood-generating processes. On the one hand, the median flood severity increased for patterns of high SMI. In this case, the catchment storage capacity is exceeded, e.g. due to long-term low-intensity rainfall, and any additional rainfall results in a runoff increase. In addition, if most parts of the catchment are saturated, a larger number of gauges may be flood affected in case of synoptic rainfall, as shown on the pan-European scale by Prudhomme and Genevier (2011). In their regional flood typology, Merz and Blöschl (2003) termed this type long-rain flood. On the other hand, the relatively dry soil moisture pattern eight shows high median severity too. This is attributable to high-intensity rainfall on relatively dry catchment conditions, which may lead to flash floods (Merz and Blöschl, 2003). The flood-generating processes are revealed in the seasonality of the soil moisture pattern types. In winter, flooding is related to high soil moisture content in the entire basin (cluster nine). The respective soil moisture pattern is persistent before and after the flood start date, indicating flooding either due to long-term low-intensity rainfall (long-rain flood) or saturated soils due to snowmelt (snowmelt flood). In summer, the flood-initiating soil moisture patterns are more variable and less persistent. On the one hand, large-scale flooding is observed. Long-lasting rainfall leads to high soil moisture content over large parts of the basin (cluster three). On the other hand, convective events (flash floods) characterized by relatively dry catchment conditions (cluster eight) occur (IKSE, 2005).

In addition to soil moisture, other patterns, in particular precipitation, are relevant for flood initiation (Brocca et al., 2008; Marchi et al., 2010; Merz and Blöschl, 2008b; Merz and Blöschl, 2009b; Parajka et al., 2010). This is indicated by the seasonal cluster distribution and the deviating seasonality of the flood start days inside the cluster (Fig. 2.7, e.g. cluster three). Furthermore, extending the pattern classification approach to e.g. precipitation patterns, the role of saturated soils limited to parts of the catchment when receiving rainfall may be pronounced.

2.6 Conclusions

Flood generation and magnitude are the result of a complex interaction between the meteorological situation and pre-event hydrological catchment conditions. The impact of catchment conditions on floods and

flood severity is expected to depend on various factors, such as season as well as flood type (e.g. snowmelt flood, long-rain flood, flash flood) and is especially difficult to decipher in large river catchments with catchment-internal variation in flood generation. To date, no studies are available that attempt to understand the space-time behavior of large-scale hydrological catchment conditions and link them to flood initiation. As a step in this direction, we propose classifying the hydrological catchment conditions and link flood occurrence to large-scale catchment state patterns. This approach is complementary to the widespread classification of circulation patterns in meteorology. As soil moisture is a key variable of hydrological catchment conditions, model-simulated soil moisture was used to answer two questions: what is the dominant space-time behavior of soil moisture at the regional catchment scale? Are there soil moisture patterns that are related to large-scale flood initiation? By applying PCA, the dimensionality of the soil moisture data was reduced to four PCs representing 86.67 % of the total soil moisture variability. The seasonally wetting and drying of the catchment represented by the first PC is the dominant mode, whereas the successive PCs describe spatially heterogeneous catchment processes. Cluster analysis assessed the similarity in daily soil moisture distribution within the catchment, and assigned each day of the investigation period to one of ten soil moisture pattern types. In parallel, 94 start days of large-scale flood events were identified and enabled a probabilistic linkage between flood occurrence and large-scale soil moisture patterns. The following conclusions can be drawn:

1. Different soil moisture patterns are not equally associated with flood occurrence.
2. Patterns with catchment-wide high soil moisture accumulate the majority of flood start days.
3. Flood-initiating soil moisture patterns vary seasonally.
4. Seasonality of soil moisture pattern frequency and seasonality of soil moisture pattern flood initiation are not identical.
5. Occurrence of a certain soil moisture pattern does not necessarily lead to flood initiation, but the probability of occurrence of a large-scale flood may be increased.

While these results underline the importance of catchment state for flood initiation and severity, (4) and (5) indicate that, beside soil moisture, other patterns are relevant for flood initiation. Therefore, future work will extend the pattern classification approach not only to circulation patterns but also to snow. A combination of hydro-meteorological pattern types would enable to quantify the interaction of patterns of hydrological catchment conditions and meteorological conditions on flood initiation and magnitude.

Acknowledgements. The first author acknowledges financial support by the AXA Research Fund project "The AXA project on Large-Scale European Flooding under climate change". We would like to thank Steffi Uhlemann for her assistance in the flood identification as well as the Potsdam Institute for Climate Impact Research (PIK) for making available the climate input data, the source code of the SWIM model and helping in setting up the model.

Chapter 3:
On the relationship between hydro-meteorological patterns and flood types

On the relationship between hydro-meteorological patterns and flood types

Abstract

Flood generation is triggered by the interaction of the hydrological pre-conditions and the meteorological conditions at different space-time scales. This interaction results in floods of diverse characteristics, e.g. spatial flood extent and temporal flood progression. While previous studies have either linked flood occurrence to weather patterns neglecting the hydrological pre-conditions or categorised floods according to their generating mechanisms into flood types, this study combines both approaches. Exemplary for the Elbe River basin, the influence of pre-event soil moisture as an indicator of hydrological pre-conditions, on the link between weather patterns and flood occurrence is investigated. Flood favouring soil moisture and weather patterns as well as their combined influence on flood occurrence are examined. Flood types are identified and linked to soil moisture and weather patterns. The results show that the flood favouring hydro-meteorological patterns vary between seasons and can be linked to flood types. The highest flood potential for long-rain floods is associated with a weather pattern that is often identified in the presence of so called 'Vb' cyclones. Rain-on-snow and snowmelt floods are associated with westerly and north-westerly wind directions. In the analysis period, 18 % of weather patterns only caused flooding in case of preceding soil saturation. The presented concept is part of a paradigm shift from pure flood frequency analysis to a frequency analysis that bases itself on process understanding by describing flood occurrence and characteristics in dependence of hydro-meteorological patterns.

Published as:

Nied, M., Pardowitz, T., Nissen, K., Ulbrich, U., Hundecha, Y., and Merz, B.: On the relationship between hydro-meteorological patterns and flood types, J. Hydrol., 519, Part D, 3249-3262, doi: http://dx.doi.org/10.1016/j.jhydrol.2014.09.089, 2014.

3.1 Introduction

Floods are generated by the interaction of various physical processes. These include hydrological preconditions (e.g. soil saturation, snow cover), meteorological conditions (e.g. amount, intensity and spatial distribution of precipitation), runoff generation processes (e.g. infiltration and lateral runoff on hillslopes), as well as river routing (e.g. superposition of flood waves). The combination of these physical controls may be important, especially at the regional scale (≥ 10,000 km²), where flooding can affect many sites simultaneously, whereas other sites remain unaffected (Merz and Blöschl, 2008b).

Three main approaches exist to describe regional flood events in terms of their spatio-temporal physical causes. They can be categorized into (1) flood event description, (2) classification into flood types and (3) linkage of flood occurrence to atmospheric circulation patterns. Following (1), detailed descriptions on e.g. soil moisture conditions, snowmelt and spatio-temporal distribution of rainfall are provided by scientific case studies. Examples in Central Europe are studies on the Elbe flood in August 2002 (Ulbrich et al., 2003a, b), the Rhine flood in January 1995 (Chbab, 1995; Engel, 1997) or the Danube flood in June 2013 (Blöschl et al., 2013). Furthermore, numerous reports and documentations about specific floods are compiled by governmental authorities and non-governmental bodies and are published as grey literature (Uhlemann et al., 2013). These descriptions are either qualitative or quantitative and in general limited to the case of severe flooding. In approach (2), the findings about individual flood events of diverse magnitude and extent are generalized by classifying them into different categories. For instance, Merz and Blöschl (2003) separated floods in accordance with their generating processes into long-rain floods, short-rain floods, flash floods, rain-on-snow floods, and snowmelt floods. Alila and Mtiraoui (2002) classified flood events based on storm type, El Niño-Southern Oscillation conditions and decadal-scale climatic variability. Hirschboeck (1987) conducted a flood classification based on precipitation, synoptic weather patterns and snowmelt. In approach (3), a probabilistic link between flood occurrence and daily atmospheric circulation patterns is sought (e.g. Bárdossy and Filiz, 2005; Duckstein et al., 1993; Petrow et al., 2009; Prudhomme and Genevier, 2011). Circulation patterns characterize the main modes of variability of atmospheric state by classifying individual weather situations. However, due to the small sample size of flood events compared to the overall number of days, Prudhomme and Genevier (2011) raised the question "if any link [between flood occurrence and circulation patterns] found is not a consequence of specific samples of events but truly is representative of physical processes". To date, this question, if and to which extent large-scale circulation patterns and flood generating processes are related, has not been explicitly addressed.

In this paper, we therefore propose to combine the process-based flood type classification approach (2) with an analysis of the link between flood occurrence and atmospheric circulation patterns (3). As different flood types have different characteristics, e.g. spatial extent and temporal flood progression, it is important to understand the conditions under which they occur. For example, climate change might alter the relative importance of the flood generating mechanisms. This might require to adapt flood management strategies (Van Loon and Van Lanen, 2012).

Another question which has not been addressed to date is how the link between circulation patterns and flood occurrence is modified by other processes amplifying or hindering flood generation. For instance, the impact of soil saturation on flood generation is widely acknowledged (e.g. Marchi et al., 2010; Merz et al., 2006; Norbiato et al., 2009; Parajka et al., 2010; Sivapalan et al., 1990) and plays a central role in flood forecasting (e.g. Fundel and Zappa, 2011). Nevertheless, it is commonly disregarded when establishing the link between circulation patterns and flood occurrence. The limitations of looking only at circulation patterns to describe flood events is further illustrated in catchments where snow processes are important resulting in a weak link between precipitation and discharge events (Parajka et al., 2010; Petrow et al., 2007).

In this paper, we identify flood types at the regional scale of the Elbe catchment, based on an adaptation of the flood typology of Merz and Blöschl (2003) and analyse their relationship to circulation patterns. The combination enables to relate large-scale atmospheric conditions to earth's surface flood processes. The objective is, on the one hand, to examine whether a particular circulation pattern favours a particular flood type. On the other hand, we study the influence of the pre-event soil moisture conditions in modifying the link between circulation patterns and flood occurrence. Complementary to the classification of atmospheric circulation patterns, we utilize a soil moisture pattern classification. We develop the approach exemplarily for the Elbe catchment.

The remainder of this paper is organized as follows: First the study area is described. The data and methods section introduces the applied techniques to identify

flood events and to classify them into flood types. Distinct daily soil moisture and weather pattern types are introduced and the method linking them to flood occurrence is explained. The results, i.e. the stratification of the identified flood events into flood types and their related hydro-meteorological patterns, are presented and discussed in Sect. 3.4 and 3.5. Section 3.6 concludes our findings.

3.2 Study area

The study region is the 148,268 km² large Elbe/Labe River basin (Fig. 3.1). The Elbe originates in the Czech Republic and crosses north-eastern Germany before flowing into the North Sea. The climate ranges between continental in the upper and middle Elbe to temperate in the lower Elbe (IKSE, 2005). Average annual precipitation is strongly modified by the relief and varies from 450 mm in the middle Elbe to above 1000 mm in the mountainous areas. In winter, precipitation falls as snow. In dependence of elevation and snow depth, snow melts predominantly in March, although it can persist until May (IKSE, 2005). The main land use types are cropland (51 %), forest (30 %) and grassland (10 %) (CORINE European Environment Agency, 2000). In the northern lowlands, sandy soils, glacial sediments and, restricted to the valleys, loamy soils are found. In the southern highlands, thin cambisols are the main soil type. In the Saale and Mulde tributaries, chernozems and luvisols dominate (Hattermann et al., 2005). The Elbe River basin has been affected by severe flood events, e.g. December 1974/January 1975 (Schirpke et al., 1978), August 2002 (Engel, 2004; Ulbrich et al., 2003a, b) and June 2013 (Conradt et al., 2013; Merz et al., 2014b).

3.3 Data and methods

Regional flood events are derived from observed discharge time series and categorized into process-based flood types. Afterwards, flood events and the identified flood types are linked to distinct patterns of hydrological pre-conditions and meteorological conditions. The analysis period is September 1957 to August 2002.

3.3.1 Flood definition and identification

Investigating the combined influence of the hydrological pre-conditions and the meteorological conditions on flood occurrence and flood type in the Elbe catchment requires a basin wide view.

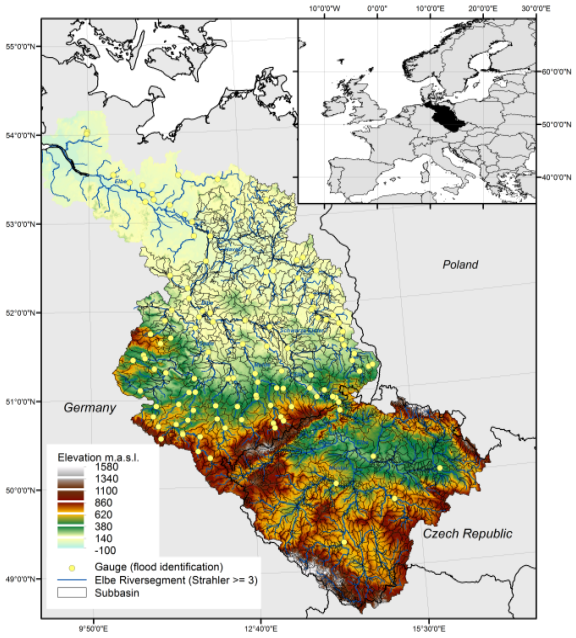

Fig. 3.1: Topographic map of the Elbe catchment. Yellow dots refer to the gauges applied in the flood event identification. Map of the regional setting of the Elbe catchment (upper right).

The flood definition has to take into account regional-scale flood generation i.e. simultaneous or time shifted flooding at several gauges. A flood identification scheme proposed by Uhlemann et al. (2010) is applied. The method consists of a systematic spatio-temporal peak flow search around each 10-year flood recorded in the river basin. Every flood event is characterized by time and location. The event start date is the date, up to 3 days in advance of a 10-year flood, at which at least one gauge in the river basin has a significant peak. At the event end date, up to 10 days after the last occurrence of a 10-year flood, the final significant peak is detected. Peak significance is ascertained by calculating the 90th percentile v of the residuals between daily observed discharge and its moving average $P(t)$ (13 days moving window). If a peak in the observed time series exceeds $P(t) + v$, it is considered significant. Two regional flood events are independent, if at least 4 days are between the event start date and the event end date of the previous flood. Daily overall discharge Q_{all} is defined as the discharge sum of all gauges in the basin standardized by their respective 2-year flood. The event centroid is the date after the occurrence of the largest increase in Q_{all} compared to the preceding day. The time period after the event start date including the event centroid date is called event build-up period. The length of the build-up period depends on flood type and spatial

extent and accounts for the catchment reaction time as well as flood routing. A schematic representation of a flood event's temporal progression and overall discharge Q_{all} is presented in Fig. 3.2.

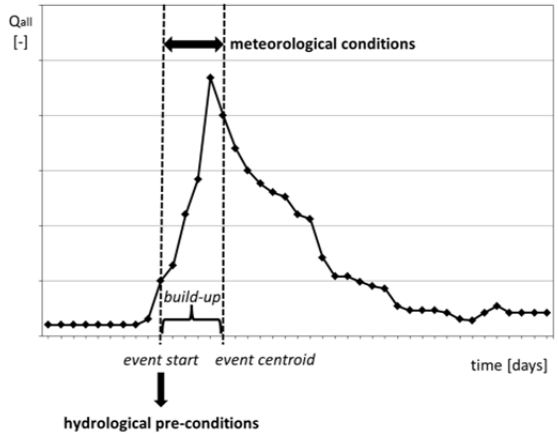

Fig. 3.2: Schematic flood event representation, denoting event start date, event centroid date, and build-up period.

Additionally, each flood event is characterized by a measure of the overall event severity S which combines spatial flood extent and flood magnitude (Uhlemann et al., 2010).

$$S = \sum_{i=1}\left(\lambda_i \frac{Q_i}{HQ2_i}\right) \mid Q_i \geq HQ2_i \ . \quad (1)$$

Q_i is the maximum daily discharge at gauge i for the considered flood event. Q_i is standardized by the 2-year flood $HQ2_i$. λ_i is a weighting factor. It describes the fraction of the regionalized river network corresponding to gauge i in relation to the overall regionalized river network i.e. $\sum\lambda_i$ equals unity. The regionalization scheme accounts for river length and river network topology and is based on the hierarchical ordering of river networks by Strahler (1964). In dependence of a gauges' Strahler-order, the total length of the upstream river stretches is estimated. In case of nested catchments, regionalization stretches from the downstream gauge to the upstream gauge. For details see Uhlemann et al. (2010). The severity estimation is restricted to gauges exceeding a 2-year flood. It is assumed that the 2-year flood corresponds to bankfull river flow below which no flood impact is expected.

The flood identification method is applied to daily average discharge time series of 114 gauges provided by various German water authorities and the Global Runoff Data Centre (GRDC, 2010). Catchment sizes vary from 104 km^2 to 131,950 km^2 and include a large number of nested catchments (Fig. 3.1, yellow dots). Half of the gauges have data that covered the entire analysis period. For each gauge, a hydrological year with more than 60 days of missing data was excluded. This resulted in between 68 (1957/1958) and 114 (1981) gauges in the analysis.

3.3.2 Classification

3.3.2.1 Soil moisture patterns

As a representative of hydrological pre-conditions, daily patterns of soil saturation are used. Nied et al. (2013) classified daily soil moisture patterns for the Elbe catchment. The soil moisture pattern classification was carried out by simulating soil moisture with a rainfall-runoff model at 1945 subbasins (Fig. 3.1) for 38 parameter realizations. Days of similar soil moisture patterns were identified using a principal component analysis and subsequent cluster analysis on the principal components. The classification into 10 soil moisture pattern types (Fig. 3.3) was identified as most suitable. The soil moisture pattern types range from soil saturation in the entire catchment (pattern 9), soil saturation restricted to parts of the catchments, i.e. upstream (pattern 3) or mountainous areas (pattern 10), to dry soil moisture conditions (pattern 7). The frequency and seasonality of the soil moisture pattern types are displayed in Fig. 3.6 a. The pattern types can be differentiated into summer (e.g. pattern 7), winter (e.g. pattern 9), and all-year patterns (e.g. pattern 5). Details on the classification approach are described in Nied et al. (2013).

3.3.2.2 Weather patterns

Daily patterns of meteorological conditions are classified using the objective classification algorithm SANDRA (Philipp et al., 2007). ERA 40 fields (Uppala et al., 2005) are evaluated on a 1.125° x 1.125° grid covering Europe (Fig. 3.1, small map). The parameters used are 500 hPa geopotential heights representing the steering circulation, temperature in 500 hPa indicating e.g. melting conditions, as well as the total column water vapour content indicating potential rainfall. In total, 40 weather pattern types are determined. The frequency and seasonality of the weather pattern types are displayed in Fig. 3.6 b. Figure 3.4 displays a selection of weather pattern types, which play a central role in this work. The complete set of weather pattern types is provided in 3.7 Appendix.

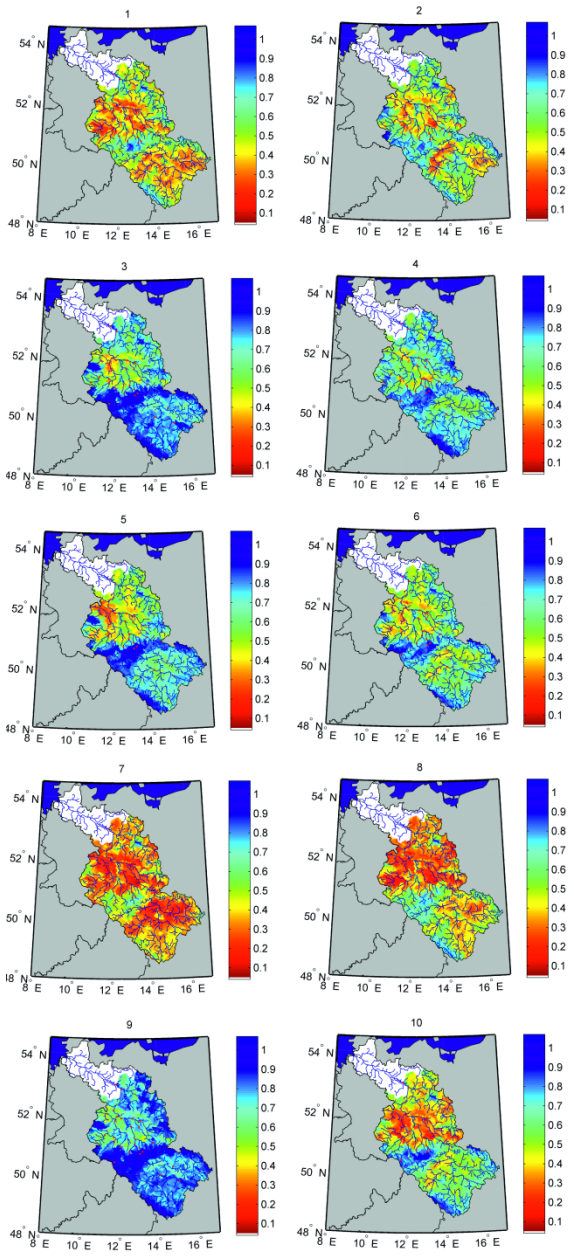

Fig. 3.3: Soil moisture pattern types as identified by Nied et al. (2013). Profile (layer-depth weighted average) soil moisture content is standardized by the field capacity of the respective soil type.

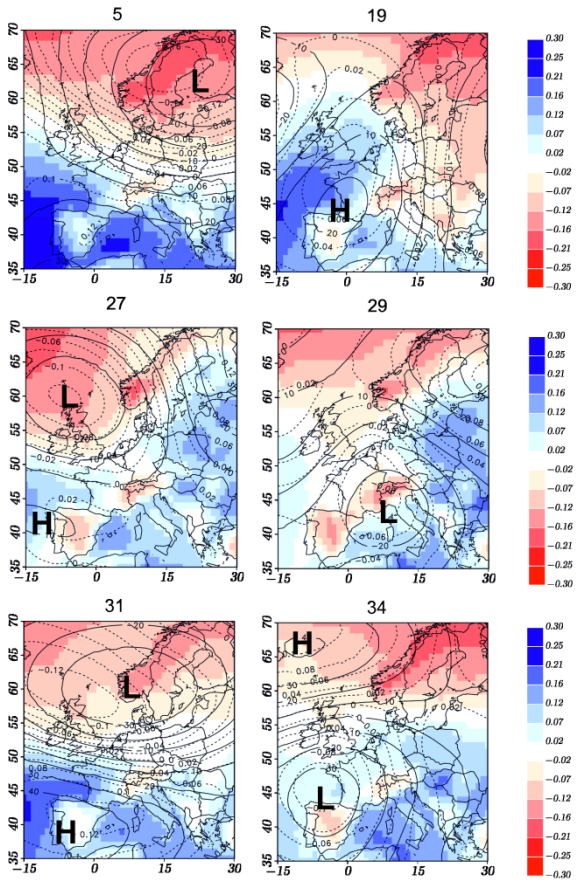

Fig. 3.4: Weather pattern types. Meteorological cluster centroids. Shaded contours show mean cluster anomalies in the vertically integrated moisture content [kg/m²], solid isolines show mean anomalies in the 500 hPa geopotential [m], and dashed isolines are mean anomalies in 500 hPa air temperature [°C].

3.3.2.3 Flood types

The flood types rain-on-snow flood, snowmelt flood, long-rain flood, short-rain flood, and flash flood by Merz and Blöschl (2003) are adapted to the scale of the Elbe River basin. The classification of the flood events into flood types is conducted manual and based on flood type indicators. Together, the flood type indicators describe specific characteristics and causative mechanisms of a flood event. For the classification of a flood event, the flood type indicators are displayed on diagnostic maps. Examples of diagnostic maps are e.g. Fig. 3.5 or Fig. 7 in Merz and Blöschl (2003). For clarity, only those flood type indicators of relevance for the particular flood event are displayed. The examination of flood type indicators is limited to those gauges and their corresponding catchments affected by at least a 2-year flood during the particular flood event (Fig. 3.5, red dots). Table 3.1 summarizes how the indicators are used to define a certain flood type. It is assumed that each flood event can be assigned to one flood type.

The following flood type indicators are applied:

- Spatial flood extent: the spatial flood extent addresses the number and spatial distribution of flood affected gauges. It can range from a single gauge to the entire river network. Floods of small spatial extent may be caused by convective storms, whereas large-scale flooding may be associated with frontal systems.
- Seasonality: as different flood types dominate in different seasons (Merz and Blöschl, 2003; Parajka et al., 2010; Petrow et al., 2007), the event start date is used as a flood type indicator.
- Snow cover: in wintertime, precipitation can fall as snow and is stored in the snowpack until melting starts. The amount and spatial distribution of snow water equivalent at the event start date and at the event centroid date are compared to shed light on snowmelt and/or accumulation.
- Air temperature: daily mean air temperature is examined in the event build-up period. It is assumed that on days with daily mean air temperature above 0 °C snowmelt occurs. Air temperature is used to separate precipitation into snowfall and rainfall. Below 0 °C precipitation is considered as snow. Above 2 °C, precipitation is considered as rainfall. In between, precipitation is considered as a mixture of rainfall and snow.
- Precipitation: the amount and spatial distribution of precipitation is examined for each day in the build-up period. For instance, short-rain floods are characterized by short duration, spatially limited, high rainfall amount, whereas long-rain floods are characterized by either basin wide stationary low rainfall or by spatially limited rainfall of high amount affecting several sites in the catchment progressively.
- Length of build-up period: the length of the build-up period is an indication of flood generation processes. For instance, the flood generating processes associated with flash floods are much faster than those associated with snowmelt. The reason in case of the latter is that the available energy (global radiation and turbulent heat exchange) controls the amount of melt (Merz and Blöschl, 2003) and causes snowmelt in different elevation zones and aspects progressively. Furthermore, the length of the build-up period is an indication of runoff processes in the river network. The length of the build-up period increases for large-scale flooding due to the downstream propagation of the flood wave.

For deriving the precipitation and air temperature indicators, daily meteorological data were provided by the German Weather Service (DWD) and the Czech Hydrometeorological Institute (CHMI). The station data were corrected for inconsistencies, data gaps and inhomogeneities (Österle et al., 2006, 2012). The Elbe catchment was subdivided into 1945 subbasins upstream of gauge Wittenberge (Fig. 3.1) and the meteorological data were interpolated on each subbasins centroid. As snow data were not available at the considered space-time scale, snow water equivalent was simulated for each subbasin with a semi-distributed rainfall-runoff model applying the degree-day method. The median simulated snow water equivalent out of 38 model realizations was used. For details see Nied et al. (2013).

3.3.3 Quantification of the flood-prone behavior of patterns

The flood identification (Sect. 3.3.1) accounts for discharge peaks of various return periods and the spatio-temporal flood development in the entire Elbe catchment. For each regional flood, a certain date which separates the hydrological pre-conditions from the event meteorology can be identified. The pre-conditions are defined as the catchment state i.e. soil moisture patterns, at the event start date, and the meteorological conditions i.e. weather patterns, are considered during the flood event build-up period (Fig. 3.2). This enables a clear separation between the influence of hydrological pre-conditions and meteorological conditions on flood occurrence as well as on flood type.

To quantify the flood-prone behaviour of patterns, the efficiency *eff* is calculated. *eff* is defined as the frequency of floods related to pattern *i* divided by the overall frequency of flood occurrence.

$$eff_i = \frac{n_{i|flood}}{N_i} \times \left(\frac{n_{flood}}{N}\right)^{-1} \quad (2)$$

where n_{flood} is the number of floods, N the number of days in the analysis period, $n_{i|flood}$ the number of floods related to pattern i and N_i the number of days related to pattern i. The efficiency is independent of the group size of the individual patterns and analogous to the performance index PI of Duckstein et al. (1993). In case $eff_i > 1$, pattern i favours the occurrence of floods and is entitled a flood-prone pattern. For instance, if $eff_i = 2$, the relative frequency of flood occurrence under pattern i is two times as high as one would expect under all groups together.

Table 3.1: Flood types.

	Flood type				
Flood type indicator	Rain-on-snow flood	Snowmelt flood	Long-rain flood	Short-rain flood	Flash flood
Spatial flood extent	Snow covered areas and optionally others	Snow covered areas and optionally their downstream regions	Regional to basin wide	Local to regional	Local
Seasonality	Winter/spring	Winter/spring	No seasonality	No seasonality	Summer
Snow cover	Yes	Yes	Possible	Possible	No
Air temperature	Above 0 °C in the snow covered areas	Above 0 °C in the snow covered areas	Above 0 °C, in the snow covered areas below 0 °C	Above 0 °C, in the snow covered areas below 0 °C	
Precipitation	Snow covered areas receiving rainfall, additionally snow free areas may receive rainfall	No	Either basin wide stationary low intensity rainfall or spatially limited high intensity rainfall affecting several sites in the catchment progressively within the build-up period (> 1 day)	Spatially limited high rainfall of short duration (~ 1 day)	Local
Length of build-up period	Medium	Long (> 4 days)	Long (> 4 days)	Medium	Short (~1 day)

Each weather pattern is weighted in accordance with the number of days it occurs in the build-up period. The weighting coefficient is the reciprocal of the length of build-up period. Thus, each flood event receives the same weight and the efficiency is independent of the length of the build-up period. To quantify the flood-prone behaviour of pattern combinations, *eff* is calculated for all combinations of soil moisture and weather patterns. The soil moisture pattern at the event start date is combined with each weather pattern in the respective build-up period. Again, it is ensured that each flood event receives the same weight independent of the length of the build-up period by weighting in accordance with the length of the build-up period. In the end, soil moisture as well as weather patterns favouring a certain flood type are identified by calculating *eff* for each pattern–flood type combination.

To test whether the determined *eff* value of a specific pattern (pattern combination) is significantly flood-prone, a bootstrap analysis is performed. The flood periods are randomly redistributed in time and *eff* is calculated for each pattern (pattern combination) as before (Eq. 2). The procedure is repeated 20,000 times resulting in 20,000 *eff* values for each pattern (pattern combination). From the distribution of the 20,000 random *eff* values, the 95th percentile is derived for each pattern (pattern combination). The *eff* value of a specific pattern (pattern combination) determined from the observed (undistributed) flood periods, is significantly flood-prone, if it exceeds the 95th percentile of the randomly obtained *eff* distribution. The bootstrap analysis is conducted for each flood type, too. Here, the flood periods associated with a particular flood type are redistributed in time.

3.4 Results

3.4.1 Flood events

Eighty-two flood events are identified in the analysed time period 1957-2002. 38 % of the events are summer (May – October) events. Ten times, the flood start date and the event centroid date are not consecutive i.e. they fall on the same day. This is especially the case for events of low severity *S* (*S* ranges between 1 and 7). In wintertime, extreme long build-up periods of more than 20 days are found. The median build-up period is 4 days.

Long-rain floods are the dominant flood type in the analysis period (Table 3.2). 22 % of flood events are classified as long-rain floods, followed by 20 % of flood events, where rain-on-snow is the dominant flood generating process. 18 % of events are short-rain floods, 17 % of events snowmelt floods. Flash floods are the smallest group containing 10 % of flood events. In accordance with the process-based flood types, rain-on-snow floods and snowmelt floods are restricted to wintertime, whereas flash floods are restricted to summertime. Short-rain and long-rain floods occur in summer as well as in wintertime, although the majority of long-rain floods are summer events. The length of the build-up period, a flood type indicator, is in the median highest for long-rain floods and snowmelt floods. The median flood severity *S*, a combined measure of event magnitude and spatial extent, is highest for rain-on-snow floods, followed by long-rain floods and snowmelt floods. As the gauging network is dense, the severity can be considered as a measure of event impact at the basin scale. In case of rain-on-snow floods, a high rainfall amount is possible beside snowmelt, resulting in a large spatial flood extent of miscellaneous magnitudes.

Table 3.2: Flood types and their characteristics.

Flood type	Events [%]	Winter events [%]	Summer events [%]	Build-up period [days] median	Flood severity *S* [-] median	Gauges ≥ HQ_2 [%] median	Gauges ≥ HQ_{10} [%] median	Regionalized river net ≥ HQ_2 [%] median
Rain-on-snow flood	20	20	0	5	77	52	7	61
Snowmelt flood	17	17	0	6	42	34	2	33
Long-rain flood	22	4	18	9	51	29	4	32
Short-rain flood	18	8	10	3	15	14	2	13
Flash flood	10	0	10	2	3	6	1	2
Unclassified	13	13	0	0	6	3	1	5
∑	100	62	38	-	-	-	-	-

The median percentage of the regionalized river network affected by rain-on-snow floods is 61 %. 52 % of gauges are affected by at least a 2-year flood and 7 % by at least a 10-year flood. Snowmelt floods have the second largest flood extent. In the median, 33 % of the regionalized river network is flood-affected. The observed flood peaks are of minor magnitude and variability. Considering the median values, 34 % of gauges are affected by at least a 2-year flood and only 2 % by at least a 10-year flood. Long-rain floods have in the median a similar flood extent as snowmelt flood (32 %), although the flood peaks are of higher magnitude. This is expressed in the higher severity and the higher percentage of gauges affected by at least a 10-year flood in case of long-rain flooding. Short-rain floods have a small spatial flood extent (13 %) of miscellaneous magnitudes. The median percentages of gauges affected by at least a 2-year flood and a 10-year flood are 14 % and 2 %, respectively. Flash floods, although they can be of high magnitude, affect only a limited part of the catchment (2 %) and have therefore a low median flood severity. 13 % of flood events are unclassified due to their not well defined flood generating processes. There is neither precipitation nor snowmelt in the build-up period.

Diagnostic maps of precipitation and snowmelt, exemplified for three flood events, are presented in Fig. 3.5. The red dots mark gauges affected by at least a 2-year flood and thus the spatial flood extent. The first flood event (Fig. 3.5, top), which lasted from 2 to 13 August 1983, is classified as a long-rain flood. In the first three days of the build-up period, a high amount of precipitation occurred, affecting progressively several sites in the Elbe catchment. For comparison, the second flood event (Fig. 3.5, middle), 1 – 11 June 1981, is classified as a short rain flood. High, spatially limited precipitation is restricted to a single day of the build-up period. The third example (Fig. 3.5, bottom) shows a snowmelt flood (15 – 31 January 1968). Within the build-up period, a high amount of snowmelt occurred due to positive air temperature (not shown) under the absence of precipitation.

Furthermore, Fig. 3.5 presents the discharge and discharge sum of the flood affected gauges normalized by their 2-year flood. The grey rectangle marks the build-up period of the respective flood event. Note that the definition of the build-up period (Sect. 3.3.1) incorporates all discharge gauges and is not limited to the flood affected gauges as shown here. In case of the long-rain flood (Fig. 3.5, top), the discharge peaks occur at three consecutive days. Few gauges show a discharge peak greater than a 2-year flood. In case of the short-rain flood (Fig. 3.5, middle), the flood-affected gauges have approximately the same magnitude and occur on two consecutive days. The snowmelt flood (Fig. 3.5, bottom) is characterized by almost constant discharge. Peak discharges are not necnecessarily restricted to the build-up period.

3.4.2 Hydro-meteorological patterns related to flood occurrence

First, the hydrological pre-conditions, i.e. soil moisture patterns, and the meteorological event conditions, i.e. weather patterns, are separately linked to the flood events. The frequency and seasonality of the flood start dates separated by soil moisture pattern type are displayed in Fig. 3.6 c. The frequency and seasonality of the flood build-up dates separated by weather pattern type are displayed in Fig. 3.6 d. Floods are unequally distributed among the patterns. For instance, 53 % of flood start dates are linked to soil moisture pattern 9, whereas weather pattern 12 was never linked to past flood occurrence. For some patterns, flood occurrence is restricted to the summer or winter season. Other patterns cause flooding year-round. For all patterns, the seasonality of the flood start dates (Fig. 3.6 c) deviates from pattern seasonality (Fig. 3.6 a). Same is true for the flood build-up dates (Fig. 3.6 b, d). For instance, weather pattern 15 is only related to flood occurrence in winter. However, the pattern occurs in summer too.

The efficiency of soil moisture as well as weather patterns is displayed at the margins of Fig. 3.7. In case of soil moisture only one pattern, pattern 9, the predominant soil moisture pattern in wintertime, exceeds an efficiency of 1 (efficiency 2.3, significant). 18 weather patterns exceed an efficiency of 1. Significant flood-prone patterns are 5 (efficiency 2.9), 15 (efficiency 2.3), 22 (efficiency 2.3), 26 (efficiency 2.6), 29 (efficiency 3.4), and 31 (efficiency 2.8). Altogether, they make up 34 % of flood event build-up days.

In the next step, soil moisture patterns and weather patterns are combined to examine their joint influence on flood generation. The matrix of Fig. 3.7 displays the efficiencies of all pattern combinations. In the analysis period, a limited number of hydro-meteorological pattern combinations have led to flood occurrence. A high efficiency is either observed if few flood events are associated with a rare pattern combination. For instance, soil moisture pattern 9 and weather pattern 29 coincided 34 times in the analysis period. 1.4 times (decimal number due to the applied weighting in the build-up period) the coincidence resulted in flood occurrence. Or if both, the absolute number of flood events and the relative frequency of the pattern combination are high. For instance, soil moisture pattern 9 coincided with weather patterns 5, 15 and 31, in total 462 times.

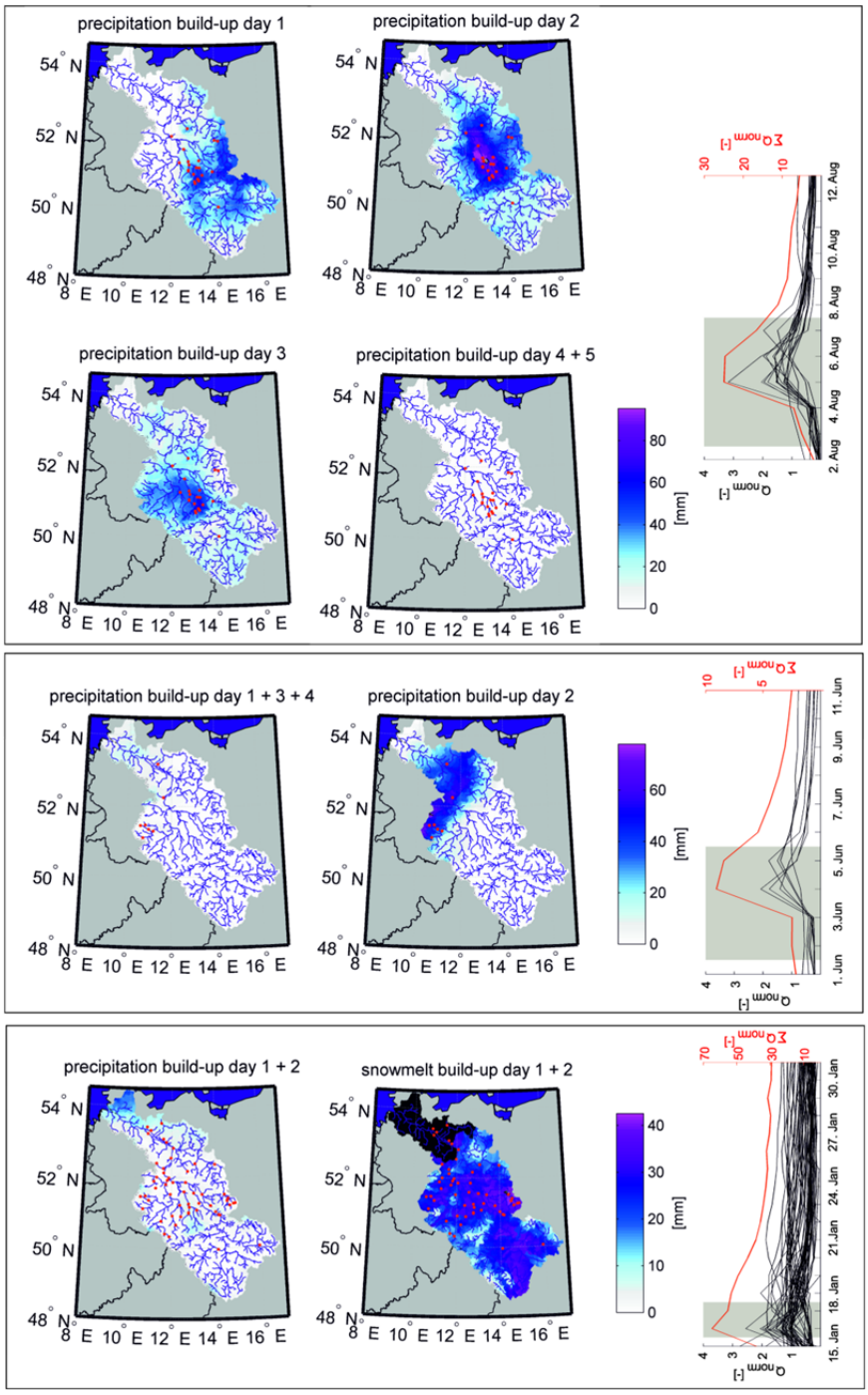

Fig. 3.5: Diagnostic maps, exemplified for three flood events. Red dots mark gauges affected by at least a 2-year flood. Top: Precipitation in the build-up period [mm]. Long-rain flood 2 – 13 August 1983. Length of the build-up period is 5 days. Severity 22. Middle: Precipitation in the build-up period [mm]. Short-rain flood 1 – 11 June 1981. Length of the build-up period is 4 days. Severity 9. Bottom: Precipitation and snowmelt in the build-up period [mm]. In the black coloured area simulated snowmelt values are not available. Snowmelt flood 15 – 31 January 1968. Length of the build-up period is 2 days. Severity 81. Discharge (black) and discharge sum (red) of flood affected gauges normalized by their 2-year flood. Grey rectangle marks the build-up period of the respective flood event.

The coincidence resulted 12.4 times in flood occurrence (15 % of flood events). Almost irrespective of the simultaneous weather pattern, soil moisture pattern 9 has a significant flood-prone efficiency. Same is true for weather pattern 29 which shows a significant flood-prone efficiency almost irrespective of the simultaneous soil moisture pattern. These findings emphasize the great flood potential of soil moisture pattern 9 and weather pattern 29. Their combination results in the highest observed efficiency (8.3, significant) which illustrates that a flood-prone soil moisture pattern together with a flood-prone weather pattern can increase the efficiency. Furthermore, a soil moisture pattern that does not favour flooding can reduce the efficiency of a flood-prone weather pattern, e.g. soil moisture pattern 1 and weather pattern 29, and vice versa, e.g. weather pattern 21 and soil moisture pattern 9. It is also observed that the combination of two flood-prone patterns can result in an efficiency decrease, e.g. soil moisture pattern 9 (significantly flood-prone) and weather pattern 34 (insignificantly flood-prone). Another interesting finding is that in certain cases, the flood favouring-conditions of a weather pattern are limited to one specific soil moisture pattern. For instance, in case of weather pattern 15, flood-prone combinations are limited to the combination with soil moisture pattern 9.

3.4.3 Hydro-meteorological patterns related to flood types

For the interpretation of the pattern-flood link (Fig. 3.7) in terms of flood generating processes, the flood types are stratified according to their soil moisture patterns (Fig. 3.8, top) as well as weather patterns (Fig. 3.8, middle, bottom). As neither the soil moisture patterns nor the weather patterns were included in the flood typology (Sect. 3.3.2.3, Sect. 3.4.1), the patterns can be regarded as independent from the flood typology. In both cases, patterns favouring a particular flood type ($eff > 1$) exist. In case of soil moisture, high efficiencies are related to soil moisture pattern 9. Highest efficiencies are found for rain-on-snow floods (efficiency 3.7, significant) and snowmelt floods (efficiency 4.0, significant). Short-rain floods have a higher efficiency (efficiency 1.7, insignificant) compared to long-rain floods (efficiency 0.8, insignificant). The efficiency of flash floods related to soil moisture pattern 9 is marginal. Flash floods show the highest efficiencies related to soil moisture patterns 1, 2, 5 and 6 (efficiency 1.9-3.8). In case of soil moisture pattern 2, the relationship is significant.

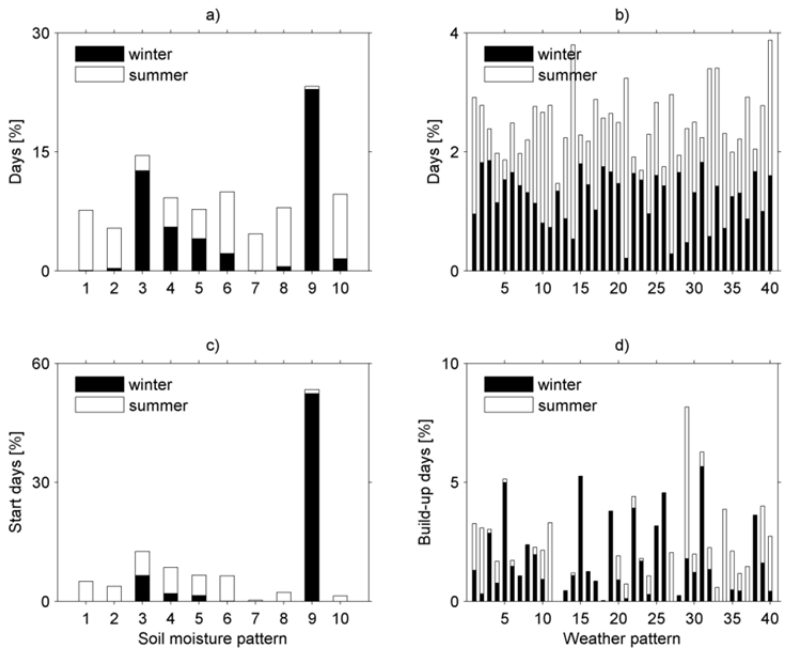

Fig. 3.6: a) Frequency and seasonality of the soil moisture pattern types in general. b) Frequency and seasonality of the weather pattern types in general. c) Frequency and seasonality of the soil moisture pattern types at the event start date. d) Frequency and seasonality of the weather pattern types during the event build-up period.

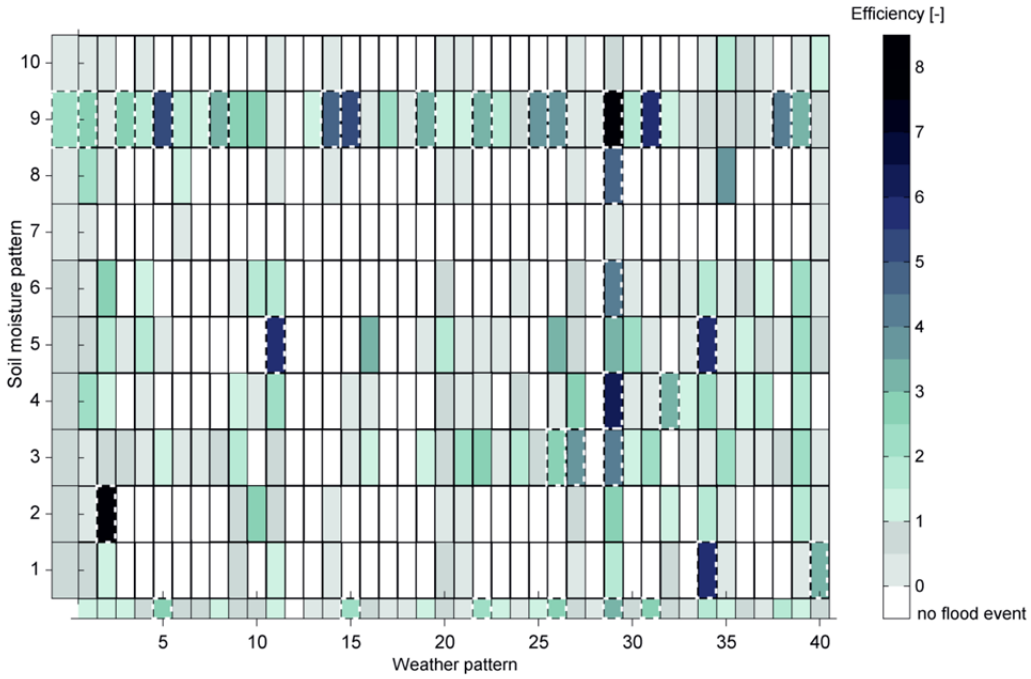

Fig. 3.7: Efficiencies of soil moisture and weather patterns respectively (margins) as well as efficiencies of soil moisture-weather pattern combinations (matrix). Soil moisture patterns are considered at the event start date. The weather patterns are considered in the event build-up period. Dashed framed panels show a significant flood-prone relationship.

Long-rain floods show high efficiencies with respect to soil moisture patterns 3, 4 and 5 (efficiency 1.5-2.0). The relationship is significant only in case of soil moisture pattern 4. Short-rain floods are linked to a variety of soil moisture patterns. Efficiencies greater than 1 are found in case of soil moisture patterns 1, 2, 4, 6 and 9. However, none of these are significant.

Compared to soil moisture patterns, several weather patterns show considerably higher efficiencies with respect to certain flood types. For instance, weather patterns 2, 11, 29 and 34 show high efficiencies (≥ 5) with respect to flash flooding. Patterns 15, 19 and 25 are predominantly linked to snowmelt floods, whereas patterns 5, 26 and 38 favour rain-on-snow events. Especially, pattern 29 is linked to long-rain flooding. Patterns 1, 9, 29, 31 and 34 are linked to short-rain flood occurrence.

For the flood events examined in detail (Fig. 3.5), the long-rain flood has a dry soil moisture pattern at the event start date (pattern 8) and 60 % of the build-up days are associated with weather pattern 29, often associated with long-rain flooding. The short-rain flood is generated on a dry soil moisture pattern (pattern 1), too. 75 % of the build-up days are linked to weather pattern 34, favouring this flood type. In case of the snowmelt flood, 50 % of the build-up days are associated with the weather pattern 19 and the remaining 50 % with the weather pattern 25, both favouring this flood type.

3.5 Discussion

3.5.1 Flood events

Adopting a catchment view, the flood identification integrates peak discharge at numerous gauges in space and time into one ‘observed’ flood event. Therefore, a flood event according to the definition provided in Sect. 3.3.1 incorporates a multiplicity of information compared to a peak discharge at a single gauge. For instance, the 82 flood events include 2370 gauges having at least a 2-year peak discharge.

The classification of the observed events into flood types shows that diverse flood generating mechanisms exist in the Elbe River catchment. The flood types along with their probability of occurrence vary seasonally. In dependence of the flood type, spatial flood extent, temporal flood progression, and flood magnitude change. Due to these different characteris-

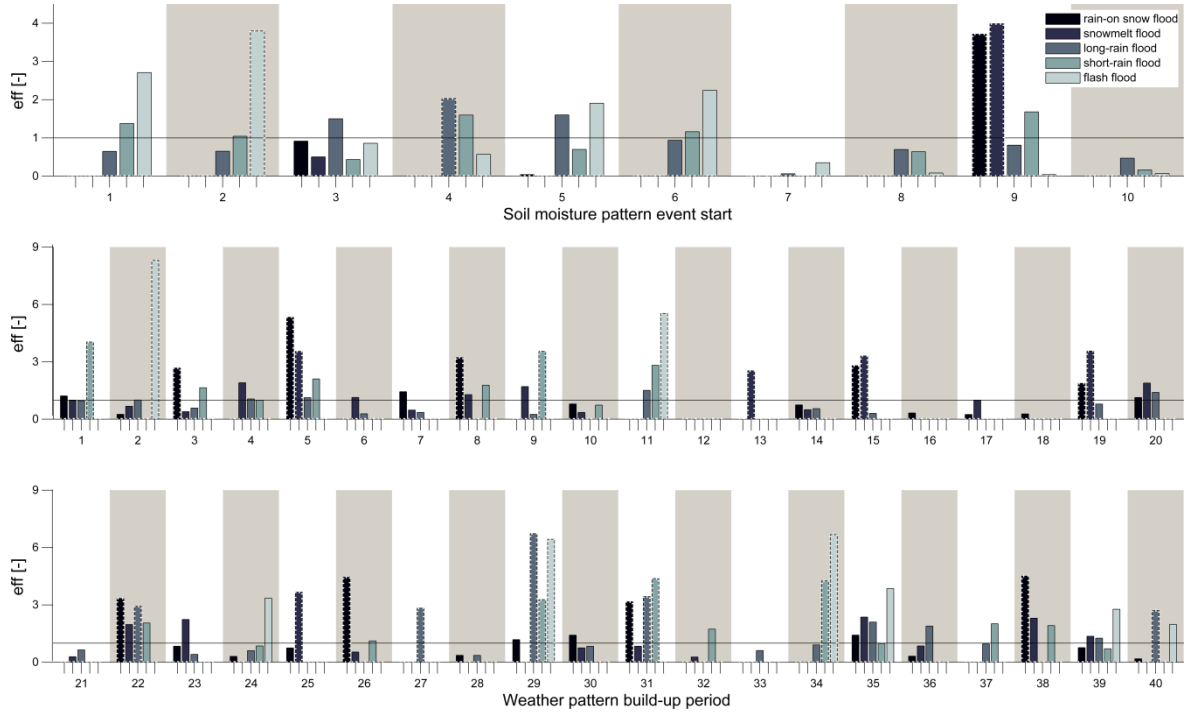

Fig. 3.8: Flood types and their associated soil moisture and weather patterns excluding unclassified flood events. Each bar represents the pattern efficiency stratified by flood type. Soil moisture patterns are considered at the event start date. The weather patterns are considered in the event build-up period. Dashed framed bars show a significant flood-prone relationship.

tics, the flood types require dissimilar flood risk management.

The classification incorporates independent information from different data sources (simulated snowmelt, observed precipitation and air temperature, as well as observed discharge), mutually affirming flood occurrence. As the relationship between these indicators is complex, a manual classification was applied. The manual classification with the help of diagnostic maps has an advantage over quantitative rules, since essential details and hydrological expert knowledge can be incorporated. For the majority of events, the assumption that one flood is the result of the same process, i.e. each flood is assigned to one flood type, is revealed by the diagnostic maps. However, similar to many natural phenomena, the boundaries between the process types are not sharp (Merz and Blöschl, 2003). For instance, snowmelt accompanied by rainfall in the high altitudes, whereas in the lowlands merely rainfall contributes to flood generation. A second example is local rainfall embedded in large scale synoptic systems as was the case in the Elbe flood in August 2002. In these cases, the prevailing process in the entire flood-affected catchment is identified with the help of the diagnostic maps and the flood event is assigned to the respective flood type. For instance, the flood in August 2002 is classified as a long-rain flood, although spatially limited high intensity rainfall (Tarolli et al., 2013) affected several sites in the catchment progressively within the build-up period.

The identified flood event set may be biased towards floods in the German part of the Elbe catchment, as only a limited number of gauges were available in the Czech part of the catchment. In particular, flood events restricted to Czech tributaries may be missing in the flood event set. However, flood events of similar characteristics may have been identified in the German tributaries.

The low percentage of detected flash floods may be attributable to their small extent and short duration behaviour. Hence, a large number of flash floods may not be represented in the precipitation and gauge data at hand. To identify a larger fraction of flash floods, discharge and precipitation data of higher spatio-temporal resolution may be necessary. Eleven flood events are unclassified due to ambiguous flood generating processes. Neither precipitation nor snowmelt is observed in the build-up period. The unclassified flood events are restricted to wintertime. They are of very short duration and low severity. In general, they are of limited spatial extent affecting several gauges

along one river reach. Therefore, discharge measurement errors are unlikely. It is hypothesized that these flood events are related to either dam drawdown or ice jams. High-intense rainfall of low spatio-temporal resolution or erroneous snowmelt simulation could also be an explanation.

3.5.2 Hydro-meteorological patterns related to flood occurrence

While the large-scale meteorological conditions have been frequently classified and linked to flood occurrence, the pre-event catchment conditions are commonly neglected. The combined linkage between hydro-meteorological patterns and flood occurrence (Sect. 3.4.2) revealed that floods are the result of a complex interaction between meteorological event characteristics and pre-event catchment conditions. The seasonal cluster distribution (Fig. 3.6 a, b) and the deviating seasonality of the flood start days (build-up dates; Fig. 3.6 c, d) inside the cluster exemplifies this complex interaction. In case of soil moisture pattern 9 and weather pattern 29, flood occurrence is widely independent of the coinciding weather/soil moisture pattern. Soil moisture pattern 9 (Fig. 3.3) is characterised by catchment wide soil saturation. A small amount of rainfall can result in flood generation. Besides soil moisture pattern 9, soil moisture pattern 3 is characterized by catchment wide soil saturation (excluding part of the western Elbe, Fig. 3.3). For 18 % of weather patterns, past flood occurrence is restricted to the coincidence with these two soil moisture patterns, i.e. they have only led to flood occurrence in case of preceding soil saturation. Soil moisture pattern 3 and 9 occur typically in winter (Fig. 3.6 a), and during associated floods snowmelt might additionally contribute to flood generation.

Weather pattern 29 (Fig. 3.4) is a low pressure system over South Europe transporting warm and moist air masses towards Central/Eastern Europe. So called ‘Vb’ cyclones which have been identified as flood-favouring in numerous studies (Jacobeit et al., 2006; Petrow et al., 2007; Ulbrich et al., 2003b) are mostly assigned to this weather pattern. This weather pattern is a summer pattern. However, in 20 % of cases it occurs in the winter season (Fig. 3.6 b). When the weather pattern 29 coincides with soil moisture pattern 9, a winter pattern, the efficiency is highest, as this rare pattern combination has a high relative frequency of flood occurrence. Thus, besides the frequency of occurrence, seasonality is of importance when combining hydro-meteorological patterns. This is further illustrated when estimating seasonal efficiencies. For instance, the all-season efficiency of soil moisture pattern 4 in combination with weather pattern 29 is 6.1 (Fig. 3.7). Restricting the efficiency estimation to the summer season, the efficiency rises to a value of 12.3, whereas the winter efficiency is 0.9.

Due to the diverse pattern seasonality, flood occurrence as well as pattern frequency of a particular soil moisture/weather pattern is non-uniformly distributed over its subgroups of pattern combinations (Fig. 3.7). As a consequence, the efficiency increases in some subgroups, whereas it decreases in others.

In the approach developed in this study, the weather patterns are considered in the event build-up period and weighted according to their relative occurrence. Thus, the linkage between weather patterns and flood occurrence is independent of the length of the build-up period as each flood event receives the same weight. The pattern persistence and succession within the build-up period are not addressed. Second, the linkage is independent of the spatial flood extent. Flood events of large spatial extent, affecting many sites in the catchment, receive the same weight as more local flood events. Thus, patterns favouring large-scale flooding are not overrepresented.

The applied linkage ensures a clear separation between hydrological pre-conditions and meteorological conditions. In addition, it takes into account the temporal flood development of the different flood events/types by an event specific build-up period (Fig. 3.2, Fig. 3.5). Similar to our approach, Duckstein et al. (1993) applied seasonal build-up periods according to seasonally varying flood generation. Other studies used a fixed time lag for all flood events. For instance, Parajka et al. (2010) estimated the relative frequency of atmospheric circulation patterns from the day and the two preceding days of the maximum annual floods, and Petrow et al. (2009) applied a time lag of one to three days in dependence of the catchment size.

The flood event set provides a range of hydro-meteorological pattern scenarios observed in the analysis period. Extending the analysis period and incorporating additional gauges, as well as a modification in the flood definition e.g. change of POT, might reveal additional flood-prone combinations and may strengthen or weaken the existing ones. Same is true for the bootstrap analysis which estimates the confidence of the calculated efficiencies under the assumption that the small (flood) sample at hand is representative of the analysed phenomena. In the present set of observed flood events, the number of some hydro-meteorological pattern combinations is rather small, although their impact on flood occurrence seems to be considerable. The sample size of flood-related hydro-meteorological pattern combinations could be extended by a modelling framework, e.g. the simulation of flood events by combining soil moisture patterns and weather patterns. This would not only

strengthen the results of our approach on the link between hydro-meteorological patterns and flood occurrence, but would enable to expand the presented pattern approach to flood severities (Eq. 1) combining the findings of Petrow et al. (2009) and Sivapalan et al. (2005). Petrow et al. (2009) identified a relationship between flood magnitude and the frequency of flood-prone circulation patterns neglecting the influence of the antecedent conditions. Sivapalan et al. (2005) demonstrated that the flood frequency curve increases dramatically if the seasonality of rainfall and antecedent soil moisture are in phase.

3.5.3 Hydro-meteorological patterns related to flood types

As the flood types have different characteristics (Sect. 3.4.1), e.g. spatial extent, magnitude and temporal progression, it is important to understand the conditions under which they occur. A dependency between flood types and soil moisture patterns as an indicator of hydrological pre-conditions is detected (Fig. 3.8). This relationship is attributable to their seasonal characteristics. Long-rain floods and flash floods predominantly occur in the summer season and are therefore linked to summer soil moisture patterns (e.g. pattern 5), whereas rain-on-snow floods and snowmelt floods are linked to pattern 9, the predominant winter soil moisture pattern. Short-rain floods are observed year-round. They appear together with summer as well as winter soil moisture patterns. In rare cases, a typical winter soil moisture pattern, e.g. pattern 3, occurs in summer (Fig. 3.6 a). Therefore, the pattern is observed in conjunction with summer flood types, too. However, the relationship is not flood-prone ($eff < 1$).

Compared to soil moisture patterns, several weather patterns show considerably higher efficiencies with respect to certain flood types (Fig. 3.8). Flash flood related patterns (pattern 2, 11, 29 and 34) are all associated with the transport of moist air from the Mediterranean towards the Elbe catchment. The large efficiencies with respect to flash floods are a consequence of the small flood type sample size (10 % of events). If only one flash flood event is related to a weather pattern of mean group size, the pattern efficiency increases to a value of 4.9.

The wind direction of rain-on-snow and snowmelt floods associated patterns (pattern 5, 15, 26 and 38) is predominantly westerly or north-westerly confirming non-evaluated observations by Beurton and Thieken (2009) and Petrow et al. (2007). These patterns occur predominantly in winter/spring and lead to mild weather and thawing conditions, as they show positive anomalies in air temperature as well as precipitation, suggesting a combination of snowmelt and rainfall. The pattern predominantly linked to snowmelt floods (pattern 19) shows positive anomalies with respect to air temperature and negative anomalies with respect to precipitation suggesting melting conditions. During this pattern subtropical air masses are transported to Central Europe. Less explicit, this is also the case for pattern 25. The previous weather patterns (5, 15, 19, 25, 26 and 38) have only led to flood occurrence in winter. This seasonal flood relevance is confirmed by their attribution to winter flood types as rain-on snow and snowmelt floods and explains why their flood-prone behaviour is restricted to soil moisture pattern 9 (Fig. 3.7). Soil moisture pattern 9 is the predominant winter soil moisture pattern when rain-on snow and snowmelt floods occur. However, the presence of snow is required for the generation of these flood types. A separation into snow-free and snow days may reveal the frequency of snow within these combinations and its influence on flood generation.

Especially important for long-rain flooding are patterns 27 and 29. Both patterns are summer patterns associated with the transport of moist Mediterranean air into the catchment. In the case of pattern 27, the cyclone is located north of the British Isles and the transport is less effective than for pattern 29, which is often identified in the presence of a ‘Vb’ cyclone passing over the Mediterranean region. The efficiency of pattern 27 rises when the soil moisture pattern gets wetter (Fig. 3.3, Fig. 3.7). This provides a further indication, how soil moisture conditions can influence flood generation. In winter, long-rain floods are associated with pattern 31, which is an intense low pressure over Northern Europe that leads to a moist and mild air transport from the Atlantic towards Central Europe. The pattern is also associated with short-rain flood occurrence in winter. Especially, patterns 1, 11, 29 and 34 are linked to short-rain floods between April and August. All of them transport Mediterranean air masses towards the Elbe catchment.

Pattern 12 is associated with the transport of dry continental air masses and was never linked to past flood occurrence in the study period.

3.6 Conclusions

Our presented approach is a step in the direction of the concept of 'flood frequency hydrology' introduced by Merz and Blöschl (2008a,b). This concept signifies a paradigm shift from pure flood frequency analysis to a frequency analysis that bases itself on process understanding of flood generation. We have demonstrated a flood identification method that enables to separate hydrological pre-conditions and meteorological conditions, and their respective influence on flood generation at the regional scale. As a result, flood occurrence is estimated with respect to hydro-meteorological patterns and pattern combinations. 18 % of weather patterns only caused flooding in case of preceding soil saturation. Irrespective of the coincident weather/soil moisture pattern, catchment wide soil saturation (pattern 9) and a weather pattern assigned to 'Vb' cyclones (pattern 29) have the highest flood potential.

The classification of flood events into flood types reveals seasonal flood generating mechanisms with diverse spatio-temporal flood extent as well as flood severity in the Elbe River catchment. In winter, rain-on-snow and snowmelt events have been observed, whereas the summer flood types are long-rain floods and flash floods. Short-rain floods occurred in both seasons.

The flood types are linked to soil moisture and weather patterns. The flood type is primarily determined by the season, by the presence of snow, and by the atmospheric conditions in the build-up period. The large-scale atmospheric conditions, i.e. weather patterns contributing to floods in the Elbe River basin, change between seasons. For different seasons and flood types, either diverse pressure systems transporting moist air masses towards the Elbe River basin or inflowing warm air masses leading to snowmelt or rain-on snow events have been identified. The dependency between flood types and soil moisture patterns is attributable to their seasonal characteristics.

While the results exemplify the influence of hydrological pre-conditions, i.e. soil moisture on the link between weather patterns and flood occurrence, and the influence of meteorological conditions on the flood type, the flood sample size is limited due to the rare nature of flood events. Therefore, future work will extend the pattern classification by a modelling framework, not only to increase the sample size but also to estimate flood risk in dependence of hydro-meteorological pattern combinations and to relate hydro-meteorological pattern combinations not only to flood occurrence but also to flood type. However, model simulations cannot replace the value of observations. It is of particular importance to maintain existing (dense) gauging station networks, as flood events recorded in high spatio-temporal resolution can further improve our understanding of flood generation which is exemplified in this study.

An advantage of the developed classification approach is its suitability to deal with inhomogeneities. As the patterns can be attributed to flood types of diverse characteristics, the flood sample can be subdivided and analysed according to the flood generating patterns. Furthermore, the developed classification approach is suitable to deal with instationarities. For instance, climate as well as land use change might alter the relative frequency of soil moisture patterns. Changes in the atmospheric conditions might alter the relative frequency of weather patterns and thus flood types. Thus, if the present weather pattern-flood (type) link is known and adequately reproduced in Global Circulation Models, their future changes could be assessed. As a result, the timing and relative frequency of the flood generating mechanisms may shift with implications for present and future flood risk management.

Acknowledgements. M. Nied, T. Pardowitz and K. Nissen acknowledge financial support by the AXA Research Fund project "The AXA project on Large-Scale European Flooding under climate change". We would like to thank the German Weather Service (DWD) and the Potsdam Institute for Climate Impact Research (PIK) for making available the climate input data. Additionally, the authors would like to thank the editor, the associate editor, and three anonymous reviewers for their detailed set of recommendations. These have certainly improved the quality of the manuscript.

3.7 Appendix

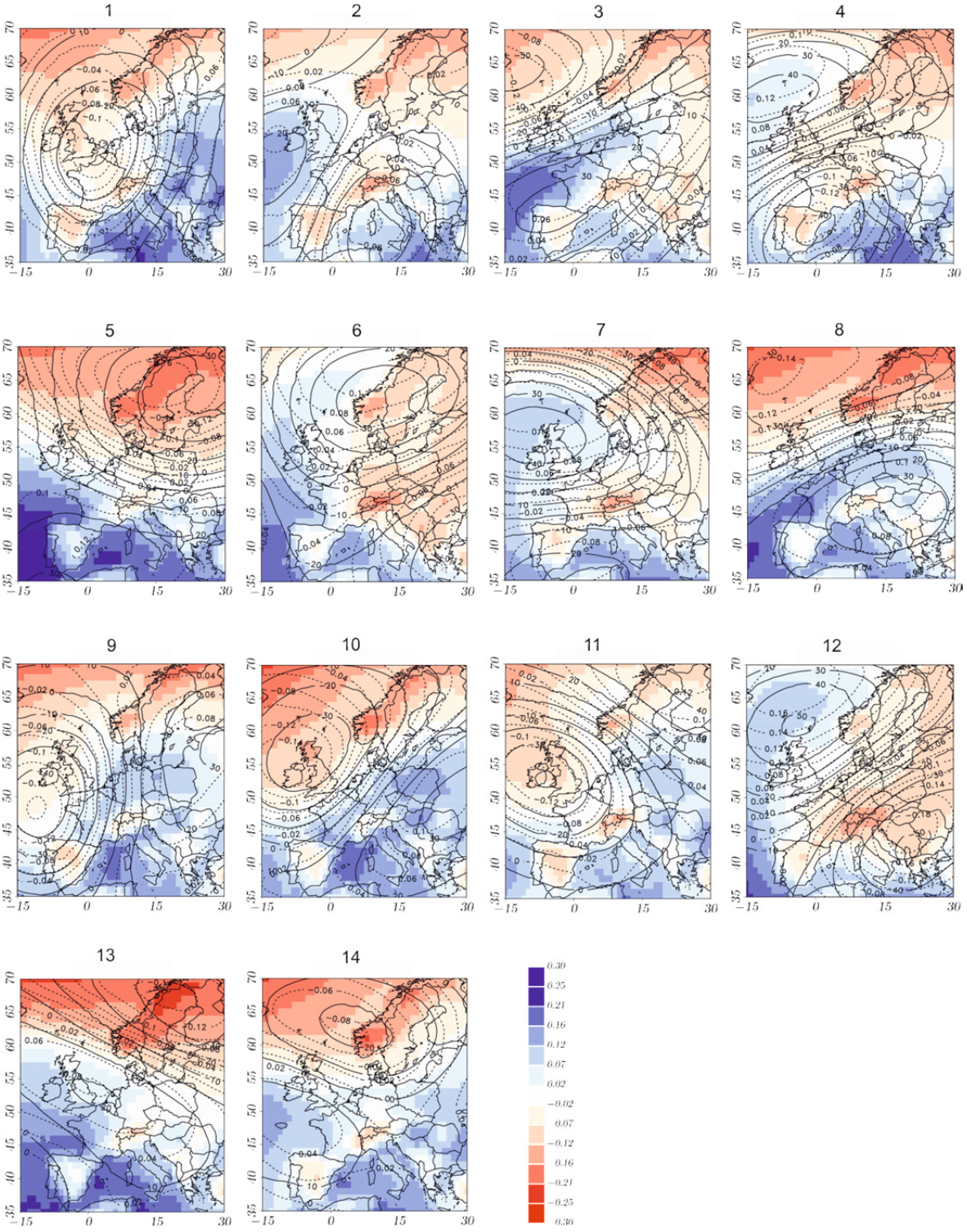

Fig. 3.9: Weather pattern types 1-14. Meteorological cluster centroids. Shaded contours show mean cluster anomalies in the vertically integrated moisture content [kg/m²], solid isolines show mean anomalies in the 500 hPa geopotential [m], and dashed isolines are mean anomalies in 500 hPa air temperature [°C].

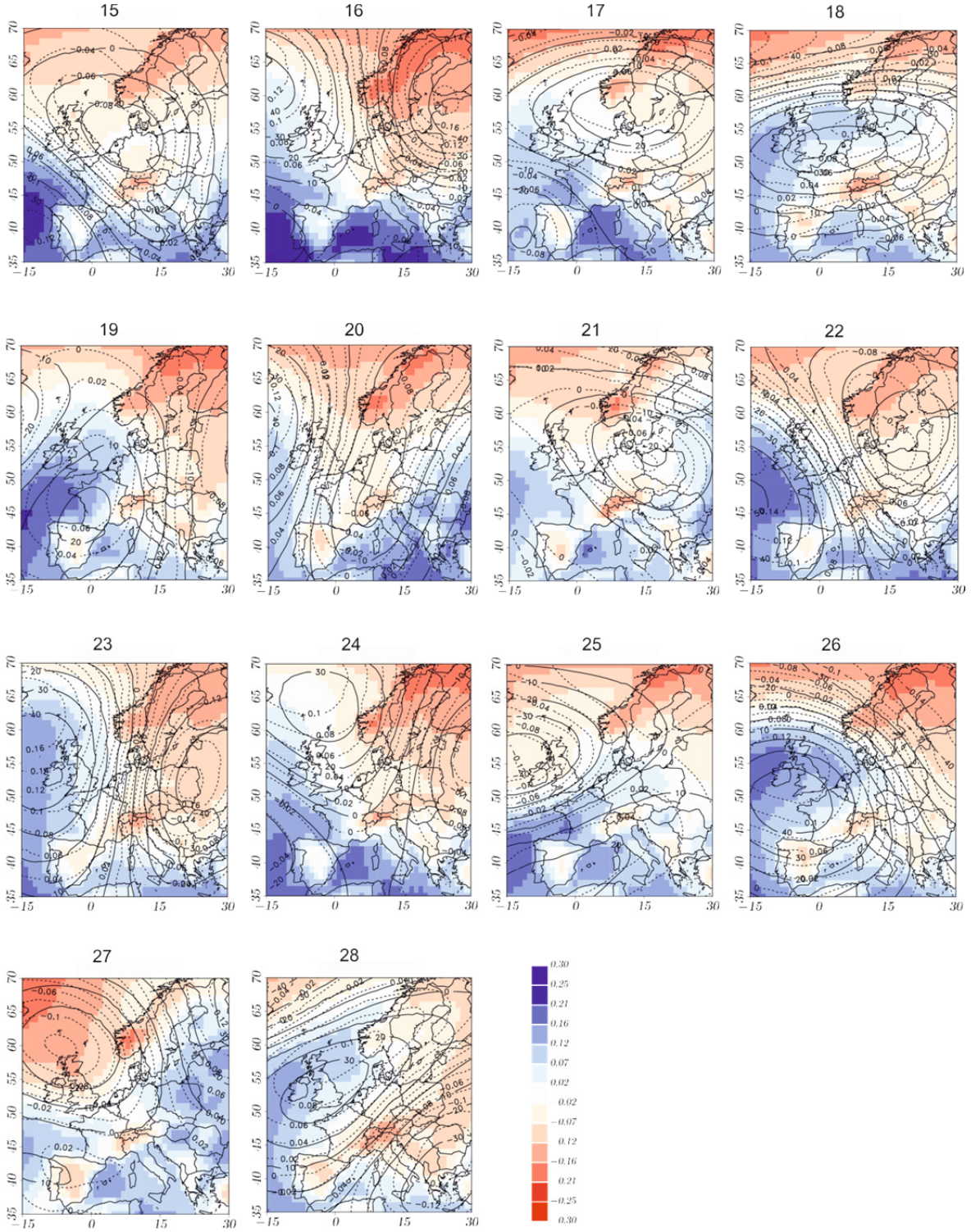

Fig. 3.10: Weather pattern types 15-28. Meteorological cluster centroids. Shaded contours show mean cluster anomalies in the vertically integrated moisture content [kg/m²], solid isolines show mean anomalies in the 500 hPa geopotential [m], and dashed isolines are mean anomalies in 500 hPa air temperature [°C].

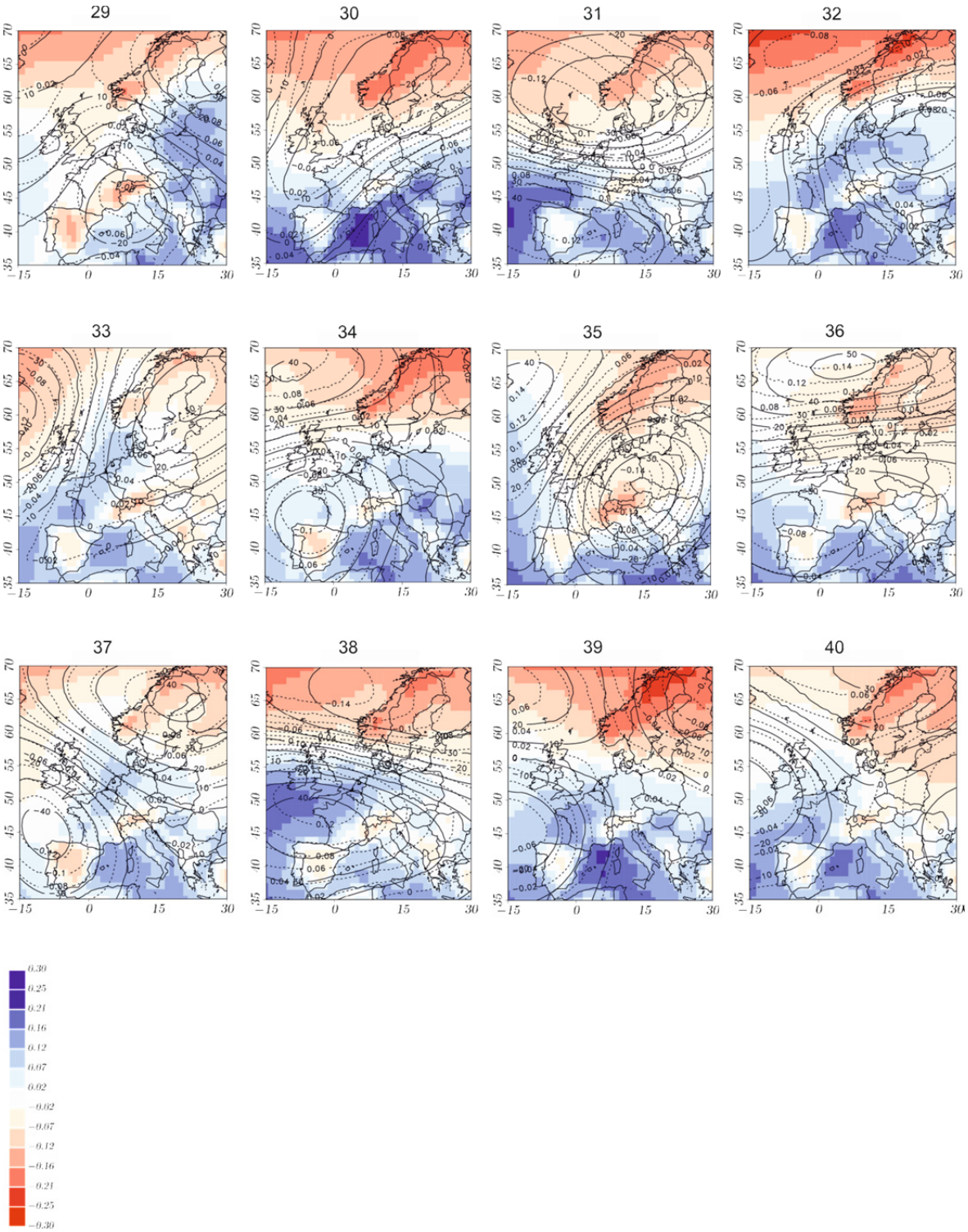

Fig. 3.11: Weather pattern types 29-40. Meteorological cluster centroids. Shaded contours show mean cluster anomalies in the vertically integrated moisture content [kg/m²], solid isolines show mean anomalies in the 500 hPa geopotential [m], and dashed isolines are mean anomalies in 500 hPa air temperature [°C].

Chapter 4:
Hydro-meteorological controls on flood characteristics

What are the hydro-meteorological controls on flood characteristics?

Abstract

Flood events can be expressed by a variety of characteristics such as flood magnitude and extent, event duration or incurred loss. Flood estimation and management may benefit from understanding how the different flood characteristics relate to the hydrological catchment conditions preceding the event and to the meteorological conditions throughout the event. In this study, we therefore investigate the hydro-meteorological controls on different flood characteristics, based on the simulation of the complete flood risk chain from the flood triggering precipitation event, through runoff generation in the catchment, flood routing and possible inundation in the river system and floodplains to flood loss. Conditional cumulative distribution functions and regression tree analysis delineate the seasonal varying flood processes and indicate that the effect of the hydrological pre-conditions, i.e. soil moisture patterns, and of the meteorological conditions, i.e. weather patterns, depends on the considered flood characteristic. In the Elbe catchment, the length of the build-up period, the event duration and the number of gauges undergoing at least a 10-year flood are governed by weather patterns. The affected length and the number of gauges undergoing at least a 2-year flood are however governed by soil moisture patterns. In case of flood severity and loss, the controlling factor is less pronounced. Severity is slightly governed by soil moisture patterns whereas loss is slightly governed by weather patterns. The study highlights that flood magnitude and extent arise from different flood generation processes and concludes that soil moisture patterns as well as weather patterns are not only beneficial to inform on possible flood occurrence but also on the involved flood processes and resulting flood characteristics.

Submitted as:

Nied, M., Schröter, K., Lüdtke, S., Nguyen V. D., and Merz, B.: What are the hydro-meteorological controls on flood characteristics?, J. Hydrol., January 2016 (in review).

4.1 Introduction

Floods can be characterized by a variety of variables, such as flood magnitude and extent, event duration and flood loss. Depending on the perspective, the flood characteristics under consideration vary. The target variable for the (re-)insurance industry is flood loss and expected annual damage (e.g. Kron et al., 2012; Pollner, 2012). Flood risk management requires details on flood magnitude and extent (e.g. BfG, 2014 to view the German flood risk map), whereas inundation duration and month of occurrence during the year are decisive for losses to agricultural crops and to flora (e.g. Van Eck et al., 2006). Flood event characteristics are the outcome of atmospheric processes that deliver the water input to the catchment, runoff generation processes, as well as flood routing and inundation processes in the river system (Merz et al., 2014a; Merz and Blöschl, 2003). For flood design, flood risk analysis and flood forecasting, it is crucial to understand how the various flood characteristics are controlled by the hydrological catchment conditions and the meteorological event conditions.

The disastrous Central European floods of August 2002 (Ulbrich et al., 2003a, b) and June 2013 (Conradt et al., 2013; Merz et al., 2014b), affecting amongst others the Elbe Basin, illustrated the interacting hydrometeorological controls on the river basin scale and the resultant spread of the event characteristics. Although the event precipitation in 2013 was not as extreme as in 2002, the hydrological severity, a combination of spatial extent and frequency of the flood peaks, was much higher than in 2002 (Schröter et al., 2015). This can be explained by the particularly wet pre-event soil moisture conditions in 2013.

The control of the meteorological conditions and the pre-event catchment conditions on flood generation and magnitude has been acknowledged in many studies (Huza et al., 2014; Nied et al., 2014; Pathiraja et al., 2012; Schröter et al., 2015). However, systematic analyses are limited to small-scale catchments (e.g. Ettrick et al., 1987; Huza et al., 2014; Paquet et al., 2013; Sivapalan et al., 2005) and flood forecasting (e.g. Fundel and Zappa, 2011; Silvestro and Rebora, 2014). At the river basin scale, first attempts to study the interplay between catchment state and event conditions indicate the large influence of antecedent catchment conditions on flood magnitude and severity (Nied et al., 2013; Schröter et al., 2015). The control on further flood characteristics such as flood duration and losses has, to our knowledge, not been investigated.

With respect to the meteorological event conditions, numerous studies identified a link between flood occurrence and weather patterns which characterize the main modes of atmospheric state variability (e. g. Duckstein et al., 1993; Jacobeit et al., 2006; Prudhomme and Genevier, 2011). Few studies examined the relation between weather patterns and flood magnitude. For instance, Bárdossy and Filiz (2005) identified flood producing circulation patterns by relating them to positive increments of discharge time series. For the Elbe River basin, Nied et al. (2014) showed that different atmospheric circulation patterns favor different flood types such as long-rain floods or snowmelt floods. For the Elbe tributary Mulde in Germany, Petrow et al. (2007) found that Vb-weather systems have the highest flood potential for floods above the 5-year return period whereas floods of lower return period are caused by a variety of circulation patterns. For different regions in Britain, Wilby and Quinn (2013) detected that normalized flood magnitudes are on average greater under specific weather patterns and established a link between circulation patterns and spatial flood extent. Time-varying flood magnitudes were also related to large scale oscillations such as the El Niño/Southern Oscillation (Ward et al., 2010; Ward et al., 2014; Waylen and Caviedes, 1986), the North Atlantic Oscillation (Bouwer et al., 2006) or to the decadal variability of the Asian monsoon (Delgado et al., 2012). However, investigations how the meteorological event conditions in combination with the hydrological pre-event conditions control different flood characteristics besides flood magnitude are lacking.

We intend to fill this gap by studying the interacting control of soil moisture patterns, as a proxy for the hydrological pre-event conditions, and of weather patterns, as a proxy for the meteorological event conditions, over a variety of flood characteristics. These characteristics include not only indicators for flood magnitude and severity but also indicators which quantify the length of the flood-affected river system or the flood impact on society.

It is not feasible to base this analysis on historic flood events alone, since the sample would not be large enough to derive statistically robust conclusions. This would be particularly problematic for the indicators which describe the societal flood impacts. Flood impact data is not well documented and is plagued by inconsistencies (Merz et al., 2010b). Hence, we propose to generate a very large number of synthetic flood events. This includes their controls, i.e. spatially coherent patterns of event precipitation and catchment pre-conditions, as well as their consequences, i.e. spatio-temporal patterns of discharge, water stage, inundation, and losses. To this end, a model chain for

assessing flood risk at the river basin scale (e.g. Falter et al., 2014; Falter et al., 2015) is applied. This model chain consists of a hydrological catchment model, a 1D/2D hydraulic model for the processes in the river system, and a damage model. It is driven by synthetically generated patterns of event precipitation and antecedent catchment conditions derived by a resampling approach. In this way, the space-time consistency of controls, processes and their interactions is taken into account. The methodology is developed for the example of the Elbe River basin introduced in Sect. 4.2. The Elbe catchment was chosen due its susceptibility to basin-wide flooding in the past years as well as due to the wealth of data and availability of models. Furthermore, both summer and winter floods are observed in the Elbe basin (Beurton and Thieken, 2009; Nied et al., 2014) which allows studying the controls on a broad range of flood types. Section 4.3 outlines the methodology, from the flood triggering precipitation and its associated weather patterns, through runoff generation compromising the soil moisture conditions, to flood identification and characterization. The results are presented and discussed in Sect. 4.4 and 4.5. The paper finalizes by concluding remarks in Sect. 4.6.

4.2 Study area

The Elbe/Labe Basin (Fig. 4.1) is located in Central Europe encompassing 148,268 km². The river originates in the Giant Mountains (Czech Republic), 1,386 m a.s.l., and flows after 1,094 km into the North Sea (IKSE, 2005). Major tributaries are the Moldau/Vltava, the Eger/Ohře, the Mulde, the Saale, the Schwarze Elster and the Havel. The main riparian states are the Czech Republic and Germany.

The basin can be subdivided into three geomorphologic units: (1) The tide influenced Lower Elbe with an elevation mainly below 75 m a.s.l. encompassing 9 % of the catchment area, (2) the lowlands of the Middle Elbe (55 % of catchment area) situated in an elevation zone below 200 m a.s.l., and (3) the Upper Elbe (36 % of catchment area) characterized by hilly country, and low to high mountain ranges (IKSE, 2005). In the lowlands, sandy soils and glacial sediments dominate. In the valleys, loamy soils and in the western Elbe loess is found. In the highlands, cambisols are the main soil type (Hattermann et al., 2005).

Climate ranges from maritime in the Lower Elbe to continental in the Middle and Upper Elbe. Mean annual evapotranspiration is 455 mm (IKSE, 2005). Basin average mean annual precipitation is 715 mm (1961-1990). However, the variation within the basin is high (IKSE, 2005). In the Middle Elbe, mean annual precipitation is around 450 mm. In the mountainous regions, mean annual precipitation is above 1,000 mm and strongly modified by the relief. In winter, precipitation is falling as snow. Snow melts predominantly in March, although it can persist until May resulting in a snowmelt influenced discharge regime.

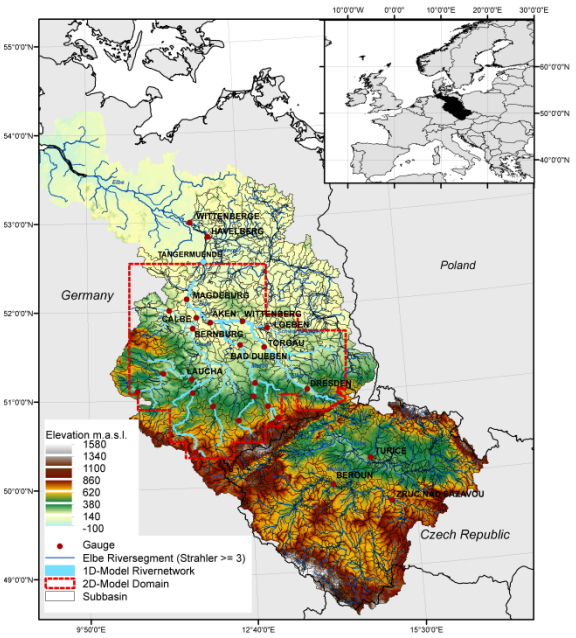

Fig. 4.1: Topographic map of the Elbe River catchment, hydrologic model domain, 1D model river network and 2D model domain. Red dots show the gauges which are used to calibrate and validate the rainfall-runoff model, and to identify large-scale flood events. Map of the regional setting of the Elbe catchment (upper right). The map delineates the spatial extent the weather pattern classification is based on.

The anthropogenic influence on the catchment is strong. 50.8 % of the catchment is cropland, 30.2 % forest and 10.2 % grassland. Settlements account for 6.5 % of the total catchment area (CORINE European Environment Agency, 2000). In the headwaters, dams have been built and along the river, dikes have been installed for flood protection purpose. Past mining activities strongly modified the Havel region.

Besides basin-wide floods, such as the disastrous summer floods of 2002 and 2013, small-scale flooding due to convective events is observed. In winter and spring, floods are predominantly generated by a combination of snowmelt and rainfall (IKSE, 2005; Nied et al., 2014; Petrow et al., 2007).

4.3 Data and methods

A process-based flood hazard and risk assessment is conducted in which soil moisture patterns are selected as a proxy for the hydrological pre-event catchment conditions and weather patterns are selected as a proxy for the meteorological event conditions. Based on 84 observed flood events in the Elbe catchment, the patterns' influence on flood generation has previously been illustrated (Nied et al., 2014). Their control on the flood characteristics is determined from an augmented sample generated by reshuffling daily fields of meteorological conditions. The reshuffling extends the available climate time series by taking into account the synoptic-scale dependence between large-scale circulation and local meteorology, as well as the seasonal variability. The reshuffled meteorological time series is used to drive the regional flood model (RFM). RFM has been developed to simulate flooding and its impact at the river basin scale (Falter et al., 2015). First, a continuous semi-distributed rainfall-runoff model simulates soil moisture as well as river discharge. Flood inundation and loss are determined by subsequently applying a hydrodynamic and a flood loss model. From these time series, flood events, their characteristics, as well as the involved soil moisture and weather patterns are identified. The relationship between patterns of hydro-meteorological conditions and flood occurrence as well as a variety of flood characteristics is deciphered by (i) conditional cumulative distribution functions to estimate the separate impact of soil moisture patterns and weather patterns on the flood characteristics, and (ii) by regression trees to analyze the combined impact of soil moisture patterns and weather patterns on the flood characteristics. The analysis period is September 1957 to August 2002. In the following, the analysis steps (Fig. 4.2) are presented in detail.

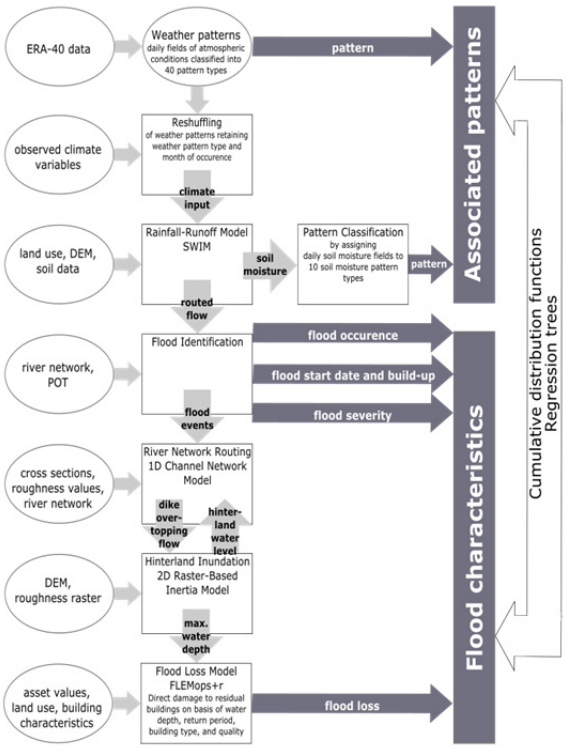

Fig. 4.2: Flow chart of the analysis: modules (rectangles), their input data (ovals) and results (arrows). Weather patterns are reshuffled and used to drive the regional flood model (RFM) composed of a rainfall-runoff model to simulate soil moisture and discharge, a hydrodynamic model to simulate inundation, as well as a flood loss model. Flood events, their characteristics, as well as the involved soil moisture and weather patterns are identified. The relationship between the patterns and flood occurrence as well as flood characteristics are analyzed by cumulative distribution functions and regression trees.

4.3.1 Hydro-meteorological patterns

4.3.1.1 Weather patterns and reshuffling

ERA-40 reanalysis data (Uppala et al., 2005) covering Europe (see Fig. 4.1, upper right) are used to derive daily weather patterns. Daily fields (1.125° x 1.125°) of geopotential height in 500 hPa representing atmospheric circulation, temperature in 500 hPa indicating e.g. melting conditions, and total column water vapor content indicating potential rainfall, were clustered by Nied et al. (2014) into 40 weather patterns using the SANDRA algorithm (Philipp et al., 2007). The flood generating weather patterns vary seasonally and can be linked to different flood types (Nied et al., 2014).

Figure 4.3 displays a selection of four weather patterns, which play a central role in this work. During weather pattern 19 subtropical air masses are transported to Central Europe. The pattern shows positive anomalies with respect to air temperature and negative anomalies with respect to precipitation in the Elbe catchment whereas weather pattern 26 is associated with positive anomalies in air temperature as well as precipitation. Wind directions are mostly westerly or north-westerly. Weather pattern 29 is a low pressure system over South Europe which transports warm and moist air masses towards Central/Eastern Europe. Flood-favoring 'Vb' cyclones are mostly assigned to this weather pattern. In case of weather pattern 34,

moist air from the Mediterranean is transported towards the Elbe catchment.

For the characterization of the local meteorological conditions in the Elbe catchment, daily data of precipitation amount, mean, maximum, and minimum air temperature, solar radiation and relative humidity are used. The station data were provided by the German Weather Service (DWD) and the Czech Hydrometeorological Institute, corrected for inconsistencies, data gaps and inhomogeneities (Österle, 2001; Österle et al., 2006).

The available climate time series are extended by a reshuffling approach. The local meteorological data are resampled by retaining the prevailing weather pattern and its month of occurrence to account for both, the synoptic-scale dependence between large-scale circulation and local meteorology, as well as the seasonal variability (Pathiraja et al., 2012). For instance, within the analysis period, a particular weather pattern occurs 62 times in August. These 62 days are randomly exchanged. The replacement is executed for all combinations of weather patterns and months simultaneously resulting in a reshuffled meteorological time series. In the median, a particular weather pattern – month combination occurs 31 times. The minimum value is 0, the maximum value 211 reflecting the different seasonality of the weather patterns. By reshuffling daily meteorological fields, the spatial coherence as well as the interdependence between the meteorological variables is preserved. However, the 'meteorological genesis' of weather phenomena lasting over several days may be disturbed. The method does neither produce new fields of meteorological variables, nor new sequences of weather patterns. Instead, it reshuffles the observed meteorological patterns, retaining the sequence of weather patterns and retaining the probability distributions of the local meteorological variables. The reshuffling is repeated 2,000 times resulting in 90,000 yearly realizations (45 years of observations x 2,000).

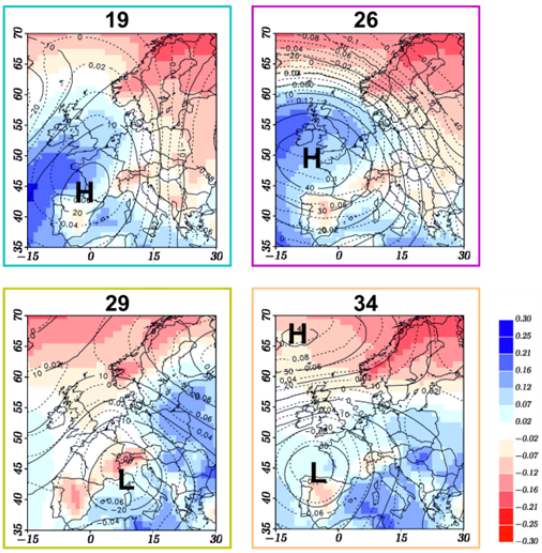

Fig. 4.3: Meteorological cluster centroids of the selected weather patterns (19, 26, 29 and 34). Shaded contours show mean cluster anomalies in the vertically integrated moisture content [kg/m²], solid isolines show mean anomalies in the 500 hPa geopotential [m], and dashed isolines are mean anomalies in 500 hPa air temperature [°C]. Weather patterns are taken from Nied et al. (2014).

4.3.1.2 Soil moisture patterns

The reshuffled meteorological time series are used to drive the subsequent flood risk model chain. From these simulations, the basin-wide distribution of soil moisture of each day is assigned to one of 10 soil moisture patterns. These patterns are taken from Nied et al. (2013). The patterns range from catchment wide soil saturation to dry conditions and vary seasonally. Figure 4.4 displays a selection of soil moisture patterns, which play a central role in this work. Pattern 9 is the wettest pattern characterized by catchment wide soil saturation.

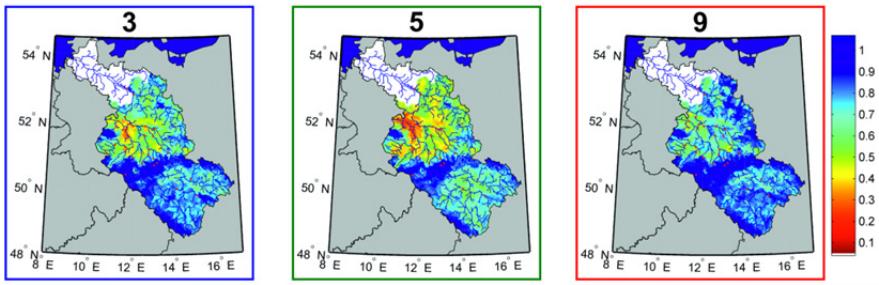

Fig. 4.4: Selected soil moisture patterns (3, 5 and 9) as identified by Nied et al. (2013). Profile (layer-depth weighted average) soil moisture content is standardized by the field capacity of the respective soil type.

Pattern 3 is characterized by catchment wide soil saturation too whereas soil saturation is limited to the upstream Elbe in case of pattern 5. Independent of the prevailing meteorological conditions, pattern 9 was identified to have the highest flood potential (Nied et al., 2013, 2014).

For their pattern classification, Nied et al. (2013) simulated soil moisture for every Elbe subbasin with the SWIM model (details see Sect. 4.3.2.1). A principal component analysis and a subsequent cluster analysis on the leading 4 principal components resulted in 10 soil moisture patterns. We use the classification of Nied et al. (2013) to assign the daily simulated soil moisture of the reshuffled model runs to these predefined patterns. The principal components (*PC)* of each reshuffled soil moisture simulation are obtained by projecting the simulated standardized (zero mean, unit variance) profile soil moisture (*SMI*) onto the eigenvectors u of the soil moisture classification of Nied et al. (2013) (eq. 1).

$$PC = SMI \times u \quad (1)$$

Subsequently, the least squared deviation between the leading 4 *PCs* of the reshuffled simulation and the 10 cluster centroids of the soil moisture classification of Nied et al. (2013) is identified for each day. Each day of the reshuffled simulation is assigned to the soil moisture pattern with the least squared difference.

4.3.2 Regional flood model (RFM)

RFM comprises a rainfall-runoff model, a coupled 1D-2D hydrodynamic model as well as a flood loss model. The model chain assesses flood hazard and risk in a spatially consistent way and has been proven to derive plausible results in meso-scale (e.g. for the 6,000 km² large Mulde catchment; Falter et al., 2015) as well as in macro-scale applications (e.g. for the Elbe catchment, Falter et al., 2014). The 1D-2D hydrodynamic model simulates the hydraulic processes in the river and adjacent flood floodplains, hence, its model domain is only a subarea of the model domain of the rainfall-runoff model (see Fig. 4.1 for the different model domains).

4.3.2.1 Rainfall-runoff model

Runoff and soil moisture are simulated with the conceptual, semi-distributed rainfall-runoff model SWIM (Krysanova et al., 1998). In the model setup, the Elbe catchment is subdivided into 1,945 subbasins upstream of gauge Wittenberge (see Fig. 4.1 for the model domain). The reshuffled meteorological time series serve as climate input to the model. The station data are interpolated on the centroid of each subbasin.

The model calculates runoff based on hydrological response units which are delineated by soil type and land use class. Information on land use is taken from the CORINE 2000 land cover data set of the European Environment Agency (CORINE European Environment Agency, 2000). The soil map is created by merging the German soil map "BUECK 1000" provided by the Federal Institute for Geosciences and Natural Resources (BGR), and the FAO-UNESCO soil map for the Czech part.

SWIM was calibrated against observed discharge at 27 discharge gauges (dots, Fig. 4.1) over the period 1981–1989, and validated from 1951 to 1980 as well as 1990 to 2003. In total, 38 sets of parameter realizations have been identified as behavioral. For each gauge, the median simulated discharge is calculated from the 38 behavioral model runs and taken for further analysis. In addition, it has been shown that the model is able to reproduce the temporal evolution of profile soil moisture by comparing simulated soil moisture against satellite derived soil moisture information (Nied et al., 2013). For more details on the model and the calibration as well as validation procedure see Nied et al. (2013).

4.3.2.2 Hydrodynamic model

As the rainfall-runoff model does not consider explicitly river channel geometry, slope and resistance, it is not able to simulate water levels and flood inundation. Therefore, a 1D river network routing model (see Fig. 4.1 for the model domain) which considers hydraulic processes by taking into account the actual river cross-sections complements the regional flood model. The routed subbasin discharge derived from the rainfall-runoff model serves as its boundary condition.

The 1D routing model solves the simplified form of the Saint-Venant equations for flow in open channel with an adaptive explicit scheme (Falter et al., 2015). The model is able to simulate overbank flow. Whenever the routed water level exceeds the dike crest level, the overtopping flow triggers a 2D hinterland inundation model. This raster-based inertial model simulates inundation propagation and is based on the simplified shallow water equation, neglecting advective acceleration (Bates et al., 2010; Falter et al., 2015). The spatial resolution is 100 m. The 1D-2D coupled model was implemented in the CUDA Fortran environment to enable model simulation on highly parallelized NVIDIA Graphical Processor Units (GPU) and multicore processor Central Processing Unit (CPU). Dike breaching is not included in the current model version. Therefore, inundation extent may be underestimated (see Falter et al., 2014).

Profiles of overbank cross-sections including dike information are the most demanding model input and

are very important for the quality of the model simulations (Falter et al., 2014). In total, 3,717 cross-sections upstream of Tangermuende have been derived from a 10 m-DEM (Federal Agency for Cartography and Geodesy in Germany) using the HEC-GeoRas tool (US Army Corps of Engineers) in ArcGIS 10.1. The cross-section profiles have been extracted in 500 m distance, perpendicular to the flow direction. Inconsistencies, e.g. due to perpendicular cross-sections overlapping each other, have been corrected manually to generate a more realistic representation of channel geometry (see Falter et al., 2015).

4.3.2.3 Flood loss model

For each flood event (see Sect. 4.3.3 for the definition of flood events), flood loss is calculated with the Flood Loss Estimation MOdel for the private sector (FLEMOps+r, Elmer et al., 2010; Thieken et al., 2008). FLEMOps+r estimates direct damage to residential buildings using a rule based multi-variable approach differentiating between five classes of maximum inundation depth (h), three building types, two classes of building quality, three classes of contamination, three classes of private precaution and three classes of flood peak return periods. In summary, the loss estimation requires spatially detailed input data of asset values, building quality and building type, as well as the event dependent variables inundation depths and return period of peak flows.

All inputs are prepared as gridded data sets (spatial resolution of 100 m) to comply with the 2D hydrodynamic modelling output. Asset values of the regional stock of residential buildings are defined on the basis of standard construction costs (BMVBS, 2005) which reflect the market price of the construction works for restoring a damaged building with reference to the year 2010. The asset values are disaggregated to the digital basic landscape model (Basic DLM) of the German ATKIS (Authoritative Topographic Cartographic Information System; BKG GEODATENZENTRUM, 2009) using the binary disaggregation scheme proposed by Wünsch et al. (2009). The characteristics of the municipal building stock are derived from the INFAS Geodaten data set (Infas Geodaten Infas Geodaten GmbH, 2009). Maximum inundation depth is the outcome of the 2D raster-based hinterland inundation model. Discharge return periods are estimated within each SWIM subbasin based on the annual maximum discharge series 1951 to 2003. As per Elmer et al. (2012), precautionary measures and contamination are not taken into account in this study. For each flood event, absolute flood losses in Euros are calculated as the product of damage ratio and location-dependent asset value per raster cell.

4.3.3 Flood event identification and characteristics

Large-scale flood events are identified according to Uhlemann et al. (2010). Flood event detection is based on daily simulated discharge at all 27 gauges (see Fig. 4.1, red dots). A systematic spatio-temporal peak-flow search is conducted around each recorded 10-year flood. In doing so, each flood event is characterized by its spatio-temporal extent. In general, a flood implies several discharge peaks of various magnitudes distributed in space and time which reflects the heterogeneity of floods at the river basin scale. The temporal flood progression is described by the event start date, the event end date and the event centroid. The event start date defines the date, up to three days in advance of a recorded 10-year flood, where the first gauge has a significant peak. The up to three days beforehand account for the catchment's concentration time which is determined by the catchment size, the catchment characteristics and its initial state. The event end date is the date where the last gauge shows a significant peak up to ten days after a 10-year flood. A peak is considered significant if it exceeds $P(t) + v$. $P(t)$ is the 13 days moving average of observed discharge and v is the 90^{th} percentile of the residuals between daily observed discharge and $P(t)$. The event centroid defines the highest daily overall discharge increase in the catchment compared to the previous date. Daily overall discharge is the discharge sum of all gauges in the catchment standardized by their respective 2-year flood (Uhlemann et al., 2010).

For each identified flood, the following characteristics, and their relationship to hydro-meteorological patterns are investigated:

- Month event start date: As different flood types dominate in different seasons (Merz and Blöschl, 2003; Nied et al., 2014), this characteristic is used to analyze the seasonal influence.
- Length build-up period: The period after the event start date including the event centroid date is named event build-up period. The length of the build-up period depends on flood type and spatial flood extent and accounts for the catchment reaction time as well as flood routing.
- Total event length: The event length marks the time between the event start date and the event end date.
- Affected length: The affected length describes the percentage of the regionalized river network affected by at least a 2-year flood. For details of the regionalization scheme see Uhlemann et al. (2010). The spatial flood extent depends on the flood type (Merz and Blöschl, 2003; Nied et al., 2014).

- Affected gauges ≥ HQ_2/affected gauges ≥ HQ_{10}: The percentage of gauges (out of the 27 gauges in the analysis) which are affected by at least a 2-year flood (10-year flood). The measure characterizes the magnitude of a flood event.
- Severity: The severity *S* is a combined measure of flood magnitude and extent

$$S = \sum_{i=1}^{n} \left(\lambda_i \frac{Q_i}{HQ2_i} \right) \mid Q_i \ \geq HQ2_i \ . \quad (2)$$

  Q_i is the maximum discharge at gauge *i* for a respective flood event which is standardized by the gauge's 2-year flood *HQ2*. Only gauges exceeding their *HQ2* are included in the severity calculation as below *HQ2* (bankfull river flow) no impact is expected. λ is a weighting factor describing the gauge's regionalized river network in relation to the overall regionalized river network.
- Losses: Flood losses are calculated according to Sect. 4.3.2.3. In contrast to the severity, flood losses also take the spatial distribution of inundation areas and their superposition with assets into account.

For the comparability of results, the threshold values *HQ2* and *HQ10*, applied in the flood identification as well as characterization, are estimated from the model simulation with undisturbed meteorological variables and kept constant for all reshuffled runs.

4.3.4 Linking patterns to flood events and their characteristics

The soil moisture patterns and weather patterns are assigned to the flood characteristics in two ways. Cumulative distribution functions analyze the separate impact of soil moisture patterns and weather patterns on the flood characteristics (Sect. 4.3.4.1) whereas a regression tree analysis (Sect. 4.3.4.2) estimates their combined impact. This allows for a quantitative investigation of the hydro-meteorological controls over the flood characteristics.

Since soil moisture patterns represent the pre-event catchment conditions, they are considered at the event start date. Weather patterns represent the meteorological influence of the event and are considered during the event build-up period. In the build-up period, each weather pattern is weighted in accordance with the number of days it occurs. The weighting coefficient is the ratio of number of days to the total length of the build-up period. Thus, each flood event receives the same weight (Nied et al., 2013; Nied et al., 2014). Minor flood events with a build-up period less than one day were removed from the analysis.

4.3.4.1 Cumulative distribution functions

A cumulative distribution function (CDF) describes the probability of a real random variable, i.e. in our case a flood characteristic. For each flood characteristic, a CDF is established to view the respective probability distribution. Second, the CDF of each flood characteristic is separated according to the prevailing soil moisture patterns as well as according to the prevailing weather patterns to view the patterns' influence on the flood characteristics.

4.3.4.2 Regression trees

Classification and regression trees (CART, Breiman et al., 1984) are binary trees to understand the structural relationship between a predictor, i.e. in our case soil moisture patterns/weather patterns and a response, i.e. the flood characteristic. Tree based models are chosen for this study as they do not make any implicit assumption on the relationship between the predictor and its response and can represent non-linear and non-monotonic dependencies. Therefore, they are well suited when there is little knowledge of the importance of the predictors as well as their interaction. However, tree based models can only reflect those structures already present in the data and therefore can't draw any conclusions beyond the utilized data.

For regression trees, the response is predicted by subsequently separating the predictor values into homogenous subgroups. The optimal split at each decision node is selected by calculating the within group variance of the response values of all possible splits. The partition that maximizes the decrease of the within group variance is chosen. This results in a tree that develops from the root node which unifies all predictor values, through the decision nodes that subsequently split the predictor values into two subgroups, to the terminal nodes (leaves) characterizing the response. Strongly ramified trees characterize the underlying data in the minutest detail. However, they can bear small leaf sample sizes where the predictive power for independent data is poor. Therefore, an optimal sized tree, complex enough to account for the relationship between predictors and response, and simple enough to avoid overfitting, has to be identified. One method is pruning. A ramified tree is sequentially pruned to a simplified subtree. Those branches are cut first that led to the smallest decrease in the predictive error. The predictive error *R* is defined over all leaves as the sum of the estimated probability of a leaf times its average squared error

$$R_T = \sum_{j=1}^{N_T} \left[\frac{T}{N} \ \frac{1}{N_T} \sum_{n=1}^{T} (y_n - \bar{y}_T)^2 \right] \quad (3)$$

where N_T is the number of leaves, N the total number of observations, T the number of observations of leaf j, y_n the observations in leaf j and $\overline{y}_n$ the simulation (median of observations in leaf j).

Ten-fold cross validation is applied to choose the tree size. The observations are randomly separated into 10 subsamples. Tree growing and pruning are repeatedly applied to the given data set excluding always one subsample. Taking the retained subsample, the predictive error of the grown tree is estimated. Afterwards, the predictive error is averaged over all subsamples and displayed as a function of the number of terminal nodes. The optimal tree is the smallest tree that is within one standard error of the subtree with the smallest predictive error.

The importance of a predictor variable (variable importance) with respect to the response is determined by estimating the predictive error at each decision node. The difference between the predictive error for the parent node and the total predictive error for the two children nodes, i.e. the decrease in the predictive error ΔI, is calculated. The importance of a variable m is defined as the sum over all ΔI where m is the splitting criteria. The higher the sum over all ΔI for a particular variable, the more important is the variable. The variable importance of the two predictor variables soil moisture patterns $\sum \Delta I_{m1}$ and weather patterns $\sum \Delta I_{m2}$ is estimated respectively for each response variable.

For the comparability of results, the delta of the variable importance is calculated for each response variable. The delta of the variable importance is defined as

$$D = \frac{\sum \Delta I_{m2}}{\max(\sum \Delta I_{m1}, \sum \Delta I_{m2})} - \frac{\sum \Delta I_{m1}}{\max(\sum \Delta I_{m1}, \sum \Delta I_{m2})} \quad (4)$$

Positive values illustrate the control of weather patterns, and negative values highlight the dominance of soil moisture patterns. The higher the absolute value, the stronger the influence of weather or soil moisture patterns on the respective flood characteristic. The maximum value is one indicating that the flood characteristic is solely controlled by weather patterns in case of a positive value or by soil moisture patterns in case of a negative value. One has to be aware that the delta of the variable importance denotes only the importance of soil moisture patterns compared to weather patterns. Predictors not included in the regression tree analysis, like flood protection and management, may have an even larger control on the flood characteristics.

4.4 Results

4.4.1 Evaluation of the regional flood model and of the reshuffling approach

To proof the capability of the regional flood model to reproduce the flood characteristics (Sect. 4.3.3), the simulated flood characteristics are compared against those retrieved from observed discharge. Therefore, the flood identification (Sect. 4.3.3) is applied to observed discharge and simulated discharge generated by the undisturbed climate data, i.e. the observed meteorology. All flood events from September 1957 to August 2002 with a minimum build-up period of one day are evaluated. From the observed discharge time series, 15 flood events are identified (Fig. 4.5, grey dashed line). The regional flood model simulates 7 events (Fig. 4.5, grey solid line) when driven with the observed meteorology.

Although the number of simulated events is half the number of observed events, the general agreement of the empirical cumulative distribution functions (CDFs), both in shape and magnitude, implies that the regional flood model is suitable to reproduce the observed event characteristics. According to the Kolmogorov Smirnov test, the hypothesis that the observed and simulated flood event characteristics are drawn from the same distribution cannot be rejected at the 5 % significance level for all characteristics.

The underestimation of the number of flood events is due to the lower number of simulated significant peaks (43,507) than observed significant peaks (60,509). As a consequence, a higher number of flood events are detected in which a single 10-year flood is simulated and no additional significant peak three days beforehand the 10-year flood is found. The events' build-up period is less one day. Including these events, 32 events are observed whereas 37 events are simulated. In the current event set where minor flood events with a build-up period less one day are neglected, the number of significant peaks during the event is in the same order of magnitude for simulated and observed flood. On average, an observed flood event comprises 53 significant peaks whereas a simulated flood event comprises 49 significant peaks. Gauges underestimating the number of significant peaks are randomly distributed within the Elbe catchment. Therefore, the underestimation may be traced back to model deficits in simulating the runoff dynamics possibly due to deficits in the climate input data where small scale precipitation features like thunderstorms may not be present. The flood characteristic losses cannot be evaluated due to the scarcity and uncertainty of historical flood loss estimates (Merz et al., 2010b).

Within the reshuffling approach, 5970 flood events (Fig. 4.5, black solid line) are identified from the reshuffled model runs. The comparison of the simulated characteristics (Fig. 4.5, grey solid line vs. black solid line) shows that the reshuffling reproduces the event characteristics. According to the Kolmogorov Smirnov test, the hypothesis that the characteristics are drawn from the same distribution cannot be rejected at the 5 % significance level for all characteristics. However, flood severity (Fig. 4.5, G), affected length (Fig. 4.5, D) and the affected gauges ≥ HQ_2 (Fig. 4.5, E) are in the median underestimated. Further, the reshuffling approach is able to generate events that are outside the range of previously (September 1957 to August 2002) observed events. For instance, the highest observed severity was 164 whereas the highest simulated severity obtained by the shuffling approach is 214. No events are generated where the entire catchment is affected by at least a 10-year flood (Fig. 4.5, F). The maximum number of gauges affected by at least a 10-year flood during one specific flood event is 70.4 %. This highlights that the commonly applied assumption of spatially uniform return periods within an entire river basin is invalid on the river basin scale and would result in overestimation of flood risk, as was shown for the Rhine river by Thieken et al. (2014). Within the reshuffling approach, about 20 % of the simulated flood events cause flood losses (Fig. 4.5, H).

4.4.2 Separate control of hydrological pre-conditions and meteorological event conditions on flood characteristics

The separate impact of the hydrological pre-conditions and the meteorological event conditions on each flood characteristic is examined by deriving CDFs (Fig. 4.6). The characteristics in dependence of weather patterns (soil moisture patterns) are shown on the left (right) hand side of each subplot. The color coded CDFs represent the patterns introduced in Sect. 4.3.1. The remaining patterns are labeled in grey. The black colored CDF is in each case identical to the black solid line in Fig. 4.5 representing the entire event set independent of the pattern. *N* is the sample size of the respective CDF.

The control of weather patterns/soil moisture patterns on a flood characteristic is expressed in the spread of the CDFs; the higher the spread the stronger the control. For instance, the CDFs of the length of the build-up period (Fig. 4.6, B) and the total event length (Fig. 4.6, C) are similar among the soil moisture patterns whereas they vary among the weather patterns. This indicates that the soil moisture conditions have little influence on these flood characteristics and that the impact of weather patterns is stronger.

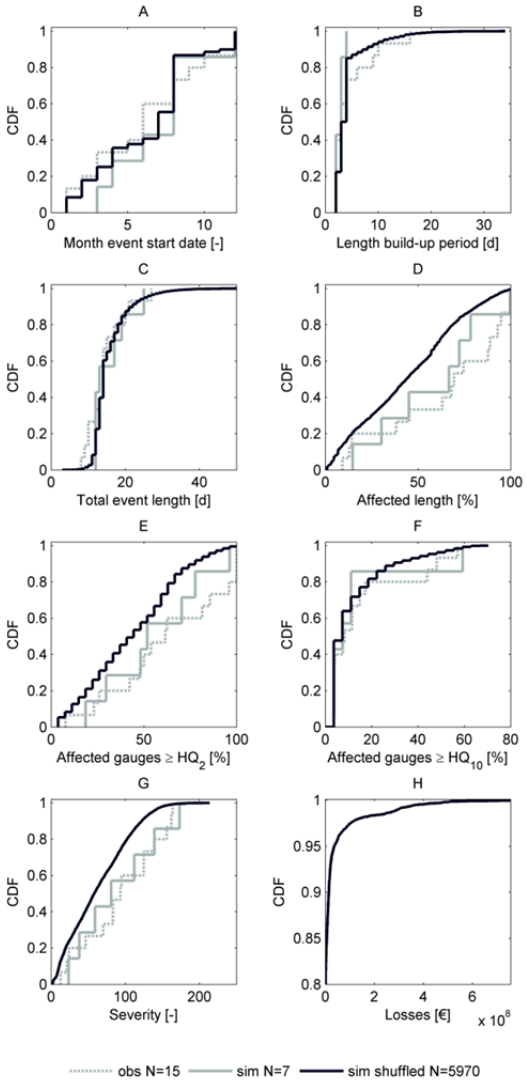

Fig. 4.5: Cumulative distribution functions (CDF) of the different flood characteristics. The flood characteristics have been derived by the flood event identification applied to observed discharge (grey dashed line), simulated discharge generated by the undisturbed climate data, i.e. the observed meteorology (grey solid line), and simulated discharge generated by the shuffling approach (black solid line).

For other characteristics, the respective influence of soil moisture and event conditions is less clear and will be further investigated and discussed in Sect. 4.4.3 and 4.5.2.

Differences in the CDFs are not only visible between weather patterns and soil moisture patterns in general but also between the characteristics for specific weather patterns and soil moisture patterns. The patterns' different behavior in relation to the various

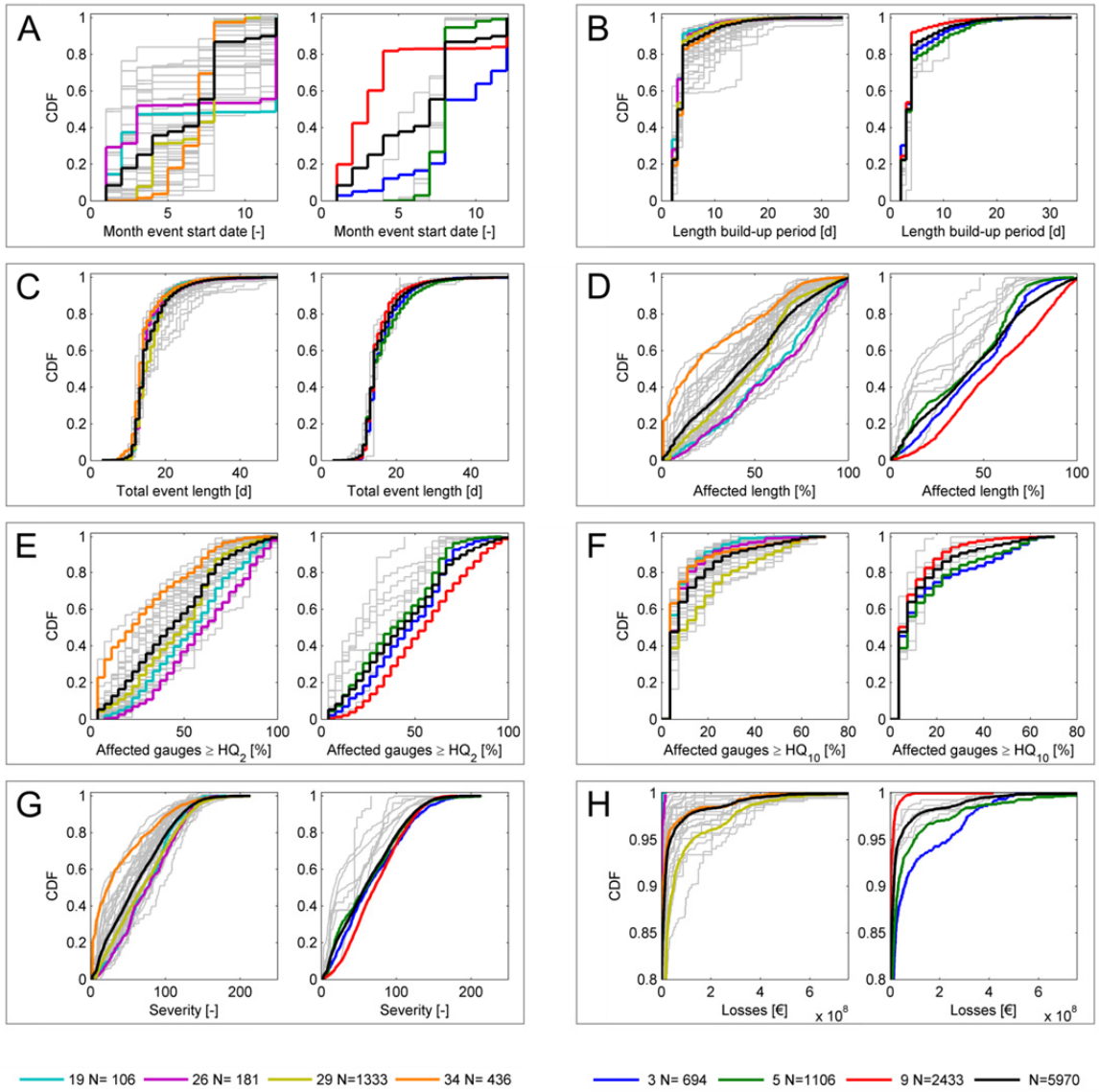

Fig. 4.6: Cumulative distribution functions (CDFs) of the flood characteristics (subplots A-H) in dependence of weather patterns and soil moisture patterns. The grey and color coded CDFs represent the 40 weather patterns (left hand side of each subplot) and the 10 soil moisture patterns (right hand side of each subplot) respectively. The light blue CDF represents weather pattern 19, the purple weather pattern 26, the olive weather pattern 29 and the orange weather pattern 34. The blue CDF represents soil moisture pattern 3, the green soil moisture pattern 5 and the red soil moisture pattern 9. The respective patterns are displayed in Sect. 4.3.1. The black CDFs represent the flood characteristics independent of patterns and are identical to the black CDFs in Fig. 4.5. *N* refers to the sample size.

characteristics can be explained by the patterns' associated flood types derived by Nied et al. (2014).

Weather pattern 19 is related to snowmelt as well as rain-on-snow events (Nied et al., 2014). In the Elbe catchment, snowmelt floods are limited to the winter season and characterized by a large spatial flood extent of minor magnitudes (Nied et al., 2014). The CDFs of weather pattern 19 reveal these characteristics. The pattern, related to flood generation in winter (Fig. 4.6, A), shows high severities (Fig. 4.6, G), a high affected length (Fig. 4.6, D), a high affected gauges $\geq HQ_2$ (Fig. 4.6, E) as well as a low affected gauges $\geq HQ_{10}$ (Fig. 4.6, F). Pattern 26 was linked to rain-on-snow events only (Nied et al., 2014). In these cases, rainfall can occur besides snowmelt (Merz and Blöschl, 2003). Therefore, CDFs of all characteristics

under consideration are slightly more extreme for pattern 26 than for pattern 19.

The highest number of flood events (1333) is linked to weather pattern 29 which is associated with floods from March to October (maximum in August; Fig. 4.6, A). The pattern is linked to short-rain floods, long-rain floods as well as flash floods (Nied et al., 2014). Flash floods are limited to the summer season. Long-rain floods predominantly occur in the winter season whereas short-rain floods have been observed all-year round (Nied et al., 2014). The CDFs of severity (Fig. 4.6, G), affected length (Fig. 4.6, D) and affected gauges $\geq HQ_2$ (Fig. 4.6, E) are around the non-stratified distribution (black solid line). However, the CDF of affected gauges $\geq HQ_{10}$ (Fig. 4.6, F) is much more extreme. Consequently, the pattern shows the most extreme loss behavior (Fig. 4.6, H) among the patterns under consideration.

Weather pattern 34 is related to flash floods as well as short-rain floods (Nied et al., 2014). In case of flash floods and short-rain floods, discharge is expected to be high but spatially limited. The CDF of weather pattern 34 reveals the small spatial extent of these flood types (Fig. 4.6, D). However, high discharge cannot be testified by the applied flood characteristics, i.e. affected gauges $\geq HQ_{10}$ (Fig. 4.6, F). The reason is that affected gauges $\geq HQ_{10}$ is related to all gauges inside the catchment and not only to the fraction of flood affected gauges which is low in case of flash floods and short-rain floods. However, flood loss (Fig. 4.6, H) gives a hint on the event impact of pattern 34 which is extreme but localized flood peaks with inundation and possibly loss. Flood loss related to pattern 34 is much higher than for the patterns associated with winter flooding (patterns 19 and 26).

Seasonal varying flood types also provide the explanation for the varying flood characteristics associated with the selected soil moisture patterns. Soil moisture pattern 9, the wettest pattern, is related to the winter flood types rain-on-snow and snowmelt, both characterized by a large spatial flood extent along with a high number of flood affected gauges (Nied et al., 2014). Accordingly, the pattern shows the most extreme CDF and even an almost linear behavior in affected length (Fig. 4.6, D) and affected gauges $\geq HQ_2$ (Fig. 4.6, E). This observation does not hold true for affected gauges $\geq HQ_{10}$ (Fig. 4.6, F). Here, the CDF of pattern 9 is even below the non-stratified distribution. In line, losses associated with soil moisture pattern 9 are far below the non-stratified distribution (Fig. 4.6, H).

Soil moisture pattern 5 related to summer flooding (Fig. 4.6, A) comes along with long-rain floods, short-rain floods as well as flash floods. Flooding in summer is either characterized by a small spatial flood extent of miscellaneous magnitudes (short-rain floods), a local flood extent of high magnitude (flash floods), or a large spatial flood extent of high magnitudes (long-rain floods, Nied et al., 2014). In the current analysis, it is not possible to assign the CDFs of pattern 5 to a particular summer flood type due to their partly contrasting characteristics, e.g. the wide range of the possible spatial flood extent. However, the CDF of affected gauges $\geq HQ_{10}$ (Fig. 4.6, F) and the CDF of losses (Fig. 4.6, H) indicate that the overall impact of this pattern is high whereas the spatial extent (Fig. 4.6, D) is less extreme which points towards the predominance of short-rain floods and flash floods in conjunction with pattern 5.

The all-year soil moisture pattern 3 (Fig. 4.6, A) has no clear conjunction to a specific flood type. The best linkage was detected to long-rain floods (Nied et al., 2014). Long-rain floods can occur all-year round but the majority of flood events related to this pattern occurs in the summer season. They are characterized by a large spatial flood extent of high magnitudes which is reflected in the CDFs of pattern 3. The CDF of losses (Fig. 4.6, H) associated with pattern 3 depicts an extreme CDF. However, it can be observed, that for the most extreme losses (higher than the 98th percentile), the CDF of soil moisture pattern 5 overtakes the CDF of soil moisture pattern 3.

Although the non-color coded patterns are not discussed for the sake of brevity, similar conclusions could be drawn for them.

4.4.3 Combined control of soil moisture patterns and weather patterns on flood characteristics

The combined impact of soil moisture patterns and weather patterns on flood characteristics is studied with the help of regression trees. A regression tree is built for each flood characteristic. The root node, the overall tree complexity, the succession of decisions nodes separating soil moisture patterns or weather patterns as well as the number of terminal nodes change in dependence of the flood characteristic under consideration.

Fig. 4.7 displays exemplarily the regression tree of the flood affected length. For reasons of simplification, only those patterns discussed in the previous section are labeled in the regression tree. Soil moisture patterns are indicated by a green number. Weather patterns are indicated by a blue number. For completeness, unlabeled patterns are indicted by their quantity. For instance '5+7P' means pattern 5 and additional 7 not further specified patterns. At each decision node visualized by a triangle, either soil moisture patterns (green triangles) or weather patterns

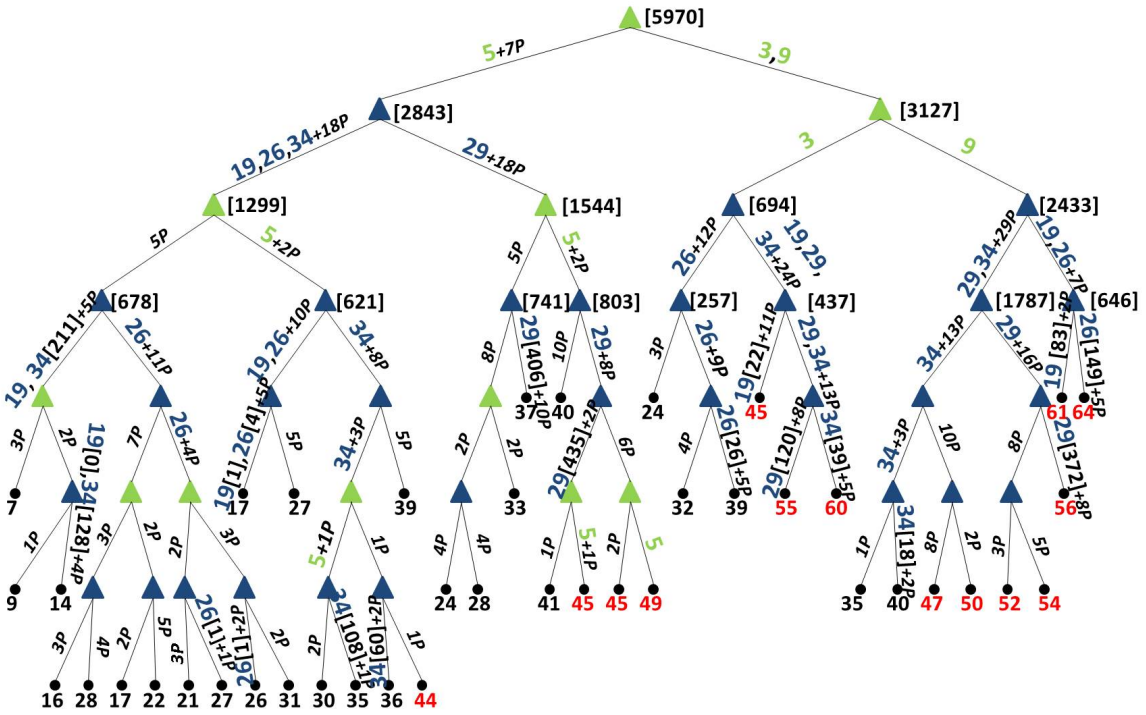

Fig. 4.7: Regression tree of the flood affected length. Soil moisture patterns are indicated by a green number, weather patterns are indicated by a blue number. Unlabeled patterns are indicted by their quantity. Decision nodes are visualized by a green triangle (soil moisture pattern) or by a blue triangle (weather pattern). The median flood affected length of each subgroup is indicated at the respective terminal node. Terminal nodes with an affected length higher than the median value of the entire event set are displayed in red. In brackets, the sample size of the specified pattern in the subgroup is indicated.

(blue triangles) are split into two subgroups. The tree has 42 terminal nodes. The minimum number of flood events in a terminal node is 30. The median flood affected length of each subgroup is indicated at the respective terminal node. Terminal nodes with an affected length higher than the median value of the entire event set derived from the solid black line in Fig. 4.5 are displayed in red. The numbers in brackets indicate the sample size of the specified pattern in the respective subgroup. The node position in the regression tree gives an indication on the importance of the respective soil moisture patterns or weather patterns. The closer a node is located to the root node the bigger is its importance for the flood characteristic under consideration.

The root node unites the entire flood event set, i.e. 5970 flood events. The first split separates the two wettest soil moisture patterns 3 and 9 to the right hand side of the tree, whereas the dryer patterns (8 in total) are pooled at the left hand side. On the right, soil moisture pattern 3 and 9 are further separated into two subgroups. All subsequent nodes separate weather patterns, as no further partition among the soil moisture patterns is possible. The first subgroup consists of 694 events all related to soil moisture pattern 3. The second subgroup consists of 2433 events all related to soil moisture pattern 9. Soil moisture pattern 9 is related to winter flooding. Therefore, the right-most branch can be considered a winter branch comprising mainly rain-on-snow and snowmelt events. Independent of the subsequent weather pattern, soil moisture pattern 9 is related to a high affected length which is characteristic for the winter flood types. The highest median affected length is observed in subgroups comprising weather pattern 19 (median of 61 %) or weather pattern 26 (median of 64 %). Among the weather patterns under consideration, these two patterns also showed the most extreme affected length in the separate view (see Fig. 4.6, B) and are, like soil moisture pattern 9, related to winter flooding. 372 flood events are associated with soil moisture pattern 9 and weather pattern 29. In the separate view, weather pattern 29 was linked to all-year flooding. It is assumed that in this branch mainly the winter events associated with weather pattern 29 are present. In contrary, soil mois-

ture pattern 3 is an all-year pattern. Hence, its branch can be considered an all-year branch.

The left hand side of the tree consists in general of soil moisture patterns related to flooding in summer. It can be considered a summer branch. Contrary to the right hand side of the tree, the node subsequent to the root node does not separate soil moisture patterns. Instead, weather patterns are separated. This indicates that the impact of weather patterns is higher in the summer branch (left hand side of the tree) whereas the impact of the soil moisture patterns is higher on the all-year/winter branch (right hand side of the tree).

In the summer branch, weather pattern 29 is grouped to the right and further separated according to the prevailing soil moisture conditions. The left hand side of the summer branch contains weather patterns 19, 26 and 34. It shows the smallest median affected length, revealing the spatial flood extent of the summer flood types flash flood and short-rain floods. As it is a summer branch, weather patterns related to winter flooding, i.e. 19 and 26, have a small sample size and are negligible. The sample size is highest for weather pattern 34 related to summer flooding.

In summary, the regression tree gives insight into which soil moisture – weather pattern combinations lead to most extreme flood impact and which ones result in small- or medium-sized impact. Second, based on the positions of the patterns in the regression tree, their importance in shaping the flood characteristic can be estimated. Finally, the regression tree delineates the seasonally varying flood processes. To derive a quantitative estimate about the importance of catchment pre-conditions versus meteorological event characteristics, the variable importance is calculated. Figure 4.8 displays the delta of the variable importance derived for each flood characteristic. The graph shows, that the length of the build-up period, the total event length as well as the affected gauges $\geq HQ_{10}$ are mostly controlled by weather patterns in the Elbe catchment. In contrary, the affected length and the affected gauges $\geq HQ_2$ are mostly controlled by soil moisture patterns. In case of severity as well as losses, the control is less pronounced. Severity is slightly governed by soil moisture patterns whereas losses are slightly governed by weather patterns.

4.5 Discussion

4.5.1 Suitability of the developed approach

The reshuffling extends time series of various meteorological variables by taking into account their space-time pattern as well as their interrelation. The reshuffling is independent of the spatial scale and in particular suited for the river basin scale as it takes into account the catchment meteorology as well as large-scale atmospheric conditions. The former is required for hydrological modelling whereas the latter can be systematically associated with floods and guarantees a homogeneous subsample as each weather pattern can be attributed to specific flood generating processes (Nied et al., 2014).

The reshuffling could be extended by altering the frequency and succession of the weather patterns to implement a change in climate. In the analysis, it is assumed that the length of the weather pattern time series is adequate to reproduce the present frequency, persistence and succession of weather patterns.

The reshuffling is similar to the concept of the Multi-Exponential Weather Pattern (MEWP) distribution (e.g. Garavaglia et al., 2011; Paquet et al., 2013). In this approach, rainfall subsamples are derived and fitted to an exponential distribution for each season and prevailing weather pattern. The composite of all subsample distributions (MEWP distribution) is used to generate synthetic rainfall events.

Studying the interacting control of soil moisture patterns, as a proxy for the hydrological pre-event conditions, and of weather patterns, as a proxy for the meteorological event conditions, over a variety of flood characteristics, the process-based approach proved its applicability (Fig. 4.5). The benefits of the presented regional flood model are: First, no assumption on e.g. the catchment's saturation state prior to flooding has to be made as the regional flood model is a continuous simulation that explicitly accounts for the different controls. Second, such a distributed approach depicts spatially heterogeneous and consistent patterns of soil moisture, precipitation, discharge, inundation and losses. Compared to a lumped approach that assumes spatially uniform conditions and return periods in the entire river basin (e.g. Alfieri et al., 2014; Merz et al., 2008), the distributed approach enables to understand flood generation and impact at the larger river basin scale in its chronological order.

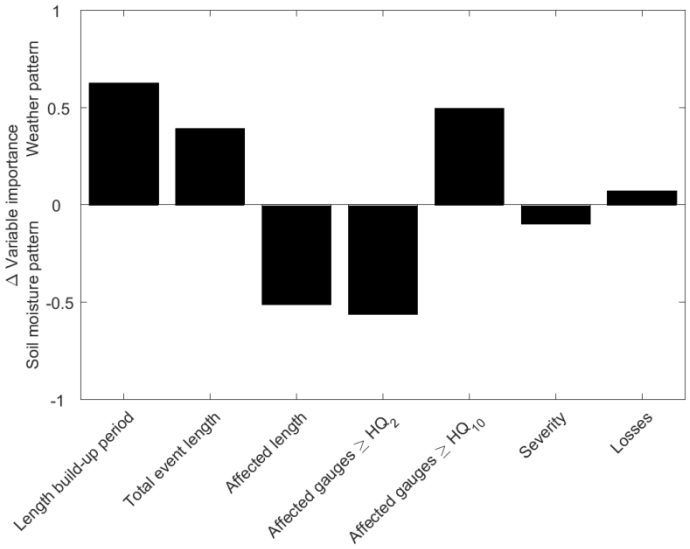

Fig. 4.8: Delta of the variable importance for each flood characteristic. Positive values highlight the dominance of the weather patterns; negative values indicate the dominance of the soil moisture patterns. The higher the absolute value the stronger the influence on the respective flood characteristic. The maximum absolute value is one.

4.5.2 Hydro-meteorological controls on the flood characteristics

Flood generation in the Elbe catchment shows a high variation in terms of spatial patterns of flood peaks and return periods and in terms of process types (Nied et al., 2014). The reshuffling allows generating large samples of flood events reproducing the observed event characteristics. It enables to retrieve distributions of the flood characteristics in dependence of the hydro-meteorological (pre-)event conditions and to study their interaction by the use of regression tree analysis. Both analyses reveal the varying nature and origin of flood events as well as the hydro-meteorological controls on the flood characteristics. They give insight into the impact of specific soil moisture – weather pattern combinations and delineate the seasonal varying flood processes.

Otherwise, the governing hydro-meteorological controls of the flood characteristics are difficult to decipher. For instance, the spatial flood extent, i.e. the affected length, is influenced by the spatial rainfall extent. A larger portion of the river network may be flood affected in case of widespread heavy rainfall. However, if a large fraction of the catchment is saturated, modest rainfall may already generate large scale flooding. Hence, it is unclear whether the affected length is controlled by the extent and magnitude of rainfall, i.e. the weather patterns, or by the share of catchment saturation, i.e. the soil moisture patterns. In the following, the hydro-meteorological controls on the flood characteristics are discussed in light of the results provided in Sect. 4.4.

Length build-up period

The control of weather patterns over the length of the build-up period is stronger than the control of soil moisture patterns. This is indicated by the higher spread of the CDFs in case of weather patterns compared to soil moisture patterns (Fig. 4.6, B), as well as by the positive delta variable importance (Fig. 4.8). The delta variable importance of the length of the build-up period has the highest absolute value and thereby highlights that the control is the strongest among all characteristics under consideration. The dominance can be traced back to the definition of the build-up period. As long as there is an increase in overall discharge the build-up period extends. The increase in overall discharge is either due to persistent rainfall or due to persistent positive air temperatures in case of a snow cover. Rainfall intensity has an influence on the length of the build-up period too. In case of intense rainfall, overland runoff can be generated if the soils' infiltration rate is exceeded. The control of the soil moisture conditions on the length of the build-up period is small compared to the weather patterns. A possible influence of the soil moisture conditions is given in case of preceding soil saturation where any rainfall is directly transformed into runoff resulting in a shorter build-up period.

Total event length

As for the build-up period, the control of the climate forcing, i.e. weather patterns, over the total event length is stronger than the control of the catchment state, i.e. soil moisture patterns. This is indicated by the higher spread of the CDFs in case of weather patterns compared to soil moisture patterns (Fig. 4.6, C), as well as by the positive delta variable importance (Fig. 4.8). For the total event length, the same considerations apply as for the length of the build-up period. Besides the increase in overall discharge, the total event length also takes the recession time, i.e. the decrease of overall discharge, into account. For discharge recession, rainfall has either to stop or to decrease significantly. In case of snowmelt events, air temperature has either to decrease below zero degrees Celsius or the snow cover has to be depleted. This results in the meteorological event conditions as the controlling factor of the total event length. Similar findings were made by Gaál et al. (2012) who attribute flood duration to the type of climatic forcing (storm type as well as snowmelt or rain-on-snow events) in Austria. However, the authors also discovered regions where catchment processes, e.g. the antecedent soil moisture state, are the governing factor for flood duration. The travel time of the flood wave in the river network has a further influence on the total event length which is in our study accounted for by the flood event definition.

Affected length

Affected length is more strongly controlled by the soil moisture patterns. This is indicated by the delta of the variable importance (Fig. 4.8). By the sole consideration of the CDFs (Fig. 4.6, D), no unambiguous conclusion would have been possible. The regression tree (Fig. 4.7) deciphered, exemplarily for all flood characteristics, the seasonal varying influence of the controls. In summer (left hand side of the regression tree in Fig. 4.7), the influence of the weather patterns is stronger than during winter (right hand side of the regression tree in Fig. 4.7). This is confirmed when estimating the variable importance separately for winter and summer. In both seasons, soil moisture patterns dominate over weather patterns. However, the absolute value of the delta variable importance is higher in winter than in summer. In addition, the regression tree showed which soil moisture – weather pattern combinations led to a high affected length and which ones resulted in small- or medium-sized affected length. As the soil moisture patterns and weather patterns can be linked to flood types (Nied et al., 2014), conclusions on the flood generation processes behind the pattern combinations can be drawn and their relative frequency can be estimated.

Affected gauges ≥ HQ_2

Like the affected length, affected gauges ≥ HQ_2 is controlled by the soil moisture conditions. Figure 4.5 D and E illustrates their similar behavior. Additionally, both characteristics have a similar regression tree (not shown). Therefore, the considerations made for the affected length hold true for the affected gauges ≥ HQ_2 too.

Affected gauges ≥ HQ_{10}

Affected gauges ≥ HQ_{10} is governed by the meteorological conditions. This can be partially explained by the upper limit of soil moisture. In case the catchment is saturated, any rainfall will be transferred into runoff. For these situations, discharge depends on precipitation only. Similarly, when the rainfall intensity exceeds the infiltration rate of the soil, discharge increases. The control of the meteorological conditions is in line with the studies which examined the relation between weather patterns and flood magnitude (e.g. Bárdossy and Filiz, 2005; Petrow et al., 2007; Wilby and Quinn, 2013). The patterns related to high affected gauges ≥ HQ_{10} are not necessarily related to high values of affected gauges ≥ HQ_2 or affected length highlighting that flood magnitude and extent arise from different flood generation processes.

Severity

Severity is a combined measure of event magnitude and extent. Event magnitude is governed by the meteorological conditions whereas flood extent is dominated by the soil moisture conditions. The control of both soil moisture and event meteorology conditions on severity is reflected in the small absolute value of the delta variable importance.

Losses

Losses are slightly governed by the meteorological event conditions. It has to be noted that losses occur only for extreme streamflow values which overtax the flood defense structures and impact areas where assets are accumulated. Having the delta variable importance of affected gauges ≥ HQ_{10} and the control of weather patterns on this characteristic in mind, a stronger governance of weather patterns on losses could have been expected. However, the CDFs showed a similar spread when separating losses according to soil moisture patterns or according to weather patterns (Fig. 4.6, H), indicating that neither the meteorological event conditions nor the catchment saturation state is the sole governing factor. Schröter et al. (2015) also have shown that large-scale flooding events can be generated either by extreme soil moisture conditions or by extreme event precipitation – or by a combination of both. In our study, soil moisture patterns 3 and 5 as well as weather pattern 29 associated with ‘Vb’ cyclones were identified as most costly with respect to

flooding. The patterns are mainly related to summer flooding. Factors such as dike breaches, flood protection and adaptation as well as flood management decisions during the event may have an even larger control on flood loss than the hydro-meteorological (pre-)event conditions but are not accounted for in this analysis.

Since this research is based on the Elbe catchment, the conclusions might not hold true for other catchments. Besides the control of the hydrological pre-conditions and the meteorological event conditions on the flood characteristics, catchment attributes such as scale, land use, geology, soils and climate (Merz and Blöschl, 2009a, b) as well as anthropogenic factors like flood mitigation and management may also have an influence. In view of land use and climate change, the approach proposed is able to cope with instationarities. Climate and land use change might alter the relative frequency of weather patterns and soil moisture patterns. If the hydro-meteorological controls on the flood characteristics are known and assumed to persist, future changes in the flood characteristics could be assessed through changes in pattern frequency.

4.6 Conclusions

Understanding flood generation and the impacts of flooding on the large river basin scale is of special interest as this is the scale where national risk policy as well as disaster management and planning have to take place (European Union, 2007). At this scale, floods have to be seen in their spatio-temporal context rather than a single extreme value at one particular location (Falter et al., 2015; Uhlemann et al., 2010).

Whereas several studies have investigated the role of hydrological pre-conditions and of the meteorological event conditions on flood generation and flood peaks in small catchments, this question has hardly been addressed for large river basins. This study deciphers for the first time the large-scale control of the hydrological pre-event conditions and the meteorological event conditions on a set of flood characteristics, including flood losses. This is achieved by generating a large number of flood events. A reshuffling approach based on weather patterns and their month of occurrence is developed. The synthetic fields of catchment meteorology are used to drive a model chain. It is demonstrated that this approach reproduces the observed flood event characteristics. It also generates flood events beyond the existing range of observed variables. A further benefit of the approach is that the antecedent moisture state is continuously simulated by the rainfall-runoff model and takes into account pattern seasonality as well as realistic dry/wet sequences.

From the analysis by means of conditional cumulative distribution functions and regression trees, we conclude that the distinct flood characteristics do not have the same hydro-meteorological controls. Delineating the seasonal varying flood processes, regression trees give insight into which soil moisture – weather pattern combinations lead to most extreme flood characteristics and which ones result in small- or medium-sized flood characteristics. Variable importance quantifies the overall impact of soil moisture patterns and weather patterns on the flood characteristics that is not possible from hydrological reasoning only. The length of the build-up period, the total event length and affected gauges $\geq HQ_{10}$ are governed by weather patterns. The affected length and affected gauges $\geq HQ_2$ are governed by soil moisture patterns. The controlling factor of flood severity, a combined measure of event magnitude and extent, is less pronounced. It is slightly governed by the pre-event catchment conditions. For the first time, flood loss has been linked to hydro-meteorological (pre-)event conditions. The results indicate that flood loss is only slightly governed by weather patterns compared to soil moisture patterns.

The results of this analysis outline that there is a potential to use soil moisture patterns as well as weather patterns not only to inform on possible flood occurrence but also on the involved flood processes and resulting flood characteristics. Furthermore, future changes in flood risk due to changes in pattern frequency evoked from climate and land use change can be embedded in the analysis.

Acknowledgements. M. Nied acknowledges financial support by the AXA Research Fund project "The AXA project on Large-Scale European Flooding under climate change". Thanks to the Potsdam Institute for Climate Impact Research for providing the climate input data.

Chapter 5:
Discussion, conclusions and outlook

5.1 Summary of achievements

The objective of this study was to systematically investigate the influence of the pre-event hydrological catchment conditions on flood generation in order to provide an estimate of the combined impact of pre-event hydrological catchment conditions and meteorological event conditions on flood occurrence, flood processes and characteristics at the river basin scale. Therefore, different classification approaches have been developed to gain insight into the flood triggering causes, their associated processes, and impacts as well as to estimate their respective probability of occurrence. In the following the main findings are summarized based on the research questions raised:

1. **Do large-scale soil moisture patterns exist? What is the dominant spatio-temporal behavior of soil moisture at the river basin scale? Do flood-prone soil moisture patterns exist?**

   Complementary to the classification of weather patterns, large-soil moisture patterns exist in the Elbe River basin. The dominant mode describing large-scale soil moisture variability is the seasonal wetting and drying that is subsequently amended by spatially heterogeneous catchment processes related to smaller scale catchment characteristics. Each day in the period under study is assigned to one out of ten soil moisture pattern types and a probabilistic link to flood initiation is established. The soil moisture patterns are not equally linked to flood initiation and vary seasonally. In winter, flood generation is initiated by catchment-wide soil saturation; a pattern which most commonly is associated with flood start days. In summer where the soil moisture conditions are less stable in time, a variety of soil moisture patterns contribute to flood initiation. In general, the occurrence of a certain soil moisture pattern does not necessarily result in a flood as other factors, in particular the meteorological event conditions, are of relevance. However, the probability of flood occurrence may be increased under a certain soil moisture pattern.

2. **Does a specific weather pattern/soil moisture pattern generate a specific flood type and can thus be linked to a particular flood generating process? How do large-scale soil moisture conditions modify the relation between weather patterns and flood occurrence by amplifying or hindering flood generation?**

   In the Elbe River basin, floods can be classified into rain-on-snow floods, snowmelt floods, long-rain floods, short-rain floods and flash floods. The seasonality, the spatial flood extent as well as flood magnitude vary between the flood types. Both, the hydrological pre-conditions as well as the meteorological event conditions can be linked to specific flood types. For instance, long-rain floods are associated with a weather pattern that is often identified in the presence of 'Vb' cyclones whereas rain-on-snow and snowmelt floods are associated with weather patterns exhibiting westerly and north-westerly wind directions. Flood occurrence at the river basin scale is estimated with respect to hydro-meteorological patterns and pattern combinations. The interaction between large-scale soil moisture conditions and weather patterns varies throughout the year. If the seasonality of a soil moisture pattern and a weather pattern are in phase, a flood-prone soil moisture pattern in combination with a flood-prone weather pattern increases the probability of flooding whereas a soil moisture pattern not-prone to flooding can reduce the flood potential of a weather pattern. The pattern of catchment wide soil saturation and the weather pattern associated with 'Vb' cyclones have the highest flood potential irrespective of the coinciding weather/soil moisture pattern. Their combination results in the highest flood-prone pattern behavior. In the analysis period 18 % of weather patterns only generate flooding in case of preceding soil saturation.

3. **Which flood characteristics are controlled by the hydrological pre-event conditions and which ones by the meteorological event conditions? Does the presence of a particular soil moisture pattern and/or weather pattern determine the magnitude of the flood characteristic under consideration? Does knowledge about the flood characteristics allow conclusions on the involved flood processes?**

   Soil moisture and weather patterns are not only beneficial to inform on flood occurrence but also on the involved processes and resulting flood characteristics. The particular control of the soil moisture conditions preceding the event and the meteorological conditions during the event varies among seasons and can be linked to flood types. Overall, weather patterns take control over the length of the build-up period, the event duration and the number of gauges undergoing at least a 10-year flood. The affected length and the number of gauges undergoing at least a 2-year flood are governed by soil moisture patterns. In case of flood severity and loss, the controlling factor is less pronounced. Severity is slightly governed by soil moisture patterns whereas loss is slightly governed by weather patterns. Based on these findings, the presence of a particular soil moisture

pattern or weather pattern as well as their combination can allow for inference on the peculiarity of a flood characteristic.

5.2 Synthesis and directions for further research

This study addresses fundamental questions towards a comprehensive process-based understanding of flood cause and effect in particular the role of the hydrological pre-event conditions and the meteorological event conditions with respect to (i) the spatial and temporal dynamics of flood events, (ii) the geophysical processes involved in the causal flood chain, and (iii) the systematic interconnections within the flood chain. This is achieved by an appropriate flood definition, the consideration of processes along the complete causal flood chain, the development of a soil moisture classification, and the classification of flood events into process-based flood types. From the tasks addressed in this work and the outcomes of the different articles, a number of aspects can be identified that need further discussion and are thereby sketching the directions for further research.

5.2.1 Spatial and temporal dynamics

The fact that a flood is a spatially and temporally dynamic phenomenon is illustrated by the study and taken into account by an event definition that incorporates the spatio-temporal flood extent as well as flood magnitude (Sect. 2.3.1, Sect. 3.3.1, Sect. 4.3.3). Due to the implementation of the complete causal flood chain (Sect. 4.3.2), floods are not only characterized by their hazard but also by their impact, in the form of direct flood loss for residential buildings, as is requested by the European Union (2007).

The flood identification method, initially developed for transbasin floods (Uhlemann et al., 2010), takes into account the spatial and temporal flood dynamics at the river basin scale and detects realistic flood events for observed as well as simulated discharge data (Sect. 2.4.1, Sect. 3.4.1, Sect. 4.4.1). The event identification is extended (Sect. 2.3.1) in order to cope with discharge time series of unequal length and thus to exploit the maximum of available discharge data. Due to the dense network of gauging stations in the Elbe River basin, the availability of long term operational discharge measurements distributed at representative locations in the entire river network is sufficient to obtain a representative flood event set.

For the first time, the flood identification method is applied to simulated discharge (Sect. 4.4.1). On the one hand, the simulated flood characteristics agree well with those observed. On the other hand, an overall fewer number of flood events is detected for the simulated flood event set. In doing so, the flood identification method reveals deficits in the short-term discharge dynamics of the simulated data. Possible explanations are deficits in the simulation of the runoff generation or a lack in the spatial resolution of either the rainfall-runoff model or the climate input data to the model. Therefore, further research is required to ascertain the reason.

Although the flood identification method takes into account the spatial and temporal behavior of flooding, the joint probability of the flood characteristics at multiple locations is unknown. Further research is required to transfer the identified flood events into a probabilistic model which is able to describe the joint probability and to assign a probability to a spatial pattern of flooding. Joint probability approaches for peak discharges have been proposed by Ghizzoni et al. (2012) and Keef et al. (2009, 2013). Ghizzoni et al. (2012) obtain joint probabilities based on a predefined event set whereas the work of Keef et al. (2009, 2013) is based on a model that includes the entire time series in the statistical model proposed by Heffernan and Tawn (2004). Thereby, the model presumes that floods in winter and summer exhibit the same spatial characteristics. In the Elbe basin, this assumption is not fulfilled as the contributions of the different flood generating processes vary seasonally. To overcome this assumption, the time series could be split according to season or according to flood generating processes/flood types/patterns as conducted in this study and the model could be applied to the sub-samples.

5.2.2 Geophysical processes

In the first place, the flood triggering physical processes are differentiated into the hydrological catchment conditions and the meteorological event conditions. For the first time, soil moisture patterns as a representative of the hydrological catchment conditions are linked to flood initiation at the river basin scale and their influence on floods is systematically deciphered. The results show the necessity of incorporating the large scale soil moisture conditions into the flood assessment. For instance, flood frequency analysis would benefit from incorporating the soil moisture conditions by separating the flood frequency analysis according to the prevailing soil moisture pattern. On average, it is assumed that a T-year precipitation event generates a T-year flood event. However, when individual events are of interest the explanatory power of flood frequency analysis is limited and the role of the soil moisture conditions may be crucial. This is for instance illustrated by the comparison of the Elbe floods of August 2002 (Ulbrich et al., 2003a, b) and

June 2013 (Conradt et al., 2013; Merz et al., 2014b). Although the event precipitation in 2002 was more extreme than in 2013, the latter was much more severe in terms of spatial extent and magnitude. The difference can be explained by the particularly wet pre-event soil moisture conditions in 2013 (Schröter et al., 2015). This work shows how the large-scale soil moisture conditions modify the established linkage between weather patterns and flood occurrence by amplifying or hindering flood generation (Sect. 3.4.2). In addition, the combined control of soil moisture patterns and weather patterns on flood characteristics such as flood magnitude and extent is outlined (Sect. 4.4.3) and further strengthens the necessity of incorporating the soil moisture conditions into flood assessment.

Moreover, the value of the current study lies in the probabilistic interconnection of soil moisture patterns/weather patterns and flood occurrence as well as flood characteristics. The developed probabilistic framework is beneficial to the seasonal prediction of flooding without having to rely on the simulation of the complete flood chain. Therefore, special emphasis should be put on the (sub-)seasonal prediction of soil moisture and weather patterns. Flood risk management, agriculture, the shipping industry and the reinsurance business will greatly benefit from an improved seasonal prediction of flooding.

The results implicate the necessity of strategically collecting soil moisture at the river basin scale in order to more directly address its impact on flooding. Due to the lack of large-scale profile soil moisture products with an adequate record length and temporal coverage, the soil moisture data for the classification are derived from simulations applying a continuous hydrological model (Sect. 2.3.2). In the recent past, the gap of soil moisture products at the river basin scale is bridged by newly developed satellite based soil moisture products as well as by land surface modelling. Several remote sensing techniques are now available. They differ in instrumentation, spatial and temporal coverage as well as soil moisture retrieval method to transfer the moisture value of the upper centimeters of the soil column to a profile value. Examples are the Soil Moisture and Ocean Salinity (SMOS) Level 2 product (Kerr et al., 2012) where soil moisture is retrieved from passive microwave remote sensing brightness temperature, the MetOp-A Advanced Scatterometer (ASCAT) product (Wagner et al., 1999) retrieving soil moisture from radar backscatter based on a change detection method or the Soil Moisture Active Passive (SMAP) satellite product (Entekhabi et al., 2010) combining active and passive sensing techniques. An example of model derived profile soil moisture is the ERA-Interim/Land product (Balsamo et al., 2015), a weather forecast model reanalysis. Due to the wide variety of modeling and retrieval approaches, the derived soil moisture products differ (Rötzer et al., 2015). For their continuous improvement, further research is required to probe the cause of these differences due to instrumentation and retrieval. Furthermore, standardized methods to integrate the satellite derived soil moisture products into hydrological catchment models have to be developed. Likewise, remotely sensed soil moisture should be used to validate simulations of soil moisture in hydrological models (Sect. 2.4.2).

In the same manner as soil moisture patterns, weather patterns can be linked to flood events and a probabilistic relationship between floods and weather patterns is detected (Sect. 3). A multitude of weather classifications exists, an overview is provided by Philipp et al. (2010). The classifications differ in the algorithm used for grouping the data, the meteorological input data, the number and type of input parameters and in the number of classes. However, not all classifications are feasible to study the link to flood occurrence (Prudhomme and Genevier, 2011). In this work, the weather pattern classification is conducted by means of the SANDRA algorithm (Philipp et al., 2007) using ERA40 data (Uppala et al., 2005) of 500 hPa geopotential height and temperature and total column water vapor. Although the SANDRA algorithm is among the most suitable classification approaches to elaborate the relationship between flood occurrence and circulation (Prudhomme and Genevier, 2011), the performance of further classification schemes has to be tested in the context of the research questions addressed here. Moreover, further research is required to investigate the influence of meteorological processes not represented by weather classifications such as convection and orographic enhancement on flood occurrence and characteristics.

In addition to the separate examination of the hydrological catchment conditions and the meteorological event conditions, feedback mechanisms between the atmosphere and soil moisture/land cover have to be taken into account. The feedback mechanism can impair the assumed independence of soil moisture and weather for example during convective situations. Convection is preferentially initiated along gradients of surface heat flux and soil moisture (Ford et al., 2015; Taylor et al., 2012) as well as along land cover boundaries (McPherson et al., 2004). However, there is also evidence that the strength of the feedback between the atmosphere and soil moisture/land cover depends on the synoptic conditions (Ford et al., 2015).

Besides the flood triggers studied, triggers acting on extended spatial and temporal scales are not yet taken into account. With respect to the meteorological event

conditions, the circulation pattern approach can be supplemented by large-scale oscillation classification. Systems which have been linked to flooding include the El Niño/Southern Oscillation (Ward et al., 2010; Ward et al., 2014; Waylen and Caviedes, 1986) or the North Atlantic Oscillation (Bouwer et al., 2006). They expand the scope of flood initiation from the European to the global and from the event based to the decadal scale. In contrast, a sufficiently large spatial scale for the hydrological catchment conditions is the river basin. Nevertheless, on a temporal scale, the hydrological catchment conditions have seasonal as well as short term components. Besides soil moisture, the snow water equivalent, groundwater levels and frozen soils trigger flood generation. A classification into patterns is deemed feasible to study their influence systematically.

The simulation of the complete causal flood chain (Sect. 4) aims to represent the catchment processes ranging from runoff generation and concentration through discharge routing to the flood loss. Each component of the model chain represents the system under study in a simplified manner and thus introduces uncertainties (Falter et al., 2014; Neal et al., 2013). The sources of uncertainties are not easy to identify as they may superimpose, amplify or compensate along the chain (Falter et al., 2014). To minimize uncertainties, observations have to be improved to raise the quality of the input and validation data. In regard to the causal flood chain, this refers in particular to the availability of long term discharge measurements, channel geometry, floodplain topography, inundation extent, floodplain exposure as well as flood losses. Second, uncertainties of the model chain with respect to structure and parameterization are of relevance (Neal et al., 2013). These can be discovered and captured by integrating manifold observational data e.g. remotely sensed soil moisture into the calibration and the validation process of the model chain. Irrespective of the vast amount of required data and the models' implementation costs, process based models are a beneficial tool to gain process understanding of flood generation at the river basin scale. They explicitly account for the different controls and consistently represent soil moisture, precipitation, discharge, inundation and floods as well as flood characteristics in spatial detail (Falter et al., 2014). The benefit of process based models is exemplified in their greater skill compared to using the severity measure when aiming to quantify the overall event impact. The implementation of the causal flood chain reveals that vulnerability has to be considered as well in order to quantify the event impact (Sect. 4.4, Sect. 4.5).

Flood loss, which is accounted for in terms of direct damage to residential buildings in this study (Sect. 4.3.2.3), is a partial description of flood impact. Flood impact also includes the potentially adverse consequences for human health, the environment, cultural heritage and economic activity (European Union, 2007). Further research should, therefore, strengthen the integration of the human factor into the assessment of floods.

5.2.3 Systematic interconnections within the flood chain

Along the complete causal flood chain, different task-oriented classification approaches such as cluster analysis (Sect. 2), regression tree analysis (Sect. 4) and diagnostic maps (Sect. 3) unveil the systematic interactions with respect to the flood triggering causes, their associated processes and characteristics. By their linkage, a deeper understanding of flood cause and effect is pursued and the probability of occurrence of different flood triggering causes, their associated processes and characteristics is estimated. First, causal mechanisms of flood occurrence can be identified by means of flood triggering circulation patterns and patterns of antecedent soil moisture state (Sect. 2, Sect. 3). Second, seasonal flood processes can be deciphered by studying the combined impact of hydrological pre-event conditions and meteorological event conditions on flood occurrence (Sect. 3.4.2). Further insight is gained by linking soil moisture and weather patterns to a flood type classification (Sect. 3.4.3). Third, the governing factors of a variety of flood characteristics including flood loss is deciphered by analyzing the control of the hydrological pre-event conditions and meteorological event conditions on the flood characteristics (Sect. 4). While the focus of this study is on patterns of antecedent soil moisture state and patterns of the meteorological conditions, the flood characteristics are summarized for each event in space and time. Whether a particular pattern of catchment/atmospheric state implies a particular pattern of e.g. inundation or flood losses is still an open question and of particular interest for flood risk management.

The classification creates homogeneous subgroups of flood cause and effect as the flood events are analyzed according to their generating patterns. This in turn enables the attribution of different process-based flood types to generating patterns (Sect. 3). Moreover, the identification of the dominant flood processes and their classification into flood types (Sect. 3) allows conclusions to be drawn on possible future changes (Merz et al., 2014a). For instance, as a consequence of climate as well as land use change, the relative frequency of soil moisture patterns and weather patterns may change. If the change of pattern frequency is adequately reproduced in Global Circulation Models and the link between the patterns and flood occurrence

is known, future changes in flood occurrence can be assessed (e.g. Nissen et al., 2013). The same applies to the prediction of flood type occurrence under climate change. Besides a change of the relative frequency of the flood generating mechanisms, their timing and succession may shift, with implications for present and future flood risk management.

Although the results of this study are not directly transferable to other river basins, the classification approaches are applicable to other regions and time periods. They allow studying floods at any scale – from the local scale through the river basin scale to the global scale. The application of consistent classification approaches would enable reporting on flood events in a standardized framework. Furthermore, a database of past events could be created allowing for the comparison among flood events as well as among catchments. Knowing the links between the classification approaches will enable a rapid flood assessment along the complete flood risk chain.

5.3 Concluding remarks

For a holistic flood view, a process-based flood perspective incorporating all factors and processes of the causal flood chain is required. The recent availability of large-scale modelling approaches as well as the increasing number of spatially extensive observations bring forward its realization.

By classification approaches along the causal flood chain, a profound knowledge on the hydrological preconditions and the meteorological conditions, their spatial and temporal characteristics, their respective influence on flood occurrence, associated flood processes and characteristics is attained at the scale of the river basin.

This knowledge contributes to a better understanding of flood generation in a probabilistic framework and is beneficial to flood risk management as a link between flood cause and effect is established.

References

Alfieri, L., Salamon, P., Bianchi, A., Neal, J., Bates, P., and Feyen, L.: Advances in pan-European flood hazard mapping, *Hydrol. Processes*, *28*, 4067-4077, 2014.

Alila, Y., and Mtiraoui, A.: Implications of heterogeneous flood-frequency distributions on traditional stream-discharge prediction techniques, *Hydrol. Processes*, *16*, 1065-1084, 2002.

Apipattanavis, S., Rajagopalan, B., and Lall, U.: Local polynomial-based flood frequency estimator for mixed population, *J. Hydrol. Eng.*, *15*, 680-691, 2010.

Arnold, J. G., Allen, P. M., and Bernhardt, G.: A comprehensive surface-groundwater flow model, *J. Hydrol.*, *142*, 47-69, 1993.

Balsamo, G., Albergel, C., Beljaars, A., Boussetta, S., Brun, E., Cloke, H., Dee, D., Dutra, E., Muñoz-Sabater, J., Pappenberger, F., de Rosnay, P., Stockdale, T., and Vitart, F.: ERA-Interim/Land: a global land surface reanalysis data set, *Hydrol. Earth Syst. Sci.*, *19*, 389-407, 2015.

Bárdossy, A., and Filiz, F.: Identification of flood producing atmospheric circulation patterns, *J. Hydrol.*, *313*, 48-57, 2005.

Bates, P. D., Horritt, M. S., and Fewtrell, T. J.: A simple inertial formulation of the shallow water equations for efficient two-dimensional flood inundation modelling, *J. Hydrol.*, *387*, 33-45, 2010.

Beurton, S., and Thieken, A. H.: Seasonality of floods in Germany, *Hydrol. Sci. J.*, *54*, 62-76, 2009.

Beven, K. J., and Binley, A. M.: The future of distributed models: Model calibration and uncertainty prediction, *Hydrol. Processes*, *6*, 279-298, 1992.

BfG: Geoportal. http://geoportal.bafg.de/mapapps/resources/apps/HWRMRL-DE/index.html?lang=de (retrieved 16.10.2015), 2014.

BKG GEODATENZENTRUM: ATKIS-Basis-DLM, 2009.

Blöschl, G., Ardoin-Bardin, S., Bonell, M., Dorninger, M., Goodrich, D., Gutknecht, D., Matamoros, D., Merz, B., Shand, P., and Szolgay, J.: At what scales do climate variability and land cover change impact on flooding and low flows?, *Hydrol. Processes*, *21*, 1241-1247, 2007.

Blöschl, G., Nester, T., Komma, J., Parajka, J., and Perdigão, R. A. P.: The June 2013 flood in the Upper Danube basin, and comparisons with the 2002, 1954 and 1899 floods, *Hydrol. Earth Syst. Sci.*, *17*, 5197-5212, 2013.

BMVBS: Normalherstellungskosten 2005 (NHK 2005), 2005.

Boer, W., Schubert, H., and Wilser, O.: Das Sommerhochwasser der Elbe im Juli 1954, Akademie-Verl. Berlin, 1959.

Bouwer, L. M., Vermaat, J. E., and Aerts, J. C. J. H.: Winter atmospheric circulation and river discharge in northwest Europe, *Geophys. Res. Lett.*, *33*, L06403, 2006.

Breiman, L., Friedman, J. H., Olshen, R. A., and Stone, C. J.: Classification and regression trees, Chapman & Hall/CRC, 1984.

Brocca, L., Melone, F., and Moramarco, T.: On the estimation of antecedent wetness conditions in rainfall-runoff modelling, *Hydrol. Processes*, *22*, 629-642, 2008.

Brocca, L., Melone, F., Moramarco, T., and Morbidelli, R.: Antecedent wetness conditions based on ERS scatterometer data, *J. Hydrol.*, *364*, 73-87, 2009.

Chbab, E. H.: How extreme were the 1995 flood waves on the rivers Rhine and Meuse?, *Phys. Chem. Earth*, *20*, 455-458, 1995.

Conradt, T., Roers, M., Schröter, K., Elmer, F., Hoffmann, P., Koch, H., Hattermann, F. F., and Wechsung, F.: Vergleich der Extremhochwässer 2002 und 2013 im deutschen Teil des Elbegebiets

und deren Abflusssimulation durch SWIM-live, *Hydrol. Wasserbewirtsch.*, *57*, 241-245, 2013.

CORINE European Environment Agency: Land Cover Data Set, 2000.

Delgado, J. M., Merz, B., and Apel, H.: A climate-flood link for the lower Mekong River, *Hydrol. Earth Syst. Sci.*, *16*, 1533-1541, 2012.

Duckstein, L., Bárdossy, A., and Bogárdi, I.: Linkage between the occurrence of daily atmospheric circulation patterns and floods: an Arizona case study, *J. Hydrol.*, *143*, 413-428, 1993.

Elmer, F., Thieken, A. H., Pech, I., and Kreibich, H.: Influence of flood frequency on residential building losses, *Nat. Hazards Earth Syst. Sci.*, *10*, 2145-2159, 2010.

Elmer, F., Hoymann, J., Düthmann, D., Vorogushyn, S., and Kreibich, H.: Drivers of flood risk change in residential areas, *Nat. Hazards Earth Syst. Sci.*, *12*, 1641-1657, 2012.

Engel, H.: The flood events of 1993/1994 and 1995 in the Rhine River basin in: Destructive Water: Water-caused Natural Disasters, their Abatement and Control, edited by: Leavesly, G. H., Lins, H. F., Nobilis, F., Parker, R. S., Schneider, V. R., and Van der Ven, F. H. M., IAHS Press, Wallingford, UK, 1997.

Engel, H.: The flood event 2002 in the Elbe river basin causes of the flood, its course, statistical assessment and flood damages, *Houille Blanche*, *6*, 33-36, 2004.

Entekhabi, D., Njoku, E. G., O'Neill, P. E., Kellogg, K. H., Crow, W. T., Edelstein, W. N., Entin, J. K., Goodman, S. D., Jackson, T. J., Johnson, J., Kimball, J., Piepmeier, J. R., Koster, R. D., Martin, N., McDonald, K. C., Moghaddam, M., Moran, S., Reichle, R., Shi, J. C., Spencer, M. W., Thurman, S. W., Tsang, L., and Van Zyl, J.: The soil moisture active passive (SMAP) mission, *Proc. IEEE*, *98*, 704-716, 2010.

Ettrick, T. M., Mawdlsey, J. A., and Metcalfe, A. V.: The Influence of Antecedent Catchment Conditions on Seasonal Flood Risk, *Water Resour. Res.*, *23*, 481-488, 1987.

European Union: Directive 2007/60/EC of the European Parliament and of the Council of 23 October 2007 on the assessment and management of flood risks, 2007.

Falter, D., Dung, N. V., Vorogushyn, S., Schröter, K., Hundecha, Y., Kreibich, H., Apel, H., Theisselmann, F., and Merz, B.: Continuous, large-scale simulation model for flood risk assessments: proof-of-concept, *J. Flood Risk Manage.*, 2014.

Falter, D., Schröter, K., Dung, N. V., Vorogushyn, S., Kreibich, H., Hundecha, Y., Apel, H., and Merz, B.: Spatially coherent flood risk assessment based on long-term continuous simulation with a coupled model chain, *J. Hydrol.*, *524*, 182-193, 2015.

Federal Agency for Cartography and Geodesy in Germany: DGM10.

Ford, T. W., Quiring, S. M., Frauenfeld, O. W., and Rapp, A. D.: Synoptic conditions related to soil moisture-atmosphere interactions and unorganized convection in Oklahoma, *Journal of Geophysical Research: Atmospheres*, *120*, 11,519-511,535, 2015.

Froidevaux, P., Schwanbeck, J., Weingartner, R., Chevalier, C., and Martius, O.: Flood triggering in Switzerland: the role of daily to monthly preceding precipitation, *Hydrol. Earth Syst. Sci.*, *19*, 3903-3924, 2015.

Fundel, F., and Zappa, M.: Hydrological ensemble forecasting in mesoscale catchments: Sensitivity to initial conditions and value of reforecasts, *Water Resour. Res.*, *47*, 2011.

Gaál, L., Szolgay, J., Kohnová, S., Parajka, J., Merz, R., Viglione, A., and Blöschl, G.: Flood timescales: Understanding the interplay of climate and catchment processes through comparative hydrology, *Water Resour. Res.*, *48*, W04511, 2012.

Garavaglia, F., Lang, M., Paquet, E., Gailhard, J., Garçon, R., and Renard, B.: Reliability and robustness of rainfall compound distribution

model based on weather pattern sub-sampling, *Hydrol. Earth Syst. Sci.*, *15*, 519-532, 2011.

Ghizzoni, T., Roth, G., and Rudari, R.: Multisite flooding hazard assessment in the Upper Mississippi River, *J. Hydrol.*, *412–413*, 101-113, 2012.

GRDC: The Global Runoff Data Centre, 56068 Koblenz, Germany, 2010.

Guha-Sapir, D., Below, R., and Hoyois, P.: EM-DAT: International Disaster Database – www.emdat.be – Université Catholique de Louvain – Brussels – Belgium, 2015.

Haberlandt, U., and Radtke, I.: Hydrological model calibration for derived flood frequency analysis using stochastic rainfall and probability distributions of peak flows, *Hydrol. Earth Syst. Sci.*, *18*, 353-365, 2014.

Hannachi, A., Jolliffe, I. T., and Stephenson, D. B.: Empirical orthogonal functions and related techniques in atmospheric science: A review, *Int. J. Climatol.*, *27*, 1119-1152, 2007.

Hattermann, F. F., Wattenbach, M., Krysanova, V., and Wechsung, W.: Runoff simulations on the macroscale with the ecohydrological model SWIM in the Elbe catchment-validation and uncertainty analysis, *Hydrol. Processes*, *19*, 693-714, 2005.

Hauptamt für Hydrologie: Witterung und Wasserstände im Juli 1954, *Wasserwirtschaft - Wassertechnik*, *Jahrgang 4*, 351-652, 1954.

Heffernan, J. E., and Tawn, J. A.: A conditional approach for multivariate extreme values (with discussion), *J. Roy. Stat. Soc. Ser. B. (Stat. Method.)*, *66*, 497-546, 2004.

Hirschboeck, K. K.: Hydroclimatically-defined mixed distributions in partial duration flood series, Hydrologic Frequency Modelling, 199-212, 1987.

Hirschboeck, K. K.: Flood Hydroclimatology, in: Flood Geomorphology, edited by: Baker, V. R., Kochel, R. C., and Patton, P. C., John Wiley & Sons, 27-49, 1988.

Hundecha, Y., and Bárdossy, A.: Modeling of the effect of land use changes on the runoff generation of a river basin through parameter regionalization of a watershed model, *J. Hydrol.*, *292*, 281-295, 2004.

Huza, J., Teuling, A. J., Braud, I., Grazioli, J., Melsen, L. A., Nord, G., Raupach, T. H., and Uijlenhoet, R.: Precipitation, soil moisture and runoff variability in a small river catchment (Ardèche, France) during HyMeX Special Observation Period 1, *J. Hydrol.*, *516*, 330-342, 2014.

Ibrahim, H. M., and Huggins, D. R.: Spatio-temporal patterns of soil water storage under dryland agriculture at the watershed scale, *J. Hydrol.*, *404*, 186-197, 2011.

IKSE: Die Elbe und ihr Einzugsgebiet. Ein geographisch-hydrologischer und wasserwirtschaftlicher Überblick, 262, 2005.

Infas Geodaten GmbH: Infas Geodaten, 2009.

Jacobeit, J., Philipp, A., and Nonnenmacher, M.: Atmospheric circulation dynamics linked with prominent discharge events in Central Europe, *Hydrolog. Sci. J.*, *51*, 946-965, 2006.

Jawson, S. D., and Niemann, J. D.: Spatial patterns from EOF analysis of soil moisture at a large scale and their dependence on soil, land-use, and topographic properties, *Adv. Water Resour.*, *30*, 366-381, 2007.

Jha, A. K., Bloch, R., and Lamond, J.: Cities and flooding: a guide to integrated urban flood risk management for the 21st century, World Bank Publications, 2012.

Joliffe, I. T.: Principal component analysis, Springer Series in Statistics, Springer, New York, 1986.

Keef, C., Svensson, C., and Tawn, J. A.: Spatial dependence in extreme river flows and precipitation for Great Britain, *J. Hydrol.*, *378*, 240-252, 2009.

Keef, C., Papastathopoulos, I., and Tawn, J. A.: Estimation of the conditional distribution of a

multivariate variable given that one of its components is large: Additional constraints for the Heffernan and Tawn model, *J. Multivar. Anal.*, *115*, 396-404, 2013.

Kerr, Y. H., Waldteufel, P., Richaume, P., Wigneron, J. P., Ferrazzoli, P., Mahmoodi, A., Al Bitar, A., Cabot, F., Gruhier, C., Juglea, S. E., Leroux, D., Mialon, A., and Delwart, S.: The SMOS soil moisture retrieval algorithm, *IEEE Trans. Geosci. Remote Sens.*, *50*, 1384-1403, 2012.

Kim, G., and Barros, A. P.: Space-time characterization of soil moisture from passive microwave remotely sensed imagery and ancillary data, *Remote Sens. Environ.*, *81*, 393-403, 2002.

Korres, W., Koyama, C. N., Fiener, P., and Schneider, K.: Analysis of surface soil moisture patterns in agricultural landscapes using empirical orthogonal functions, *Hydrol. Earth Syst. Sci.*, *14*, 751-764, 2010.

Kron, W., Steuer, M., Löw, P., and Wirtz, A.: How to deal properly with a natural catastrophe database – analysis of flood losses, *Nat. Hazards Earth Syst. Sci.*, *12*, 535-550, 2012.

Krysanova, V., Meiner, A., Roosaare, J., and Vasilyev, A.: Simulation modelling of the coastal waters pollution from agricultural watershed, *Ecol. Model.*, *49*, 7-29, 1989.

Krysanova, V., Müller-Wohlfeil, D.-I., and Becker, A.: Development and test of a spatially distributed hydrological / water quality model for mesoscale watersheds, *Ecol. Model.*, *106*, 261-289, 1998.

Maidment, D. R.: Handbook of Hydrology, McGraw-Hill, Inc. New York, 1993.

Marchi, L., Borga, M., Preciso, E., and Gaume, E.: Characterisation of selected extreme flash floods in Europe and implications for flood risk management, *J. Hydrol.*, *394*, 118-133, 2010.

McPherson, R. A., Stensrud, D. J., and Crawford, K. C.: The Impact of Oklahoma's Winter Wheat Belt on the Mesoscale Environment, *Monthly Weather Review*, *132*, 405-421, 2004.

Merz, B., Hall, J., Disse, M., and Schumann, A.: Fluvial flood risk management in a changing world, *Nat. Hazards Earth Syst. Sci.*, *10*, 509-527, 2010a.

Merz, B., Kreibich, H., Schwarze, R., and Thieken, A.: Review article "Assessment of economic flood damage", *Nat. Hazards Earth Syst. Sci.*, *10*, 1697-1724, 2010b.

Merz, B., Aerts, J., Arnbjerg-Nielsen, K., Baldi, M., Becker, A., Bichet, A., Blöschl, G., Bouwer, L. M., Brauer, A., Cioffi, F., Delgado, J. M., Gocht, M., Guzzetti, F., Harrigan, S., Hirschboeck, K., Kilsby, C., Kron, W., Kwon, H. H., Lall, U., Merz, R., Nissen, K., Salvatti, P., Swierczynski, T., Ulbrich, U., Viglione, A., Ward, P. J., Weiler, M., Wilhelm, B., and Nied, M.: Floods and climate: emerging perspectives for flood risk assessment and management, *Nat. Hazards Earth Syst. Sci.*, *14*, 1921-1942, 2014a.

Merz, B., Elmer, F., Kunz, M., Mühr, B., and Schröter, K.: The extreme flood in June 2013 in Germany, *Houille Blanche - Revue internationale de l'eau*, *1*, 5-10, 2014b.

Merz, R., and Blöschl, G.: A process typology of regional floods, *Water Resour. Res.*, *39*, 1340, 2003.

Merz, R., Blöschl, G., and Parajka, J.: Spatio-temporal variability of event runoff coefficients, *J. Hydrol.*, *331*, 591-604, 2006.

Merz, R., and Blöschl, G.: Flood frequency hydrology: 2. Combining data evidence, *Water Resour. Res.*, *44*, 2008a.

Merz, R., and Blöschl, G.: Flood frequency hydrology: 1. Temporal, spatial, and causal expansion of information, *Water Resour. Res.*, *44*, W08432, 2008b.

Merz, R., Blöschl, G., and Humer, G.: National flood discharge mapping in Austria, *Nat. Hazards*, *46*, 53-72, 2008.

Merz, R., and Blöschl, G.: A regional analysis of event runoff coefficients with respect to climate and catchment characteristics in Austria, *Water Resour. Res.*, *45*, 2009a.

Merz, R., and Blöschl, G.: Process controls on the statistical flood moments - a data based analysis, *Hydrol. Processes*, *23*, 675-696, 2009b.

Munich RE: Loss events worldwide 1980 – 2014, 10 costliest floods ordered by overall losses, *Münchener Rückversicherungs-Gesellschaft, Geo Risks Research, NatCatSERVICE*, 2015.

Nash, J. E., and Sutcliffe, J. V.: River flow forecasting through conceptual models. Part I. A discussion of principles., *J. Hydrol.*, *10*, 280-290, 1970.

Neal, J., Keef, C., Bates, P., Beven, K., and Leedal, D.: Probabilistic flood risk mapping including spatial dependence, *Hydrol. Processes*, *27*, 1349-1363, 2013.

Nied, M., Hundecha, Y., and Merz, B.: Flood-initiating catchment conditions: A spatio-temporal analysis of large-scale soil moisture patterns in the Elbe river basin, *Hydrol. Earth Syst. Sci.*, *17*, 1401-1414, 2013.

Nied, M., Pardowitz, T., Nissen, K., Ulbrich, U., Hundecha, Y., and Merz, B.: On the relationship between hydro-meteorological patterns and flood types, *J. Hydrol.*, *519, Part D*, 3249-3262, 2014.

Nissen, K. M., Pardowitz, T., Ulbrich, U., and Nied, M.: Will climate change affect weather types associated with flooding in the Elbe river basin?, *EGU General Assembly Conference Abstracts*, *EGU2013-7938*, 2013.

Norbiato, D., Borga, M., Merz, R., Blöschl, G., and Carton, A.: Controls on event runoff coefficients in the eastern Italian Alps, *J. Hydrol.*, *375*, 312-325, 2009.

Österle, H.: Reconstruction of daily global radiation for past years for use in agricultural models, *Phys. Chem. Earth (B)*, *26*, 253-256, 2001.

Österle, H., Gerstengarbe, F. W., and Werner, P. C.: Ein neuer meteorologischer Datensatz für Deutschland, 1951 - 2003, in: Proceedings der 7. Deutschen Klimatagung, Klimatrends: Vergangenheit und Zukunft, Meteorologisches Institut der Ludwig-Maximilians-Universität, München, 3, 2006.

Österle, H., Schmidt, S., Hauf, Y., and Wechsung, F.: Erstellung und Prüfung eines synoptischen meteorologischen Tagesdatensatzes von 1951 bis 2003 für den tschechischen Teil des Elbe-Einzugsgebietes, in: Die Elbe und ihr Einzugsgebiet im globalen Wandel, edited by: Wechsung, F., Hartje, V., Kaden, S., Venohr, M., Hansjürgens, B., and Gräfe, P., Weißensee Verlag Berlin, 2012.

Overland, J. E., and Preisendorfer, R. W.: A significance test for principal components applied to a cyclone climatology, *Mon. Weather Rev.*, *110*, 1-4, 1982.

Paquet, E., Garavaglia, F., Garçon, R., and Gailhard, J.: The SCHADEX method: A semi-continuous rainfall–runoff simulation for extreme flood estimation, *J. Hydrol.*, *495*, 23-37, 2013.

Parajka, J., Naeimi, V., Blöschl, G., Wagner, W., Merz, R., and Scipal, K.: Assimilating scatterometer soil moisture data into conceptual hydrologic models at the regional scale, *Hydrol. Earth Syst. Sci.*, *10*, 353-368, 2006.

Parajka, J., Kohnová, S., Bálint, G., Barbuc, M., Borga, M., Claps, P., Cheval, S., Dumitrescu, A., Gaume, E., Hlavcová, K., Merz, R., Pfaundler, M., Stancalie, G., Szolgay, J., and Blöschl, G.: Seasonal characteristics of flood regimes across the Alpine-Carpathian range, *J. Hydrol.*, *394*, 78-89, 2010.

Pathiraja, S., Westra, S., and Sharma, A.: Why continuous simulation? The role of antecedent moisture in design flood estimation, *Water Resour. Res.*, *48*, 1-15, 2012.

Perry, M. A., and Niemann, J. D.: Analysis and estimation of soil moisture at the catchment scale using EOFs, *J. Hydrol.*, *334*, 388-404, 2007.

Petrow, T., Merz, B., Lindenschmidt, K. E., and Thieken, A. H.: Aspects of seasonality and flood generating circulation patterns in a mountainous catchment in south-eastern Germany, *Hydrol. Earth Syst. Sci.*, *11*, 1455-1468, 2007.

Petrow, T., Zimmer, J., and Merz, B.: Changes in the flood hazard in Germany through changing

frequency and persistence of circulation patterns, *Nat. Hazard Earth Sys.*, *9*, 1409-1423, 2009.

Philipp, A., Della-Marta, P. M., Jacobeit, J., Fereday, D. R., Jones, P. D., Moberg, A., and Wanner, H.: Long-Term Variability of Daily North Atlantic–European Pressure Patterns since 1850 Classified by Simulated Annealing Clustering, *J. Clim.*, *20*, 4065-4095, 2007.

Philipp, A., Bartholy, J., Beck, C., Erpicum, M., Esteban, P., Fettweis, X., Huth, R., James, P., Jourdain, S., Kreienkamp, F., Krennert, T., Lykoudis, S., Michalides, S. C., Pianko-Kluczynska, K., Post, P., Álvarez, D. R., Schiemann, R., Spekat, A., and Tymvios, F. S.: Cost733cat - A database of weather and circulation type classifications, *Phys. Chem. Earth Pt A/B/C*, *35*, 360-373, 2010.

Pollner, J.: Financial and Fiscal Instruments for Catastrophe Risk Management: Addressing the Losses from Flood Hazards in Central Europe, World Bank Publications, 2012.

Preisendorfer, R. W.: Principal component analysis in meteorology and oceanography, Dev. Atmos. Sci., 17, edited by: Mobley, C. D., Elsevier, Amsterdam, 425 pp., 1988.

Priestley, C. H. B., and Taylor, R. J.: On the assessment of surface heat flux and evaporation using large-scale parameters, *Mon. Weather Rev.*, *100*, 81-92, 1972.

Prudhomme, C., and Genevier, M.: Can atmospheric circulation be linked to flooding in Europe?, *Hydrol. Processes*, *25*, 1180-1990, 2011.

Ritchie, J. T.: Model for predicting evaporation from a row crop with incomplete cover, *Water Resour. Res.*, *8*, 1204-1213, 1972.

Rodda, H. J. E.: The development and application of a flood risk model for the Czech Republic, *Nat. Hazards*, *36*, 207-220, 2005.

Rötzer, K., Montzka, C., and Vereecken, H.: Spatio-temporal variability of global soil moisture products, *J. Hydrol.*, *522*, 187-202, 2015.

Schirpke, H., Richter, I., and Rieß, B.: Analyse der Hochwassersituation im Oktober 1974 / Dezember 1974 / Januar 1975 in den Flußgebieten der Oberen Elbe, der Schwarzen Elster und den Mulden, in: Ablauf der Winterhochwässer 1974/75 im Gebiet der DDR, Mitteilungen des Instituts für Wasserwirtschaft, 41, 33-119, 1978.

Schröter, K., Kunz, M., Elmer, F., Mühr, B., and Merz, B.: What made the June 2013 flood in Germany an exceptional event? A hydro-meteorological evaluation, *Hydrol. Earth Syst. Sci.*, *19*, 309-327, 2015.

Silvestro, F., and Rebora, N.: Impact of precipitation forecast uncertainties and initial soil moisture conditions on a probabilistic flood forecasting chain, *J. Hydrol.*, *519, Part A*, 1052-1067, 2014.

Sivapalan, M., Wood, E. F., and Beven, K. J.: On hydrologic Similarity 3. A Dimensionless Flood Frequency Model Using a Generalized Geomorphologic Unit Hydrograph and partial area Runoff Generation, *Water Resour. Res.*, *26*, 43-58, 1990.

Sivapalan, M., Blöschl, G., Merz, R., and Gutknecht, D.: Linking flood frequency to long-term water balance: Incorporating effects of seasonality, *Water Resour. Res.*, *41*, W06012, 2005.

Strahler, A. N.: Quantitative geomorphology of drainage basins and channel networks, Handbook of Applied Hydrology, edited by: Chow, V. T., and Hill, M., New York, 39-76 pp., 1964.

Tarolli, M., Borga, M., Zoccatelli, D., Bernhofer, C., Jatho, N., and Janabi, F.: Rainfall space-time organization and orographic control on flash flood response: The Weisseritz event of August 13, 2002, *J. Hydrol. Eng.*, *18*, 183-193, 2013.

Taylor, C. M., de Jeu, R. A. M., Guichard, F., Harris, P. P., and Dorigo, W. A.: Afternoon rain more likely over drier soils, *Nature*, *489*, 423-426, 2012.

Thieken, A. H., Olschewski, A., Kreibich, H., Kobsch, S., and Merz, B.: Development and evaluation of FLEMOps - a new Flood Loss Estimation MOdel for the private sector, in: Flood Recovery, Innovation and Response, edited by: Proverbs, D.,

Brebbia, C. A., and PenningRowsell, E., WIT Trans. Ecol. Environ., WIT Press, Southampton, 315-324, 2008.

Thieken, A. H., Apel, H., and Merz, B.: Assessing the probability of large-scale flood loss events: a case study for the river Rhine, Germany, *J. Flood Risk Manage.*, 2014.

Uhlemann, S., Thieken, A. H., and Merz, B.: A consistent set of trans-basin floods in Germany between 1952 - 2002, *Hydrol. Earth Syst. Sci.*, *14*, 1277-1295, 2010.

Uhlemann, S., Bertelmann, R., and Merz, B.: Data expansion: the potential of grey literature for understanding floods, *Hydrol. Earth Syst. Sci.*, *17*, 895-911, 2013.

Ulbrich, U., Brücher, T., Fink, A. H., Leckebusch, G. C., Krüger, A., and Pinto, J. G.: The central European floods of August 2002: Part 1 - Rainfall periods and flood development, *Weather*, *58*, 371-377, 2003a.

Ulbrich, U., Brücher, T., Fink, A. H., Leckebusch, G. C., Krüger, A., and Pinto, J. G.: The central European floods of August 2002: Part 2 - Synoptic causes and considerations with respect to climate change, *Weather*, *58*, 434 - 442, 2003b.

Uppala, S. M., KÅllberg, P. W., Simmons, A. J., Andrae, U., Bechtold, V. D. C., Fiorino, M., Gibson, J. K., Haseler, J., Hernandez, A., Kelly, G. A., Li, X., Onogi, K., Saarinen, S., Sokka, N., Allan, R. P., Andersson, E., Arpe, K., Balmaseda, M. A., Beljaars, A. C. M., Berg, L. V. D., Bidlot, J., Bormann, N., Caires, S., Chevallier, F., Dethof, A., Dragosavac, M., Fisher, M., Fuentes, M., Hagemann, S., Hólm, E., Hoskins, B. J., Isaksen, L., Janssen, P. A. E. M., Jenne, R., McNally, A. P., Mahfouf, J. F., Morcrette, J. J., Rayner, N. A., Saunders, R. W., Simon, P., Sterl, A., Trenberth, K. E., Untch, A., Vasiljevic, D., Viterbo, P., and Woollen, J.: The ERA-40 re-analysis, *Q. J. Roy. Meteorol. Soc.*, *131*, 2961-3012, 2005.

US Army Corps of Engineers: HEC-GeoRAS.

USDA Soil Conservation Service: National Engineering Handbook, 1972.

Van Eck, W. H. J. M., Lenssen, J. P. M., Van De Steeg, H. M., Blom, C. W. P. M., and De Kroon, H.: Seasonal dependent effects of flooding on plant species survival and zonation: A comparative study of 10 terrestrial grassland species, *Hydrobiologia*, *565*, 59-69, 2006.

Van Loon, A. F., and Van Lanen, H. A. J.: A process-based typology of hydrological drought, *Hydrol. Earth Syst. Sci.*, *16*, 1915-1946, 2012.

Wagner, W., Lemoine, G., and Rott, H.: A method for estimating soil moisture from ERS scatterometer and soil data, *Remote Sens. Environ.*, *70*, 191-207, 1999.

Ward Jr., J. H.: Hierarchical grouping to optimize an objective function, *J. Am. Stat. Assoc.*, *58*, 236-244, 1963.

Ward, P. J., Beets, W., Bouwer, L. M., Aerts, J. C. J. H., and Renssen, H.: Sensitivity of river discharge to ENSO, *Geophys. Res. Lett.*, *37*, L12402, 2010.

Ward, P. J., Eisner, S., Flörke, M., Dettinger, M. D., and Kummu, M.: Annual flood sensitivities to El Niño–Southern Oscillation at the global scale, *Hydrol. Earth Syst. Sci.*, *18*, 47-66, 2014.

Waylen, P. R., and Caviedes, C. N.: El Niño and annual floods on the north Peruvian littoral, *J. Hydrol.*, *89*, 141-156, 1986.

Wilby, R. L., and Quinn, N. W.: Reconstructing multi-decadal variations in fluvial flood risk using atmospheric circulation patterns, *J. Hydrol.*, *487*, 109-121, 2013.

Wittrock, V., and Ripley, E. A.: The predictability of autumn soil moisture levels on the Canadian Prairies, *Int. J. Climatol.*, *19*, 271-289, 1999.

Wünsch, A., Herrmann, U., Kreibich, H., and Thieken, A.: The Role of Disaggregation of Asset Values in Flood Loss Estimation: A Comparison of Different Modeling Approaches at the Mulde River, Germany, *Environ. Manage.*, *44*, 524-541, 2009.

Author's declaration

I prepared this dissertation without illegal assistance. The work is original except where indicated by special reference in the text and no part of the dissertation has been submitted for any other degree. This dissertation has not been presented to any other University for examination, neither in Germany nor in another country.

Manuela Nied
Karlsruhe, March 2016